EXPERIMENTAL VERIFICATION OF SOME MODAL ANALYSIS METHODS

by
B. V. VASUDEVA RAO

DEPARTMENT OF MECHANICAL ENGINEERING
INDIAN INSTITUTE OF TECHNOLOGY KANPUR

October, 1988

EXPERIMENTAL VERIFICATION OF SOME MODAL ANALYSIS METHODS

A Thesis Submitted
In Partial Fulfilment of the Requirements
for the Degree of
MASTER OF TECHNOLOGY

by
B. V. VASUDEVA RAO

to the
DEPARTMENT OF MECHANICAL ENGINEERING
INDIAN INSTITUTE OF TECHNOLOGY KANPUR
October, 1988

ACKNOWLEDGEMENTS

I express my gratitude to my guide Dr.H. Hatwal for his invaluable guidance and constant encouragement at all stages of work.

I thank Jaspal for his help and cooperation during this work.

My thanks are due to Mr. M.M. Singh and Mr.Majumdar of Vibration Lab. for all the help extended to me.

I express my thanks to Bannur, Sharath, Satish, Venkat, Anuj, Shastri and a host of other friends for making my stay at IIT a most enjoyable and memorable one.

B.V. VASUDEVA RAO

21/X/88.

CERTIFICATE

This is to certify that the work entitled, "Experimental Verification of Some Modal Analysis Methods" by B.V. Vasudeva Rao has been carried out under my supervision and has not been submitted elsewhere for a degree.

Hatwal

October, 1988.

(H. HATWAL)
Assistant Professor
Department of Mechanical Engineering
Indian Institute of Technology
Kanpur

CONTENTS

Page

LIST OF TABLES

LIST OF FIGURES

NOTATIONS

${}_rA^*_{jk}$	Modal constant (mode r, FRF jk)
$a^*(\omega)$	Accelerance
$\hat{a}$	Acceleration response
${}_rB^*_{jk}$	Residual term, FRF approximation for other modes
$[C]$	Viscous damping matrix
$f(t),\ f^*$	Force
$[H]$	Hysteretic damping matrix
$[K]$	Stiffness matrix
$[M]$	Mass matrix
N	Number of DOF in MDOF system
x, x^*, X	Displacement response
Y^*	Mobility
α^*	Receptance
$\{\emptyset\}_r$	Normalised eigenvector of r^{th} mode
η_r	Hysteretic damping loss factor for r^{th} mode
ω	Frequency of vibration
ω_r	Natural frequency
λ^*_r	Damped natural frequency
${}_RM_{jk}$	Mass residual (FRF, jk)
${}_RK_{jk}$	Stiffness residual (FRF, jk)

ABSTRACT

One of two objectives of the present work is to investigate the advantage of Modal parameter extraction by Multidegree of Freedom (MDF) method over single degree of freedom (SDF) method, when the structure is highly damped and has closely placed modes. The MDF curve fit method used is a least square error minimisation technique. It has been tested on two structures. One was a plate held in hand and the other was a structure made up of four beams interconnected at their ends by bolts. It was found that the MDF method gave improved parameters compared to the parameters obtained by SDF method. The other objective of this work was to predict the response model of a coupled structure using the response models of the substructures. The method adopted was the impedance coupling method. Measured response model of the two substructures, a beam and a U-shaped structure has been used to predict the response model of the structure, formed by coupling the substructures at two co-ordinates.

CHAPTER-1

INTRODUCTION

1.1 Introduction

Measurement of the dynamic characteristics of materials and structures is an increasingly important part of the design and development of air and space crafts, automotive and rail road vehicles, machine tools and other equipment. Aided by the development of electronics and computers in the last two decades, dynamic modelling and testing has been simplified and refined considerably.

The dynamic behavior of a mechanical structure can be characterised by three types of models, namely the spatial model, the modal model and the response model [1]. Spatial model characterises the physical properties, namely mass stiffness and damping of the system. Modal model is defined by the natural frequencies, damping loss factors and mode shape vectors. The response model is a set of responses at a given point due to a unit amplitude sinusoidal force applied to each point individually and at every frequency within a specified range [1].

Experimental methods of obtaining the above mentioned models is called 'Modal testing'. The first step in Modal testing is the determination of the response models. This is found by exciting the structure, measuring the responses and determining.

the transfer function of the system on the spectrum analyser. This constitutes the 'Hardware' of modal testing. The response model is then analysed to yield the modal and spatial models. This analysis constitutes the 'software' of modal testing.

Analytical methods like Finite element methods, can also derive the mathematical models. The advantage of these analytical methods lies in the fact that the system characteristics can be determined and modified at the design stage itself. But the system characteristics thus predicted may differ from the actual performance due to complexity of structure, nonhomogenity of material etc. These analytical models can be improved by comparing it with the models obtained by modal testing. Modal testing can also help in monitoring the condition of structures and in predicting the possible failures of the structure before hand.

1.2 Literature Review

Literature of modal analysis dates back to 1940's, when the principle of Modal testing was given by Kennedy and Pancu [2]. The literature concerning the development of Modal testing is given in a recent work by Jaspal Singh [3].

Testing techniques can be divided into single shaker and multiple shaker tests. In single shaker testing, the structure is vibrated at one particular point and responses are measured at one or more points. Multiple shaker technique is used for large structures such as aircraft structures. A large

amount of energy can be uniformly fed into the structures than the single point excitation. A number of exciters can be positioned judiciously at different points on the structure so that the modes of interest can be excited individually[4,5].

Methods which determine the modal parameters namely, the natural frequency, modal damping and mode shapes, from the transfer function can be classified as single degree of freedom (SDF) methods and multidegree of freedom (MDF) methods. The type of method selected depends upon the closeness of resonances and the amount of damping. SDF methods extract parameters of one mode at a time. The most widely used method is the circle fit method [1]. The near resonance points of the transfer function (Frequency response function) will form an arc of a circle or a complete circle, depending on the amount of damping. The algorithm for a least square error circle fit is given by Brandon and Cowley [6].

MDF methods may be used in both time and frequency domains. The MDF method given by Gaukroger, Skingle and Heron [7] is widely applicable since it can be used for curve fitting a large number of close resonances. The damping considered was of viscous type. In this method a linearised iterative least square procedure is followed.

A MDF method in which many frequency response functions are simultaneously curve fitted, with excitation at only one point is given by Goyder [8]. The difference of Gaukroger algorithm [7] with that of Goyder [8] is that the later method

considers each mode separately, that data for each mode being taken from all the FRF's collectively. Thus a single mode is isolated and curve fitted for all frequency response functions.

Ewins [1] has outlined a MDF method in time domain, called the complex exponentials method. This method is based on fitting a complex exponential function to the time impulse function.

Most of the MDF methods require a lot of computation. A relatively simple method is described by Ewins and Gleeson [9]. for lightly damped structure. This method uses only the real part of frequency response function to determine the parameters.

The literature on coupled structures is relatively small. Ewins [1] has outlined a method called the impedance coupling method. Here the measured frequency responses of two separate components of a structure are used to predict the response of the coupled structure, formed by combining the two components, at one or more co-ordinates. A very interesting practical problem of predicting the response of a coupled helicopter carrier has been carried out by Ewins, Silva and Maleci[10].

Spatial model may be easily derived from the modal model. A procedure to calculate the mass, stiffness matrices of a mechanical structure has been given by Fritzen[11].

The spatial modal derived is not always unique. Interaction with spatial model is more meaningful if already such a model has been formulated and now validity or modification is needed. Done and Hughes [12,13] have analysed the effect of adding mass or stiffness to the existing structure and have established methods for obtaining the bounds within which the response of the modified structure will lie.

1.3 Objective and Scope of Present Work

This work was undertaken to investigate the advantage of MDF over SDF method and to study the behaviour of a coupled structure. The MDF curve fit method was used to improve the modal parameters of a structure with high damping or closely placed modes. This iterative method required initial estimates, which were obtained by SDF circle fit method. Two specimens, a plate held in hand and a structure with four beams interconnected at the ends with bolts were analysed by MDF curve fit method. The former was heavily damped while the latter had two very closely placed modes, thus providing good cases to test the MDF curve fit method.

The other purpose of this work has been to predict the response of a coupled structure formed by two substructures coupled at two coordinates. The two substructures were, a beam and a U-shaped structure. The method adopted was the impedance coupling method outlined by Ewins [1] . The predictions were made utilizing the measured responses of the two substructures analysed separately. This was compared with the measured responses of the physically coupled structure.

The subject matter is presented in the following order. Chapter 2 deals with the theoretical basis of modal analysis. In Chapter 3, modal parameter extraction methods, namely SDF circle fit method and MDF curve fit method are described. Chapter 4 describes the impedance coupling method. Chapter 5 presents the instrumentation and the theory of signal analysis, essential for Modal testing. Results and discussion are given in Chapter 6.

Chapter - 2

Theory of Modal Analysis

2.1 Introduction

This chapter outlines the theoretical aspects of Modal analysis for multidegree of freedom (MDF) systems. The first section gives the basic equations of motion for a linear vibrating system, in time domain as well as frequency domain. The next section gives the response, Modal and spatial models for the undamped MDF system. The frequency response functions FRF's are also defined in this section. The models for the general case hysteretic damping is given next. The last section gives the different ways of displaying the FRF data.

2.2 Equations of Motion for MDF System

The matrix formulation of the equation of motion of a discrete linear structure with viscous damping is

$$[M]\{\ddot{x}(t)\} + [C]\{\dot{x}(t)\} + [K]\{x(t)\} = f(t) \tag{2.1}$$

where $[M]$, $[C]$, $[K]$ are the mass, viscous damping and stiffness matrices, $\{x(t)\}$ is a vector of displacements and $\{f(t)\}$ is the vector of the forcing functions.

If the forcing and displacements are assumed to be sinusoidal with frequency ω, then $\{x\} = \{x^*\} e^{i\omega t}$ and $\{f\} = \{f^*\} e^{i\omega t}$, and (2.1) reduces to

$$(-\omega^2 [M] + i\omega [C] + [K]) \{x^*\} = \{f^*\} , \qquad (2.2)$$

The equivalent equation for harmonic motion in the case of hysteretic damping is

$$(-\omega^2 [M] + i [H] + [K]) \{x^*\} = \{f^*\} \qquad (2.3)$$

The study of undamped case is discussed first because it is simpler than that of damped case and also aids in a better understanding.

2.3 Undamped MDF System

If in the above equations (2.2) and (2.3), $[C]$ and $[H]$ are zero then

$$(-\omega^2 [M] + [K]) \{x\} = \{f\} \qquad (2.4)$$

This is the general equation for an undamped MDF system. For systems under free vibration,

$$([K] - \omega^2 [M]) \{x\} = \{0\} \qquad (2.5)$$

The solution of this eigen value problem yields $\lceil \omega_r^2 \rfloor$ and $[\{\phi_r\}]$, where ω_r is the system's natural frequency and $\{\phi_r\}$ is its corresponding normalised mode shape vector.

The matrix $[\phi]$ possess the orthogonality property, which is expressed mathematically as

$$[\phi]^T \; [M] [\phi] = \lceil 1 \rfloor \tag{2.6}$$

$$[\phi]^T \; [K] [\phi] = \lceil \omega_r^2 \rfloor \tag{2.7}$$

The forced response of the undamped system is governed by

$$([K] - \omega^2 \; [M]) \{x\} = \{f\} \tag{2.8}$$

This may be written as

$$\{x\} = [\alpha(\omega)] \quad \{f\} \tag{2.9}$$

where,

$$[\alpha(\omega)] = ([K]) - \omega^2 \; [M])^{-1} \tag{2.10}$$

Any element α_{jk} of the above matrix represents the response of a point j on the structure to a unit sinusoidal force at point k i.e.

$$\alpha_{jk} = \frac{x_j}{f_k} \tag{2.11}$$

This α_{jk} is known as the transfer receptance for $j \neq k$ and is called the point receptance for $j = k$. Also $[\alpha(\omega)]$ is symmetric.

The relation between the system's response and the force may be alternately expressed with respect to the velocity (v) and acceleration $(\hat{a})$, as

$$\text{Mobility } Y_{jk}(\omega) = \frac{v_j}{f_k} = i\omega \; \alpha_{jk}(\omega) \tag{2.12}$$

$$\text{Accelerance } a_{jk}(\omega) = \frac{\hat{a}_j}{f_k} = -\omega^2 \alpha_{jk}(\omega) \tag{2.13}$$

The above terms receptance, mobility and accelerance are generally known as frequency response functions (FRF).

Rewriting (2.10) as,

$$([K] - \omega^2[M]) = [\alpha(\omega)]^{-1},$$

and premultiplying by $[\phi]^T$ and postmultiplying by $[\phi]$ on both sides, one gets

$$[\phi]^T ([K] - \omega^2 [M]) [\phi] = [\phi]^T [\alpha(\omega)]^{-1} [\phi]$$

using the orthogonality relations expressed in (2.7) and (2.8)

$$\lceil(\omega_r^2 - \omega^2)\rfloor = [\phi]^T [\alpha(\omega)]^{-1} [\phi]$$

or

$$[\alpha(\omega)] = [\phi] \lceil(\omega_r^2 - \omega^2)\rfloor^{-1} [\phi]^T \tag{2.14}$$

Thus the element α_{jk} of the receptance matrix $[\alpha(\omega)]$ is

$$\alpha_{jk}(\omega) = \sum_{r=1}^{N} \frac{({}_r\phi_j)\ ({}_r\phi_k)}{(\omega_r^2 - \omega^2)} \tag{2.15}$$

The above product $({}_r\phi_j \cdot {}_r\phi_k)$ is represented by ${}_rA_{jk}$ and is called the 'Modal Constant'. The equation (2.15) is then rewritten

$$\alpha_{jk}(\omega) = \sum_{r=1}^{N} \frac{{}_rA_{jk}}{\omega_r^2 - \omega^2} \tag{2.16}$$

The Modal constants ${}_rA_{jk}$, yield information about the Modal matrix $[\phi]$, which in turn leads to the $[M]$ and $[K]$ matrices by virtue of its orthogonality property given by (2.6) and (2.7).

2.4 Hysteretic Damping

For structural or hysteretic damping, the general MDF equation of motion with harmonic excitation is given by (2.3). In absence of external excitation, the free vibration equation is

$$(-\lambda^{*2}[M] + [K] + i[H])\ \{x^*\} = \{0\} \tag{2.17}$$

This complex eigen value problem yields the eigenvalue matrix $[\backslash \lambda_r^{*2} \backslash]$ and the eigenvector matrix $[\phi^*]$, where both the matrices are complex. λ_r^{*2} is the damped natural frequency given by

$$\lambda_r^{*2} = \omega_r^2\ (1 + i\ \eta_r) \tag{2.18}$$

where, ω_r is called the natural frequency and η_r is the damping loss factor for the r^{th} mode. This $[\phi^*]$ matrix also possess the orthogonality property with respect to $[M]$ and $[K+iH]$ matrices.

For forced response the receptance matrix is now given by

$$[\alpha^*(\omega)] = ([K] + i[H] - \omega^2 [M])^{-1} \quad (2.19)$$

Proceeding is the same way as in the undamped case, one can express an element of $[\alpha^*(\omega)]$ matrix by

$$\alpha^*_{jk}(\omega) = \sum_{r=1}^{N} \frac{{}_r\phi^*_j \cdot {}_r\phi^*_k}{\omega_r^2 - \omega^2 + i\eta_r\,\omega_r^2} \quad (2.20)$$

Writing $({}_r\phi^*_j \cdot {}_r\phi^*_k)$ as ${}_rA^*_{jk}$, the receptance is expressed as

$$\alpha^*_{jk}(\omega) = \sum_{r=1}^{N} \frac{{}_rA^*_{jk}}{\omega_r^2 - \omega^2 + i\eta_r\,\omega_r^2} \quad (2.21)$$

2.5 Display of FRF

FRF (i.e. receptance etc.) is a complex quantity and is frequency dependent. In order to effectively show the information of FRF, two types of plots are usually used .

(a) Bode Plot: It has two parts (i) magnitude of FRF vs. frequency, (ii) Phase of FRF vs. frequency.

A wide range of values of magnitude has to be shown. This is effectively done by using logarithmic scales for the modulus axis or sometimes for both the modulus axis and frequency axis. A peak in the magnitude plot indicates the existence of a mode. The frequency at which this peak occurs indicate the natural frequency of that mode.

(b) Nyquist Plot: It is a graph of real part vs. imaginary part of FRF. It does not contain the frequency information explicitly. The advantage of the nyquist plot is that it displays the important region of resonance effectively. This plot of the resonance region will be an arc of a circle or a complete circle, depending on the damping. This circle called as nyquist circle contains the information about all the modal parameters namely the modal constant, damping loss factor and the natural frequency. This inherent information about modal parameters existing in the nyquist circle is effectively used by SDF circle fit method to estimate the modal parameters. This method is described in Chapter 3.

Chapter - 3

Modal Parameter Extractions for a Structure

3.1 Introduction

This chapter first briefly explains the method of treating each mode as a single degree of freedom approximation and then extracting the modal parameter values using circle fit method. The next section discusses the multidegree of freedom curve fit method where all the modes of FRF are considered together to yield the modal parameters.

3.2 Single Degree of Freedom Analysis with Circle Fit Method

The basic assumption for the single degree of freedom (SDF) method is that, in the vicinity of the resonance, the response is dominated by that particular mode (nyquist plot will be an arc of a circle) and the contribution of other modes may be represented by a constant term. Therefore the equation for receptance for hysteretic damping, may be written as [1]

$$\alpha^*_{jk}(\omega) = \frac{{}_rA^*_{jk}}{\omega_r^2 - \omega^2 + i\,\eta_r\omega_r^2} + {}_rB^*_{jk} \qquad (3.1)$$

The parameters ${}_rA^*_{jk}$, ω_r, η_r and ${}_rB^*_{jk}$ of the r^{th} mode may be evaluated by following the sequence.

(1) Select about 10 to 15 points on either side of the resonance, taking care to see that the points selected encompass a good part of the arc of the nyquist circle.

(2) Fit a circle to these points. The algorithm given by Brandon and Cowley [6] is used for this. This algorithm is given in Appendix A. If the quality of fit is better for receptance, when compared to that of mobility, then the type of damping included in the analysis is the hysteretic damping. Conversely, if the mobility gives a better fit, the type of damping considered is viscous damping.

(3) A better estimate of natural frequency may be obtained from the point where the maximum sweep rate $(d\theta/d\omega^2)$ occurs (Fig. 3.1). Since the points are placed at equal increments, finite difference is used to pinpoint the natural frequency with the precision of 10% of the frequency increment.

(4) Damping estimates are obtained by using combinations of points below and above resonance frequency ω_r^2, and the average value of all these estimates is taken as the damping for that mode.

(5) The diameter, passing through ω_r^2, of the fitted circle and the orientation of this diameter with the

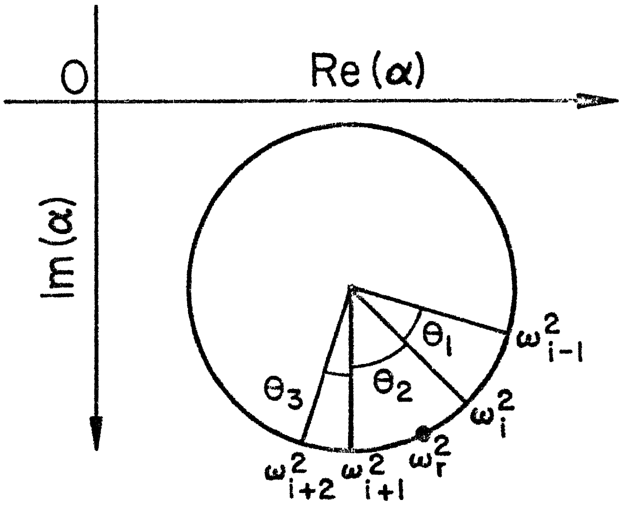

Fig. 3.1 Natural frequency location

imaginary axis, are used in the estimation of magnitude of ${}_{r}A^{*}_{jk}$ and its argument. The distance of the points, which is diametrically opposite to the natural frequency, from the origin and its orientation with respect to the imaginary axis, is used to calculate the term ${}_{r}B^{*}_{jk}$.

(6) The structures, considered in this work, are tested in free-free condition. Hence at low frequencies, the FRF exhibits mass like behaviour and at high frequencies, it exhibits a stiffness like behaviour. In order to account for these, the basic receptance equation may be modified by including these residuals as follows:

$$\alpha^{*}_{jk} = -\frac{1}{\omega^{2}\ {}_{R}M_{jk}} + \left(\Sigma \frac{{}_{r}A^{*}_{jk}}{\omega_r^2-\omega^2+i\,\eta_r\omega_r^2}\right) + \frac{1}{{}_{R}K_{jk}} \tag{3.2}$$

where ${}_{R}M_{jk}$ and ${}_{R}K_{jk}$ are the mass and stiffness residuals respectively.

The above various steps and their inherent mathematical details, has been given in a recent work [3].

In practice, one finds that the modes may be closely placed and may have very high damping. Under these conditions the effect of other mode/modes in the vicinity of a particular resonance is quite significant. The regeneration of FRF using SDF methods, may not be accurate enough. Hence

the single mode assumption of each resonance is not valid.

3.3 Multidegree Curve Fitting Method

As explained above, the SDF methods treat data around each resonant frequency separately. This method requires simple and small amount of computation. For closely placed modes or for some structures with high damping, not enough points can be identified as belonging solely to a particular mode. This may necessitate other methods like Multi Degree Freedom (MDF) curve fitting.

In MDF curve fitting methods, an FRF is considered as a single curve and the modal parameters are adjusted so as to achieve the best curve fit. This method, then obviously requires more computing power. One such method, based on the work by Gaukroger, Skingle and Heron [7], is briefly explained in the following.

3.3.1 Details of Analysis

With the hysteretic damping, the receptance as a function of frequency is

$$\alpha^*_{jk}(\omega) = -\frac{1}{\omega^2\, {}_R M_{jk}} + \left(\sum_{r=1}^{N} \frac{{}_r A^*_{jk}}{\omega_r^2 - \omega^2 + i\,\eta_r\, \omega_r^2} \right) + \frac{1}{{}_R K_{jk}} \qquad (3.3)$$

The parameters to be estimated in the above equation,

are the residuals ${}_{R}M_{jk}$, ${}_{R}K_{jk}$ and the modal parameters of the r^{th} mode - ${}_{r}A^{*}_{jk}$ (both real and imaginary parts), ω_r and η_r, where $r = 1...N$; N = number of modes in the FRF. Hence the total number of parameters to be obtained are (4N+2).

If α^{*}_{m} is the mathematical receptance and α^{*}_{e} is the measured receptance, then the least square error e is given by

$$e = \sum_{\substack{\text{over the frequency}\\ \text{range of interest}}} (\alpha^{*}_{e} - \alpha^{*}_{m})(\bar{\alpha}^{*}_{e} - \bar{\alpha}^{*}_{m}) \tag{3.4}$$

where $\bar{\alpha}^{*}_{e}$ and $\bar{\alpha}^{*}_{m}$, are the conjugates of α^{*}_{e} and α^{*}_{m}, respectively. This error e given by (3.4), is to be now minimised with respect to each of the parameters k_i, where $i = 1,....,(4N+2)$.

This essentially reduces to the expression given below (See Appendix B).

$$[P]\{\delta k\} + \{R\} = 0 \tag{3.5}$$

where the elements of matrix $[P]$, P_{ij} is given by

$$P_{ij} = \frac{\partial^2 e}{\partial k_i . \partial k_j} = \sum_{\substack{\text{over the frequency}\\ \text{range of interest}}} \left(\frac{\partial \alpha^{*}_{m}}{\partial k_j} . \frac{\partial \bar{\alpha}^{*}_{m}}{\partial k_i} + \frac{\partial \bar{\alpha}^{*}_{m}}{\partial k_j} . \frac{\partial \alpha^{*}_{m}}{\partial k_i}\right) \tag{3.6}$$

The elements of the vector {R}, R_i is given by

$$R_i = \frac{\partial e}{\partial k_i} = - \sum_{\substack{\text{over the frequency} \\ \text{range of interest}}} (\alpha_e^* - \alpha_m^*)$$

$$\frac{\partial \bar{\alpha}_m^*}{\partial k_i} + (\bar{\alpha}_e^* - \bar{\alpha}_m^*) \frac{\partial \alpha_m^*}{\partial k_i} \qquad (3.7)$$

Vector { δk} is the unknown, which is added to the initial approximation k_1', k_1' ..... $k'_{(4N+2)}$, of the parameters, to obtain new estimates.

As a first step, the matrix [P] and the vector {R} are formed using the initial approximations k_1', k_2',.... k'_{4n+2}. A good initial approximation may be taken as the modal parameter values obtained from SDF. The equation (3.5) is then solved to obtain δk_1, δk_2,...δk_{4N+2}. New values $(k_1'+\delta k_1)$, $(k_2 + \delta k_2)$..... are then used in (3.6) and (3.7) and this process is repeated until an acceptably accurate solution is obtained.

The elements of the vector {R}, R_i is given by

$$R_i = \frac{\partial e}{\partial k_i} = - \sum_{\substack{\text{over the frequency}\\ \text{range of interest}}} (\alpha_e^* - \alpha_m^*)$$

$$\frac{\partial \bar{\alpha}_m^*}{\partial k_i} + (\bar{\alpha}_e^* - \bar{\alpha}_m^*) \frac{\partial \alpha_m^*}{\partial k_i} \qquad (3.7)$$

Vector $\{\delta k\}$ is the unknown, which is added to the initial approximation k_1', k_1' ..... $k'_{(4N+2)}$, of the parameters, to obtain new estimates.

As a first step, the matrix [P] and the vector {R} are formed using the initial approximations k_1', k_2',.... k'_{4n+2}. A good initial approximation may be taken as the modal parameter values obtained from SDF. The equation (3.5) is then solved to obtain δk_1, δk_2,...δk_{4N+2}. New values $(k_1' + \delta k_1)$, $(k_2 + \delta k_2)$..... are then used in (3.6) and (3.7) and this process is repeated until an acceptably accurate solution is obtained.

Chapter 4

Coupled Structures

4.1 Introduction

This chapter explains briefly the procedure of predicting the response characteristics of a coupled structure, knowing the response characteristics of the substructures. The method used in this work is called the Impedance Coupling Method [1] . First this method is outlined for the coupling of two substructures at a single coordinate . Further on, the procedure for coupling at more than one co-ordinate is given. This section also examines, how one can include in the analysis, coordinates which are not involved in coupling.

4.2 Impedance Coupling Method

This method is also called as stiffness method [1] . The underlying principle is given below.

Consider two components A and B (Fig. 4.1) which are coupled at a single co-ordinate to form the coupled structure C. The coupling coordinate is designated by numeric 1 and the coincident coupling points on substructures A and B are denoted by ^1a and ^1b, respectively. The coupling coordinate on the coupled structure is denoted by ^1c.

If the system A at the connection co-ordinate ^1a is excited harmonically by $f^*_{1_a}\, e^{i\omega t}$, the resulting response $x^*_{1_a}$ $e^{i\omega t}$ is given by

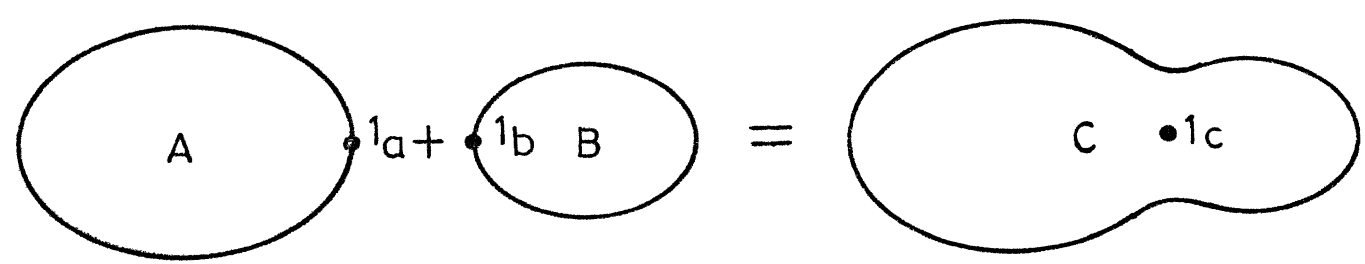

Coupling of Two Substructures at a Single Co-ordinate

FIG. 4·1

$$x^*_{1_a} \; e^{i\omega t} = \alpha^*_{1_a 1_a}(\omega) \; f^*_{1_a} \; e^{i\omega t} \tag{4.1}$$

or

$$x^*_{1_a} = \alpha^*_{1_a 1_a}(\omega) \; f^*_{1_a} \tag{4.2}$$

Similarly for subsystem B,

$$x^*_{1_b} = \alpha^*_{1_b 1_b}(\omega) \; f^*_{1_b} \tag{4.3}$$

Applying the compatability and equilibrium conditions at the connection co-ordinates one gets

$$x^*_{1_c} = x^*_{1_a} = x^*_{1_b} \tag{4.4}$$

$$f^*_{1_c} = f^*_{1_a} + f^*_{1_b} \tag{4.5}$$

Substitution of (4.2) and (4.3) in (4.4) and using the result in (4.5), the relationship between the receptances is

$$\frac{1}{\alpha^*_{1_c 1_c}} = \frac{1}{\alpha^*_{1_a 1_a}} + \frac{1}{\alpha^*_{1_b 1_b}} \tag{4.6}$$

or,

$$Z^*_{1_c 1_c} = Z^*_{1_a 1_a} + Z^*_{1_b 1_b} \tag{4.7}$$

where, Z denotes the impedance.

Thus the FRF of the coupled structure C can be obtained in terms of the FRF properties of the substructures analysed separately.

The above analysis can be extended to the systems connected at more than one co-ordinate. The co-ordinates which are not involved in coupling may also be included. The whole process involves the partition of the subsystem impedance matrices into submatrices which are involved in coupling and those which are not and then adding together only those submatrices which are involved in coupling.

Therefore, if $[\alpha^*_A(\omega)]$ and $[Z^*_A(\omega)]$ are the receptance and impedance matrices, respectively, of subsystem A and $[\alpha^*_B(\omega)]$ and $[Z^*_B(\omega)]$ are the corresponding matrices of subsystem B, and if the coupling coordinates are collectively designed by q, the coordinates not involved in coupling by p for subsystem A, then the receptance matrix is partitioned as

$$[\alpha^*_A(\omega)] = \begin{bmatrix} \alpha^*_{p_a p_a} & \alpha^*_{p_a q_a} \\ \alpha^*_{q_a p_a} & \alpha^*_{q_a q_a} \end{bmatrix} \tag{4.8}$$

$$[Z_A^*(\omega)] = [\alpha_A^*(\omega)]^{-1} = \begin{bmatrix} Z^*_{p_a p_a} & Z^*_{p_a q_a} \\ Z^*_{q_a p_a} & Z^*_{q_a q_a} \end{bmatrix} \tag{4.9}$$

Similarly the impedance matrix for the subsystem B, is given by

$$[Z_B^*(\omega)] = [\alpha_B^*(\omega)]^{-1} = \begin{bmatrix} Z^*_{r_b r_b} & Z^*_{r_b q_b} \\ Z^*_{q_b r_b} & Z^*_{q_b q_b} \end{bmatrix} \tag{4.10}$$

where, r denotes the coordinates on subsystem B which are not involved in coupling.

As before, applying the compatibility and equilibrium condition, the impedance matrix $[Z_C^*(\omega)]$ for the coupled structure can be obtained in the form,

$$[Z_C^*(\omega)] = [Z_A^*(\omega)] + [Z_B^*(\omega)]$$

$$= \begin{bmatrix} Z^*_{p_a p_a} & 0 & Z^*_{p_a q_a} \\ 0 & Z^*_{r_b r_b} & Z^*_{r_b q_b} \\ Z^*_{q_a p_a} & Z^*_{q_b r_b} & Z^*_{q_a q_a} + Z^*_{q_b q_b} \end{bmatrix} \tag{4.11}$$

The receptance matrix $[\alpha_c^*(\omega)]$ for the combined system is obtained by the inverse of $[Z_c^*(\omega)]$ as

$$[\alpha_c^*(\omega)] = [Z_c^*(\omega)]^{-1} \qquad (4.12)$$

From modal testing point of view, the impedances required for the substructures may be evaluated by any one of the options mentioned below.

(i) Using the modal Model and evaluating the receptance matrix using the formula

$$[\alpha^*(\omega)] = [\phi^*] \left[\diagdown (\lambda_r^{*2} - \omega^2) \diagdown \right]^{-1} [\phi^*]^T \qquad (4.13)$$

where

$$\lambda_r^{*2} = \omega_r^2 (1 + i\eta_r)$$

(ii) Calculating the inverse of the receptance FRF matrix obtained by direct measurement.

(iii) Calculating the inverse of the regenerated receptance FRF matrix.

The results presented in section 6 are by using the last method of utilizing the regenerated FRFs.

Chapter - 5

Instrumentation and Signal Analysis

5.1 Introduction

Experimental modal analysis involves exciting a system, measuring the excitation and response time signals and then operating on these time signals to determine the system transfer function. The instrumentation used in this work is shown by the block diagram in Fig. 5.1. The impact hammer, the accelerometer and the preconditioning amplifier are first described briefly in the followings. The signal analysis is later described in section 5.2.

Excitation by Impact hammer is one of the commonly used excitation technique . The impact excitation does not not require elaborate fixture and it is ideal for use in restricted spaces where an exciter would not fit. Structures of masses in the range of approximately 2 kg to 1000 kg can be excited by impact-hammer. The equipment consists of an impactor with different types of tips and heads, which serve to extend frequency and force level ranges of excitation. Just below the tip of the impactor is a force transducer, which detects the magnitude of the force felt by the impactor.

Accelerometers are piezoelectric transducers used to measure the response (acceleration) of a system. The piezoelectric crystal attached to a seismic mass, senses the inertial force of the seismic mass. This force generates an electric charge across the end faces of the crystal, which is proportional to the acceleration felt by the accelerometer. Accelerometers are preferred over other types of pickups, namely the velocity and displacement pickups, because accelerometers are much smaller in size and can cover a wider frequency range.

Amplifiers are used to boost the very small electrical charge that is generated by the piezoelectric transducers into a signal strong enough to be measured by the analyser. There are two types of amplifiers namely charge amplifier and voltage amplifiers. Charge amplifiers are preferred over voltage amplifier, mainly due to the reason that the sensitivity and gain are not affected by the length and properties of the connecting cable in case of charge amplifiers, but is adversely affected in case of voltage amplifiers.

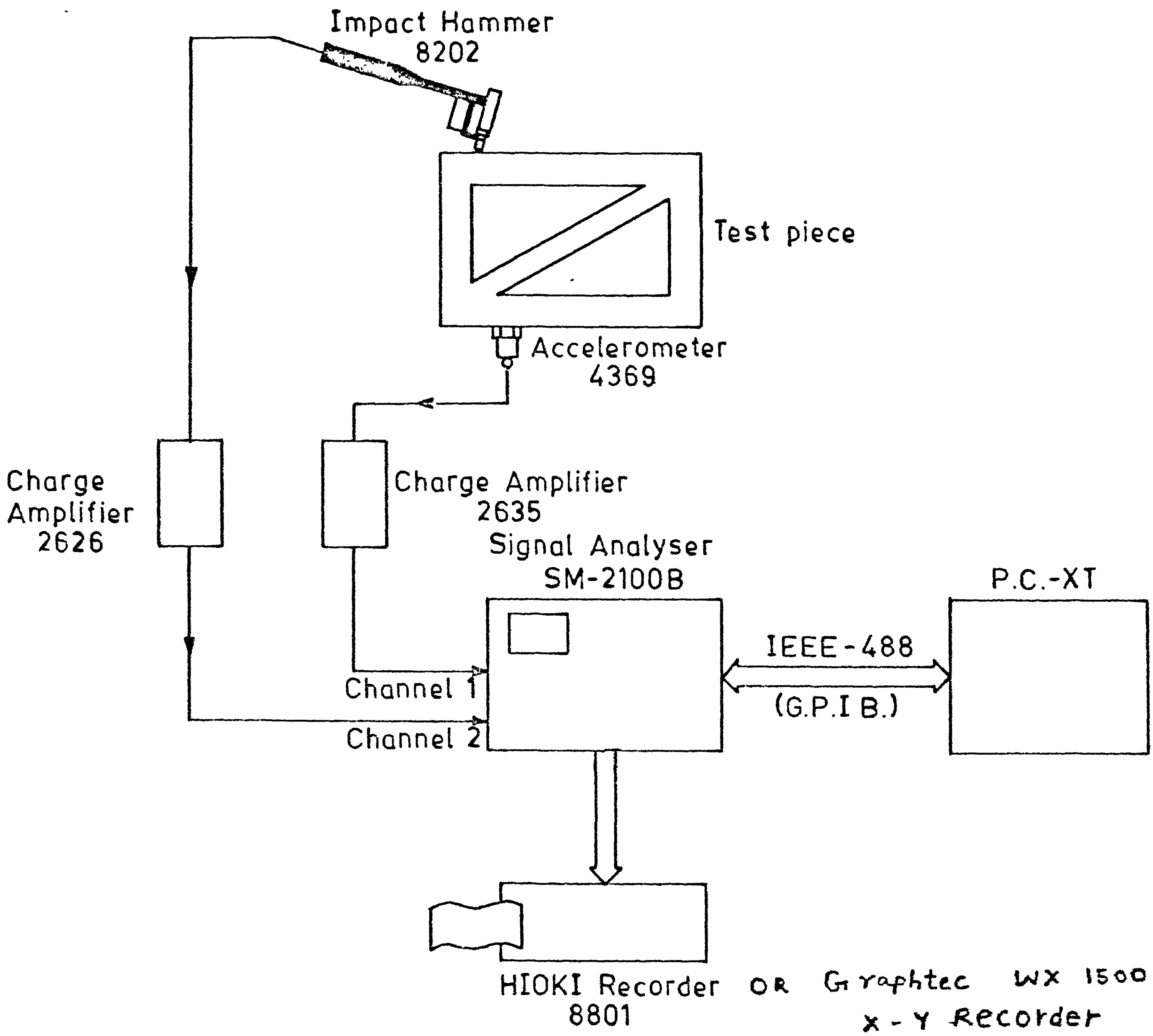

Block Diagram of Experimental Setup.

Fig. 5.1

The spectrum analyser receives the two time signals namely, the excitation and response signals. The analyser operates on these time signals, to determine the system transfer functions or frequency response function. The specifications of the instruments used are indicated in Fig. 5.1.

5.2 Signal Analysis

5.2.1 Fourier Transforms

The first step in modal testing is to relate the input (excitation f(t)) and the output (response x(t)) of the system in the frequency domain. This is done by performing dual channel FFT analysis on a spectrum analyser.

If f(t) and x(t) are the input and output of a system in time domain, then the function relating these two in time domain is called the Impulse Response Function h(t). This relationship is given by

$$x(t) = \int_{-\infty}^{+\infty} h(\tau)\, f(t-\tau)\, d\tau \qquad (5.1)$$

In frequency domain this relation is

$$X^*(\omega) = H^*(\omega) \,.\, F^*(\omega) \qquad (5.2)$$

The steps involved in arriving at (5.2) from (5.1) are given in Appendix C .

In (5.2), $X^*(\omega)$ and $F^*(\omega)$ are the fourier transforms of $x(t)$ and $f(t)$ respectively and $H^*(\omega)$ is the frequency response function of the system.

If $x(t)$ and $f(t)$ satisfy the Dirichlets' condition, then

$$X^*(\omega) = \frac{1}{2\pi} \int_{-\infty}^{+\infty} x(t)\, e^{-i\omega t}\, dt \qquad (5.3)$$

and

$$F^*(\omega) = \frac{1}{2\pi} \int_{-\infty}^{+\infty} f(t)\, e^{-i\omega t}\, dt \qquad (5.4)$$

5.2.2 <u>Autospectra, Cross Spectra, Transfer Function and Coherence</u>

5.2.2.1 <u>Auto Spectra</u>

Auto spectra of $x(t)$ and $f(t)$ are defined as

$$\left.\begin{aligned} S_{xx}(\omega) &= X^*(\omega) \,.\, \tilde{X}^*(\omega) \\ S_{ff}(\omega) &= F^*(\omega) \,.\, \tilde{F}^*(\omega) \end{aligned}\right\} \qquad (5.5)$$

where $\underset{\sim}{x}^{*}(\omega)$ and $\underset{\sim}{F}^{*}(\omega)$ are the complex conjugates of $X^{*}(\omega)$ and $F^{*}(\omega)$ respectively. The autospectrum is a real quantity and it indicates the distribution of power in a signal as a function of frequency.

5.2.2.2 Cross-Spectrum

It is the basic function which correlates the input and output signals. The cross-spectrum between the two signals x(t) and f(t) is given by

$$\begin{aligned} S^{*}_{fx}(\omega) &= \underset{\sim}{F}^{*}(\omega) \; . \; X^{*}(\omega) \\ S^{*}_{xf}(\omega) &= F^{*}(\omega) \; . \; \underset{\sim}{X}^{*}(\omega) \\ S^{*}_{xf} &= \underset{\sim}{S}^{*}_{fx} \end{aligned} \tag{5.6}$$

5.2.2.3 Transfer Function

This function relates the input and output of the system. Thus from (5.2), the transfer function as a function of frequency is

$$H^{*}(\omega) = \frac{X^{*}(\omega)}{F^{*}(\omega)} \tag{5.7}$$

Alternately, the transfer function is defined in terms of the autospectrum and the cross spectrum as,

$$H^{*}(\omega) = S^{*}_{fx}(\omega) \,/\, S_{ff}(\omega) \tag{5.8}$$

or

$$H^*(\omega) = S_{xx}(\omega) \,/\, S^*_{xf}(\omega) \tag{5.9}$$

The division in (5.8) is by a real quantity which is more convenient on the spectrum analyser.

5.2.2.4 Coherence

For exact measurements, (5.8) and (5.9) should yield identical results. Based on this a coherence function $\gamma^2(\omega)$ is determined as

$$\gamma^2(\omega) = \frac{|S^*_{fx}(\omega)|^2}{S_{ff}(\omega)\; S_{xx}(\omega)} \tag{5.10}$$

The coherence is ideally equal to one for linear, deterministic, noise free system and is between zero and one otherwise. Thus, the coherence forms a good measure of faithfulness of the experimental data. Later in Chapter 6, the coherence is utilized to justify the measurement of accelerance rather than receptance.

5.2.3 Discrete Fourier Transform DFT

With the advent of digital computers, the focus is entirely on discretization of analog signals. In evaluating DFT, both the time and frequency domain data are in discrete form.

The time signal $x(t)$ recorded for a sample length T, is discretised to obtain N discrete evenly spaced values. The sampling rate, ω_s is given by

$$\omega_s = 2\pi N/T \tag{5.11}$$

DFT, $X^*(\omega)$, of this time signal, may also have N discrete values. If so, then the frequency range is zero to ω_s, with a frequency resolution of $\Delta\omega$, where $\Delta\omega = \omega_s/N$. The forward transform will have the form

$$X^*(k) = \frac{1}{N} \sum_{n=0}^{N-1} x(n)\, e^{-i\frac{2\pi kn}{N}}, \quad k = 0,1,\ldots N-1 \tag{5.12}$$

and the inverse transform takes the form

$$x(n) = \sum_{k=0}^{N-1} X^*(k)\, e^{i\frac{2\pi kn}{N}}, \quad n = 0,1\ldots N-1 \tag{5.13}$$

Equation (5.12) is expressed as,

$$\{X^*\} = \frac{1}{N} [A^*]\{x\} \tag{5.14}$$

where $\{X^*\}$ is a vector representing the N complex frequency components, $[A^*]$ is a square matrix of unit vectors (order NxN) and $\{x\}$ is a vector representing the N, discrete time signal values.

Equation (5.12) indicates that obtaining N frequency components from N time samples requires N^2 complex multiplications. Using fast Fourier transform (FFT) algorithm given by Cooley and Tukey [14], the same result can be obtained with a greatly reduced number of complex multiplications (of the order of $N \, Log_2^N$).

5.2.4 Aliasing

This problem is associated with digital spectral analysis. If the sampling rate, ω_s, is too slow, then the high frequencies in the original time signal may be misinterpreted as low frequencies. This form of error is known as aliasing. This problem of aliasing is illustrated in Fig. 5.2. Figure 5.2(a) shows the case in which the sampling rate ω_s is higher than the frequency of the sinusoid. Hence on performing DFT, the actual frequency is correctly recognised. For the case shown in Fig. 5.2(b), the sampling rate, ω_s, is lower than the frequency of the sinusoid. As can be seen from the same figure, the sampling points are now situated in such a way that on performing DFT, a lower frequency is recognised instead of the actual frequency.

The relationship between the sampling rate and the frequency content of the time signal is expressed in Shannon's sampling theorem [14], which states that a sampled (discretised) time signal must not contain components of frequencies above half the sampling rate (called the nyquist frequency). The maximum frequency contents of the time signal,

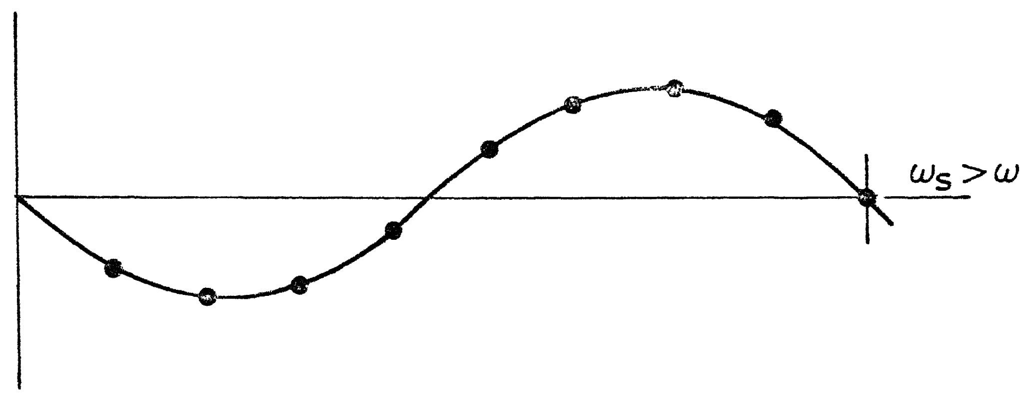

FIG. 5·2 (a)

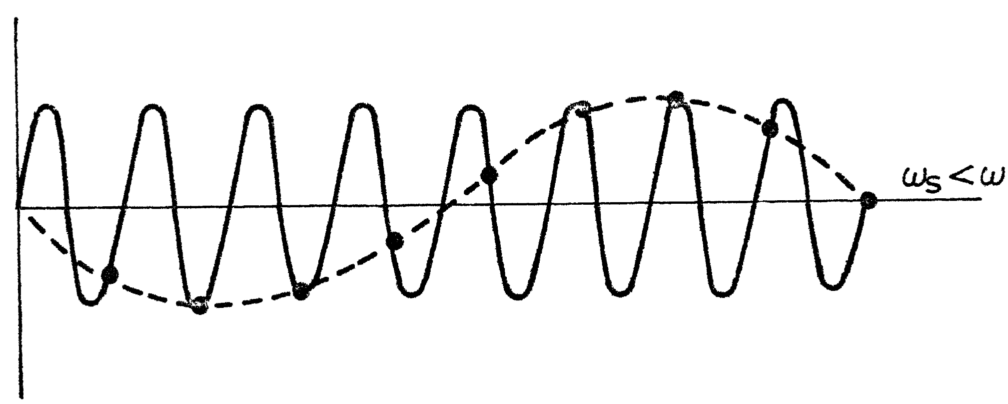

Phenomenon of Aliasing

FIG. 5·2 (b)

ω_{max} is,

$$\omega_{max} = \omega_s/2 . \tag{5.15}$$

and the resolution of the frequency spectrum, $\Delta\omega$ is

$$\Delta\omega = \omega_s/N \tag{5.16}$$

It should be noted here, that with this restriction of ω_{max}, the number of discrete frequency points is N/2. Equations (5.12), (5.13), then get modified as

$$X^*(k) = \frac{1}{N} \sum_{n=0}^{N-1} x(n)\, e^{-i\frac{2\pi kn}{N}} , \quad k = 0,1\ldots(\tfrac{N}{2} - 1)$$

$$X^*(n) = \sum_{k=0}^{N/2 - 1} x(t)\, e^{i\frac{2\pi kn}{N}} , \quad x = 0,1\ldots(N-1) \tag{5.17}$$

In the frequency domain, the error caused due to alising is depicted in Fig. 5.3(a). If the time signal does have contents of high frequency then the signal is passed through an anti-alising filter to cut off the higher frequency signals. This cutoff frequency is decided by the frequency of sampling rate, ω_s. One such filter and the filtered signal spectrum is shown in Fig. 5.3(b).

5.2.5 Leakage

The time signal is recorded for a finite length of time history and the signal is assumed to be periodic in this time length. If this signal is not fully periodic,

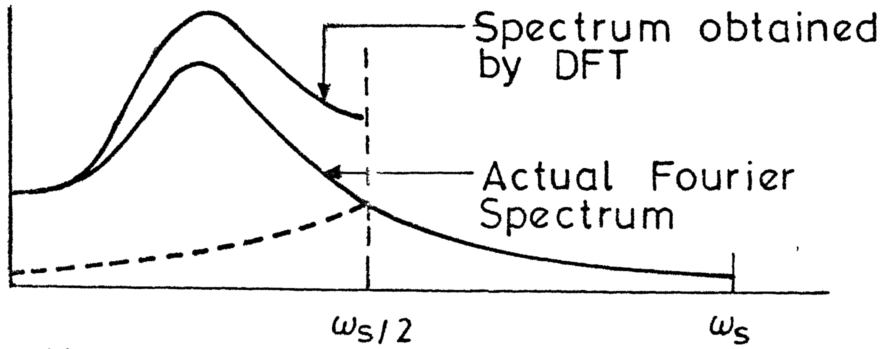

Alias Distortion of Spectrum by DFT
FIG.5·3(a)

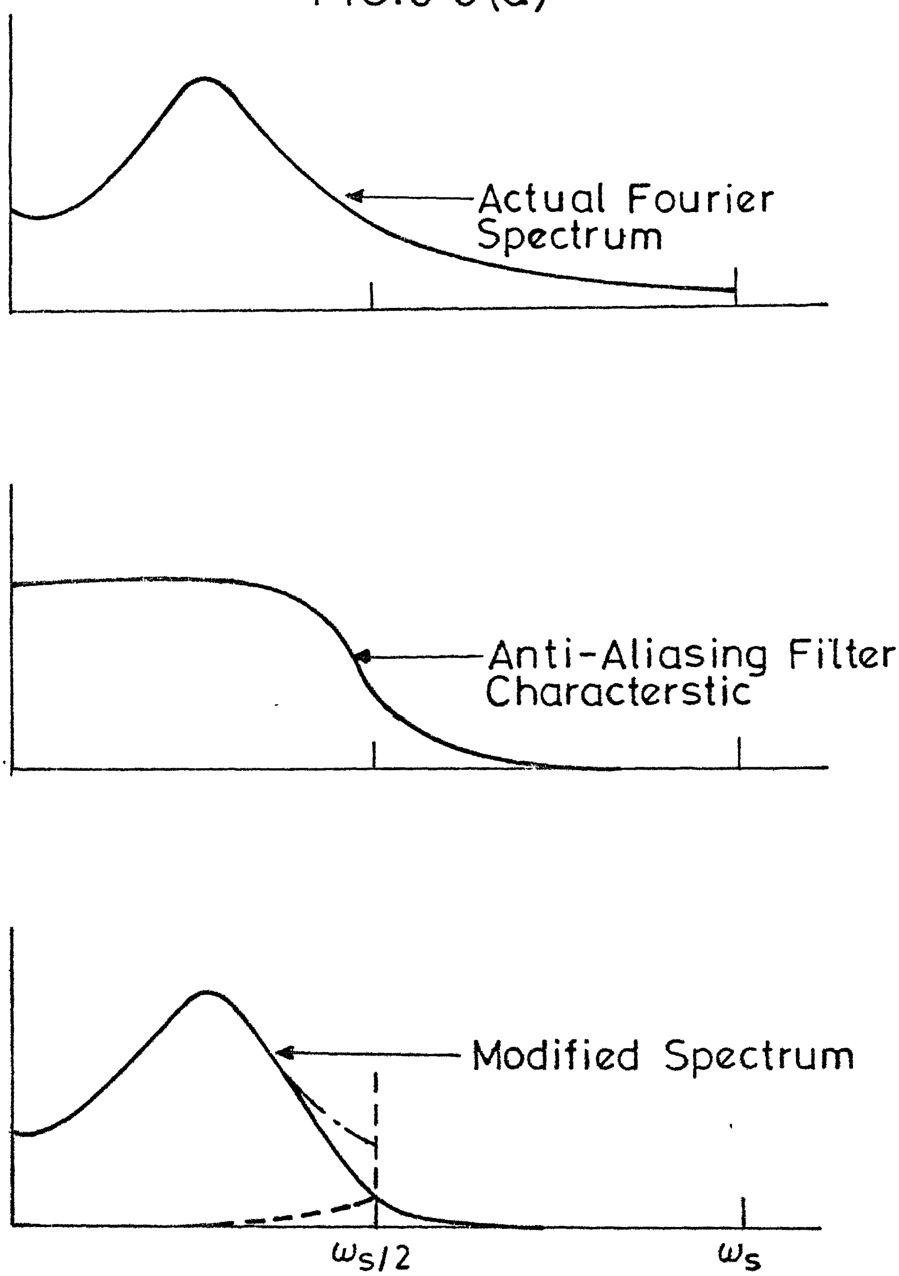

Anti-Aliasing Filter Proccess
FIG. 5·3(b)

then the problem of leakage appears. This can best be illustrated by the following example. Two samples of the same signal are recorded at slightly different record lengths. The signal shown in Fig. 5.4(a) is fully periodic and hence the DFT indicates the single frequency shown in the same figure. The signal shown in Fig. 5.4(b) is not fully periodic and the DFT does not show a single frequency as in Fig. 5.4(a). This indicates that the energy has leaked into a number of the spectral lines close to the true frequency. When the signal frequencies are low, this leakage problem can be greatly disturbing. The problem of leakage can be solved by proper 'windowing', described in the next subsection.

5.2.6 Windowing

Windowing involves the weighting or imposition of a prescribed profile on the time signal x(t) prior to performing the Fourier transform. The weighting is denoted by W(t). The analysed signal $x'(t)$ is given as

$$x'(t) = x(t) \cdot W(t) \qquad (5.17)$$

Some common types of windows used are shown in Fig. 5.5. The Iwatsu spectrum analyser offers rectangular and Hanning windows and there are described briefly in the following.

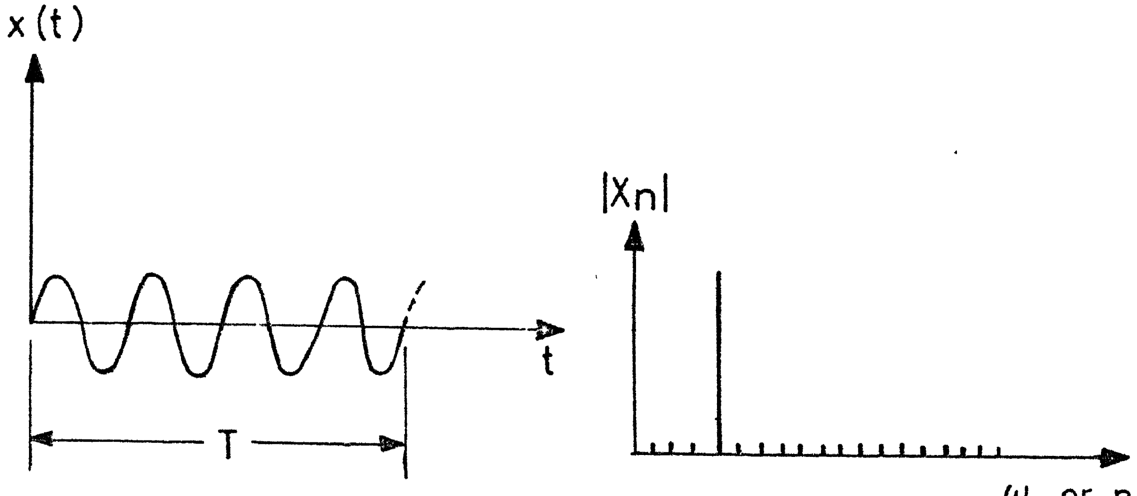

FIG. 5·4 (a)

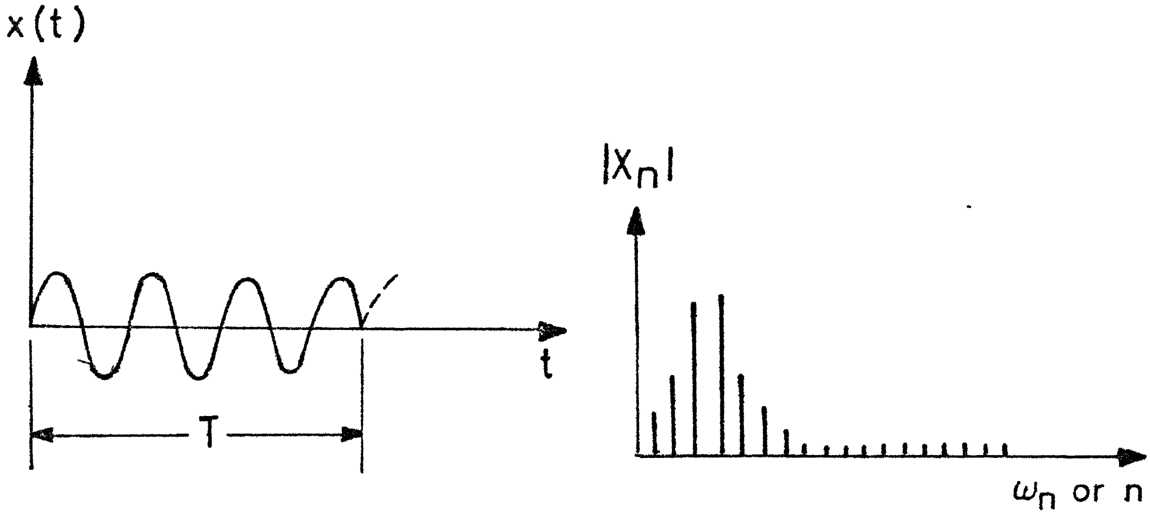

Leakage of Spectrum

FIG. 5·4 (b)

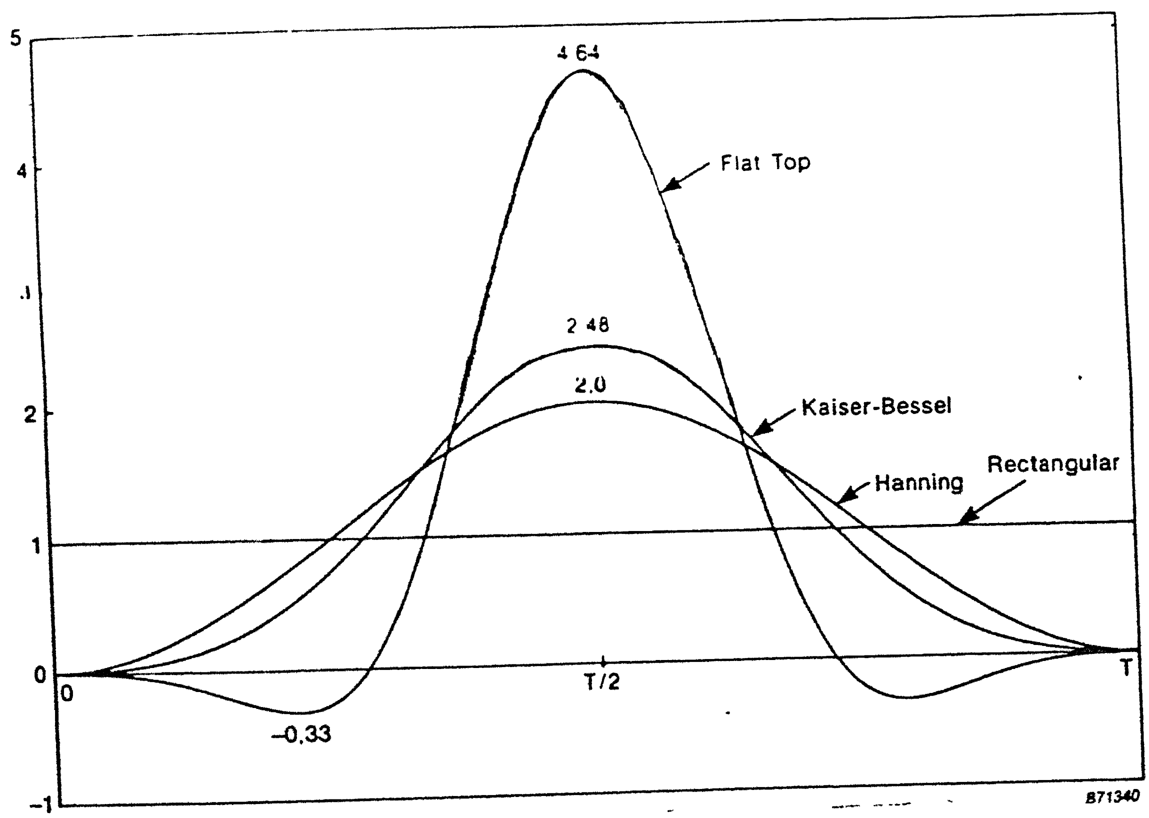

Fig. 5.5 : Some Common Types of Windows

(i) Rectangular Window

The rectangular windowing or weighting, also called flat or Boxcar weighting, in actually no weighting, at all on the finite time record (T). It is defined as

$$W(t) = 1 \quad \text{for } 0 \leq t \leq T$$
$$W(t) = 0 \quad \text{elsewhere.} \tag{5.18}$$

The practical use of the rectangular window is for analysing transients with shorter durations then the record length T. Rectangular windows are easily the first choice for all types of signals.

(ii) Hanning Window

Hanning window is a sum of rectangular window and period of a cosine of equal amplitude. Hanning weighting is defined as

$$W(t) = 1 - \cos 2\pi t/T \qquad \text{for } 0 \leq t \leq T$$
$$W(t) = 0 \quad \text{otherwise.} \tag{5.19}$$

Hanning windows are typically used for continuous signals such as produced by steady periodic or random vibration. It reduces effectively the problems of leakage. This is illustrated by using the hanning windowing for the example given in Fig. 5.4. The improvement gained by using hanning windowing is evident in Fig. 5.6.

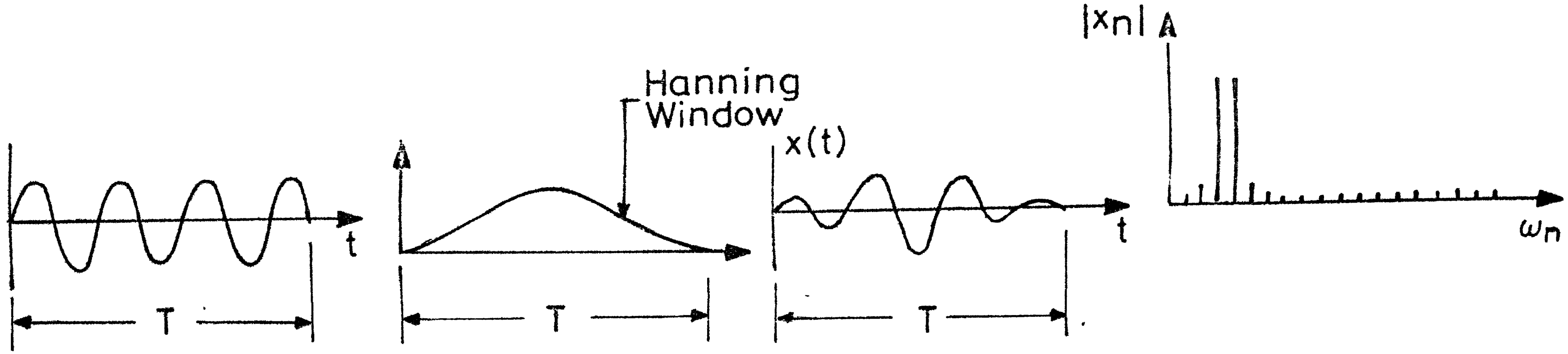

Effect of Hanning Window on DFT

FIG. 5·6

5.2.7 Averaging Modes

Averaging of a number of samples of time signal are done usually for processing random signals. When analysing random vibration, it is the estimates of the spectral densities and correlation functions, which actually characterise the type of signal. Three modes of averaging are usually provided in the spectrum analyser.

(a) Sum Mode: This operation is executed by assuming the weight of each signal as 1/N. The noise of the averaging signal is decreased with the increase of the number of samples averaged.

(b) Exponential Mode: This operation is executed by an exponential weighting of the samples of time signals. In other words, the starting samples are given more weighting than the latter samples.

(c) Peak Mode: This operation compares the size of each sample of time signal to select the sample with maximum value.

5.2.8 Iwatsu Spectrum Analyser and the Options Selected

The front panel of Iwatsu Spectrum Analyser offers a large class of analysing functions by operating function selection keys. The function used in this work was coherence function. The use of this function automatically also calculates autopower, crosspower and the transfer functions, which are registered in separate blocks by the inbuilt functions. These autopower functions could also have been

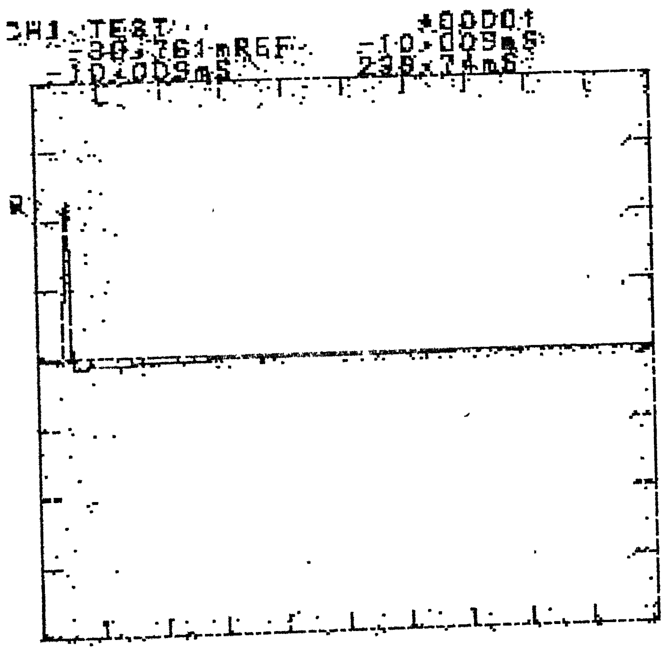

5.7(a) : Time history of impulse excitation signal

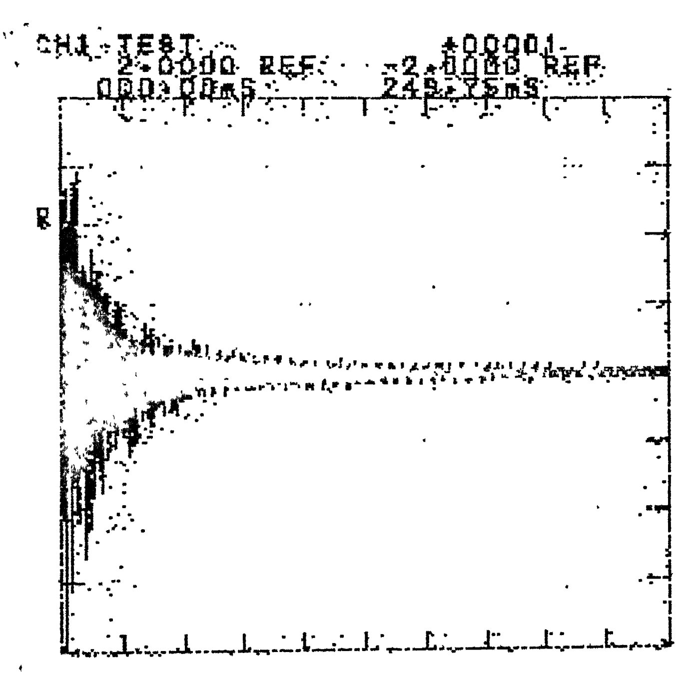

Fig. 5.7b : Time history of response signal (2K)

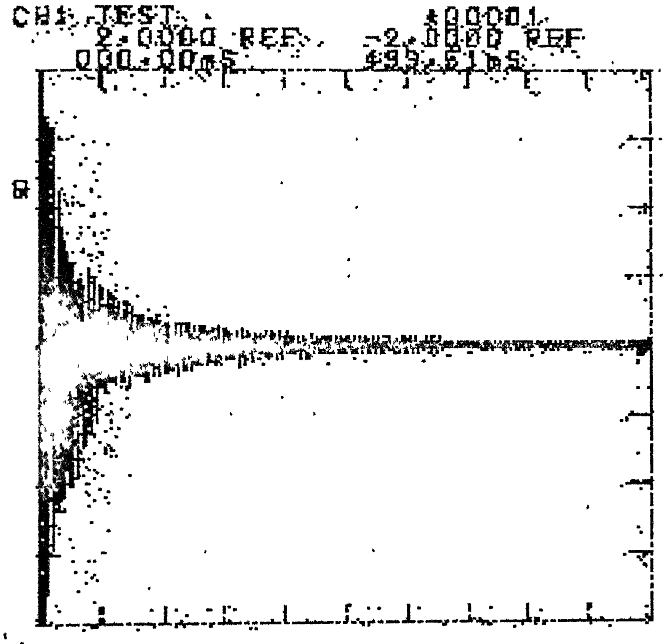

Fig. 5.7b : Time history of response signal (4K)

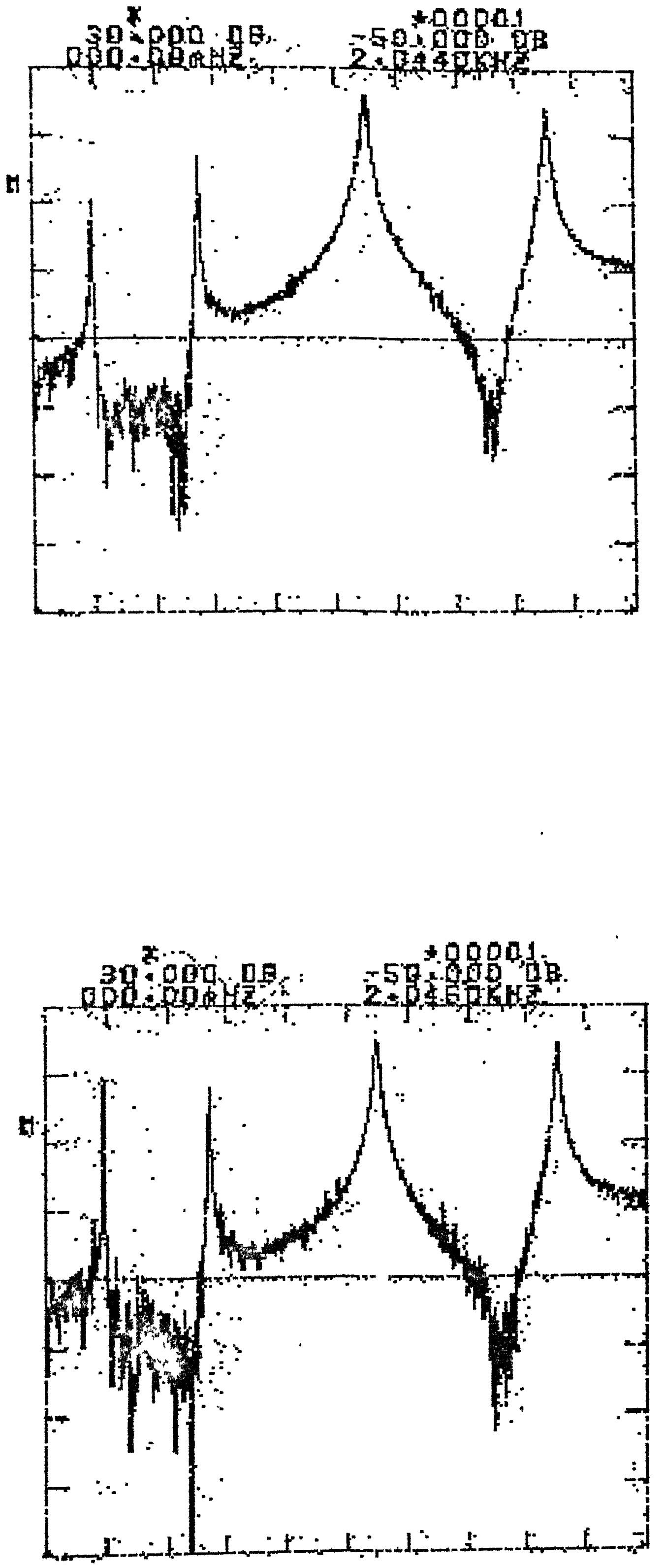

Fig.5.8 : FRF obtained from response signals of different record lengths

calculated separately by individual processing keys.

The time signal is recorded by selecting the data length (i.e., N) and the upper limit of analysing frequency. The latter choice automatically fixes the pass band frequency of the antialiasing filter. The sampling rate, ω_s, is decided by (5.16).

As explained in Section 5.2.6, a proper choice of window function is needed. This is to be guided by the type of signal to be recorded. The impact hammer produces an impulse signal of very short duration, the signal being produced at the beginning instants, as shown in Fig. 5.7(a). This calls for an rectangular window as discussed in Section 5.2.6. The two channels of the analyzer are guided by the same window. A typical response signal with data length as 2K and upper frequency range as 2 KHz is shown in Fig.5.7(b) and it is clear that with the record time of 250 msec, the signal has not decayed completely. In order to have faith in in the results, the response signal was also recorded over 500 msec with data length as 4K, and upper free range as 2 KHz. The resulting FRF's using these two signals are compared in Fig. 5.8 and it is evident that the record time of 250 msec is sufficient to yield the correct information.

The extraction of modal parameters from the recorded data needs post processing of the FRF's. For this post processing the FRF data registered in spectrum analyser is

transferred to the IBM PC/XT via GPIB (IEEE - 488) bus. The results are later transferred back to signal analyzer for the display and recording purposes. The data transfer commands are executed from the PC/XT.

Chapter - 6

Results and Discussion

6.1 Introduction

A previous work [1] reported results using Modal analvsis through a SDF method, namely the circle fit method. This chapter first discusses results for a hanging plate held with hand to illustrate the inadequacy of the circle fit method when damping is high, eventhough the modes are well separated. An MDF curve fit method is used to modify the modal parameter values and the MDF method is found to generate more accurate results. The next section discusses the problem of a structure with last two of the five modes being closely spaced and the MDF method is again shown to yield better results for the modal parameters.

The last section presents the results for a coupled structure. Here the two substructures are separately analyzed for modal parameters and the FRF's for receptance of the coupled structure is generated using the values of modal parameters of the substructures. This is checked against the experimentally obtained FRF for the same coupled structure.

The FRF's displayed in the chapter are for accelerances but the modal parameter extraction are done from the receptances. The accelerance is measured instead of the required receptances. Receptances are calculated by (2.13). This additional computation required is due to the fact that the double integration process in charge amplifier results in the usage of high gain in amplifier which introduce noise. This can be clearly seen by observing coherence for both acceleration and receptance measurement [3].

6.2 Improvement by MDF Curve Fit Method over SDF Circle Fit Method

A case where the SDF fit method gives inaccurate estimates of the Modal parameters has been studied. The structure was a plate which was held lightly by hand to induce high damping. Upto a frequency range of 500 Hz, this structure exhibited two modes, of which the first is highly damped. A regenerated FRF obtained by SDF circle fit method superimposed on the measured FRF is shown in Fig. 6.1, where the experimental curve is shown by the jagged natured plot. From this figure it is evident that the SDF circle fit method has given a bad fit for the first mode. With MDF curve fit method, described in Chapter 3, the regenerated FRF has been improved. This structure was used mainly to illustrate the improvement of modal parameters, mainly the damping ratios. So the residual terms are neglected and thus eight parameters need to be considered in (3.5). The initial estimates required for MDF curve fit method has been taken from the parameter values provided by SDF circle fit method.

The number of iterations and error after each iteration is given in Table 6.1. For this case, the results converge after only three iterations. The initial estimate of parameters taken from SDF circle fit method along with their refined values from MDF curve fit method after 5 iterations are shown in Table 6.2 The regenerated FRF

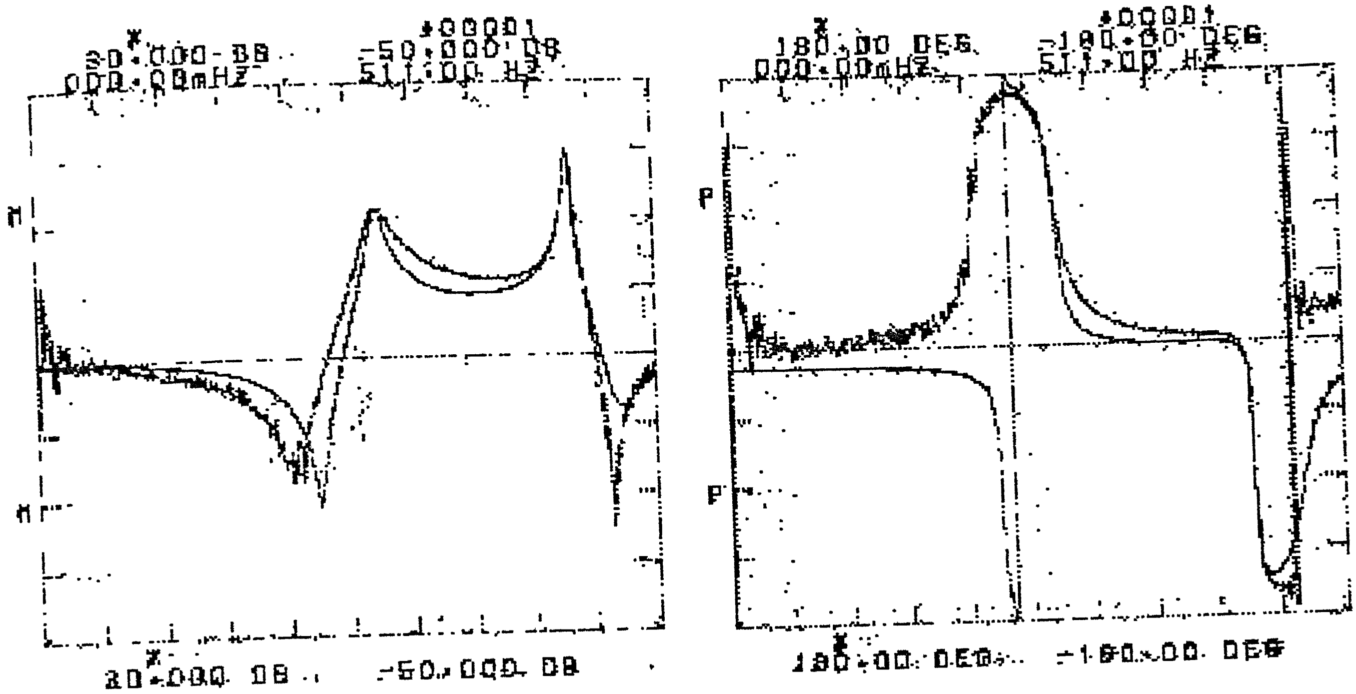

Fig. 6.1 : Measured and re erated (SDF method) FRF for plate held in hand.

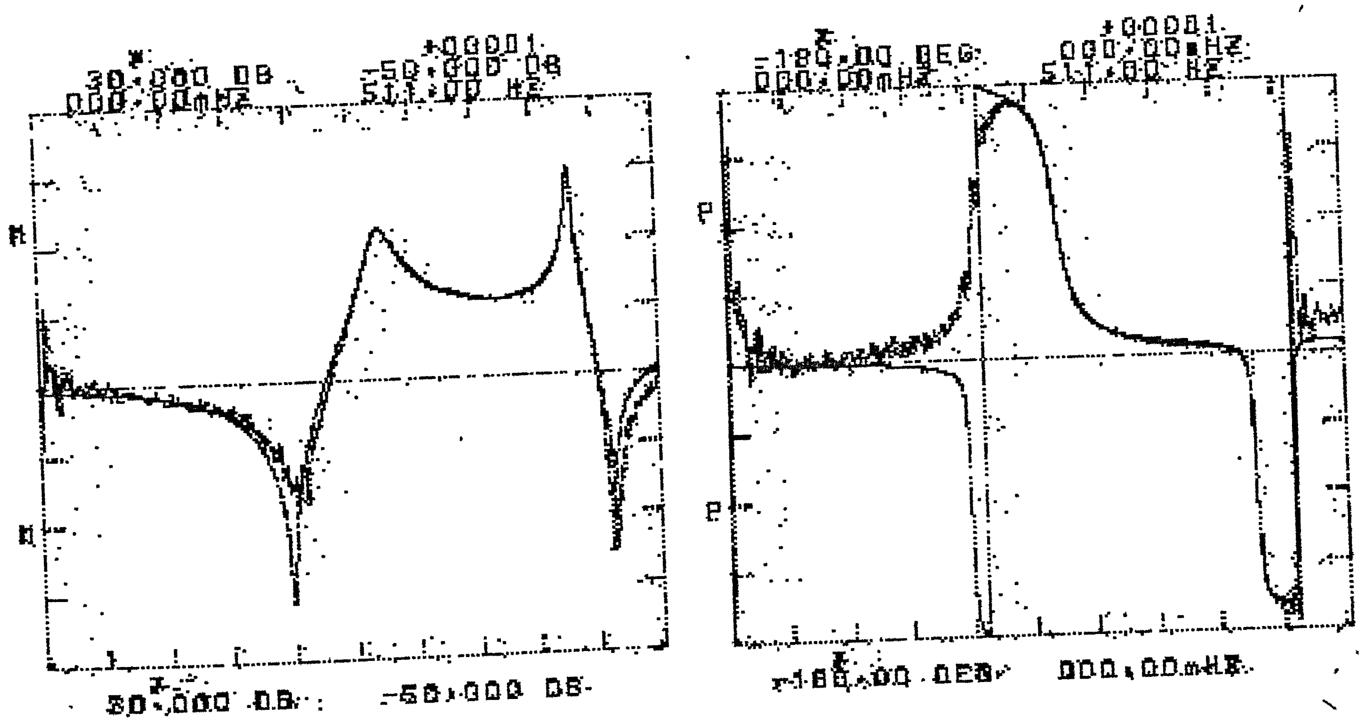

Fig. 6.2 : Measured and regenerated (MDF method) FRF for plate held in hand

Table 6.1 : Error after each iteration of MDF curve fit method for a plate held in hand

Error after SDF circle fit method = 72.942

Iteration No.	Error after each iteration
1	11.094
2	7.458
3	7.413
4	7.408
5	7.407

Time taken for each iteration $\approx$ 100 seconds

Table 6.2 : Parameters obtained by SDF circle fit method compared with improved values obtained by MDF curve fit method for the plate held in hand

Parameters	SDF circle fit method	MDF curve fit method
η_1	0.042665	0.0721406
ω_1	277.8	278.11051
$({}_1A^*_{jk})_{real}$	0.166144	0.279986
$({}_1A^*_{jk})_{imag}$	0.008244	0.052724
η_2	0.009244	0.0092857
ω_2	439.3	439.35958
$({}_2A^*_{jk})_{real}$	-0.091384	-0.09195
$({}_2A^*_{jk})_{imag}$	-0.011683	-0.008507

obtained from these improved values superimposed on the measured FRF is shown in Fig. 6.2. Comparing Fig. 6.2 with Fig. 6.1, it is evident that the MDF curve fit method yields significantly better results. The improvement of the first modal damping constant η_1, as well as of the modal constant, ${}_1A^*_{jk}$ is noticable from Table 6.2.

6.3 Numerical Procedures and Results for a Jointed Structure

6.3.1 Jointed Structure Configuration

The structure is made up of four beams interconnected at the ends as shown in Fig. 6.3. This structure offers an advantage that by changing the included angles between the limbs, the position of the modes along the frequency axis can be shifted. This structure with included angles as 68° and 112°, shown in Fig. 6.3, was analyzed in an earlier work [3].

When the included angles are not near 90°, the modes are well separated for a frequency range upto 500 Hz. This can be clearly seen from the FRF of Fig. 6.4, which has been reproduced here from [3], and exhibits five well separated modes. The modeshapes of these five modes are also reproduced in Fig. 6.5.

In the present work, the same structure has been studied when the included between the limbs are very close to 90°. The structure with this configuration is shown in Fig. 6.6. A typical FRF a^*_{14}, obtained by measuring the response at 1 with impact excitation at 4, is shown in

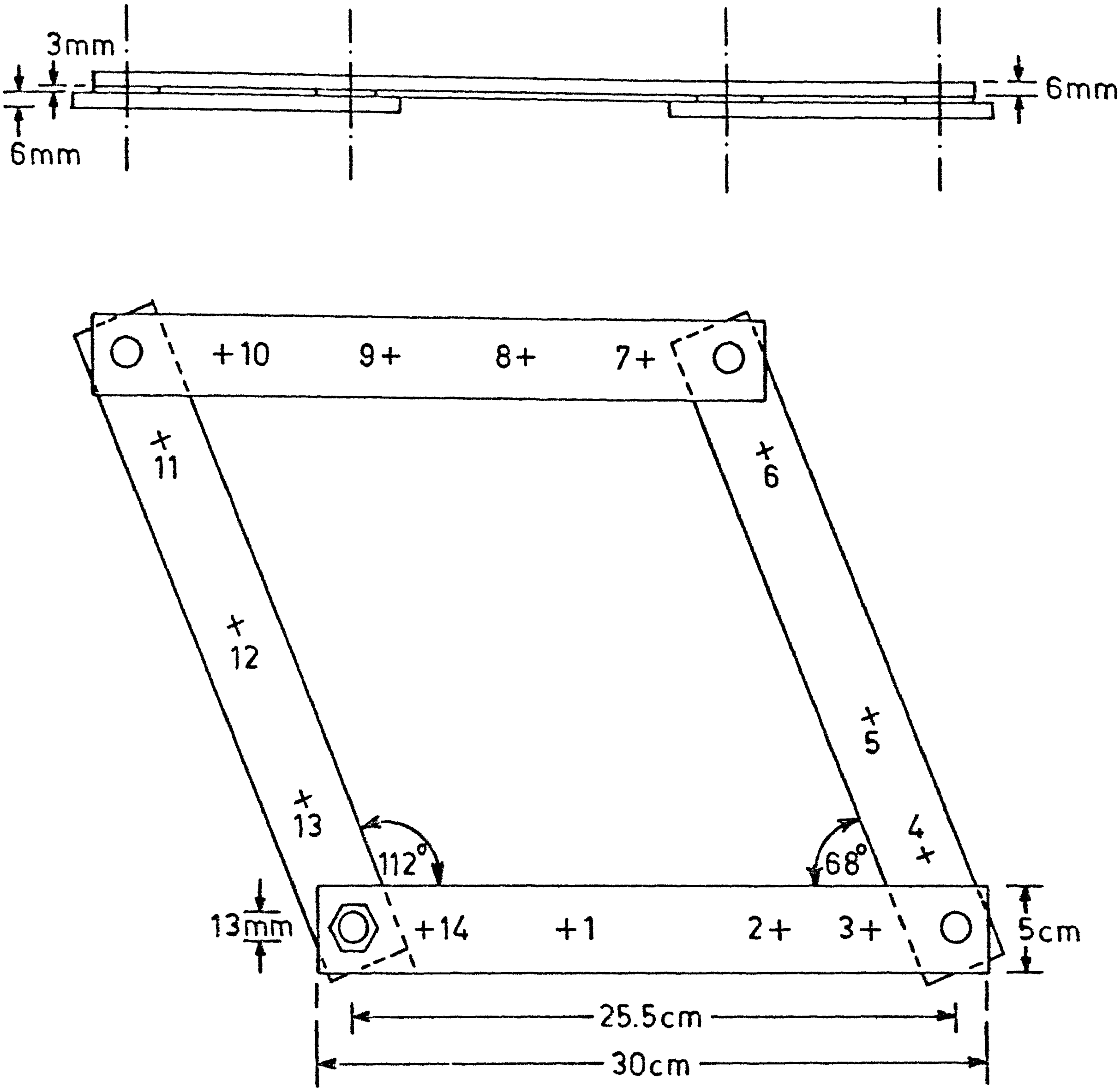

DIMENSIONS AND LOCATION OF TEST POINTS ON RHOMBUS SHAPED STRUCTURE

Fig. 6.3

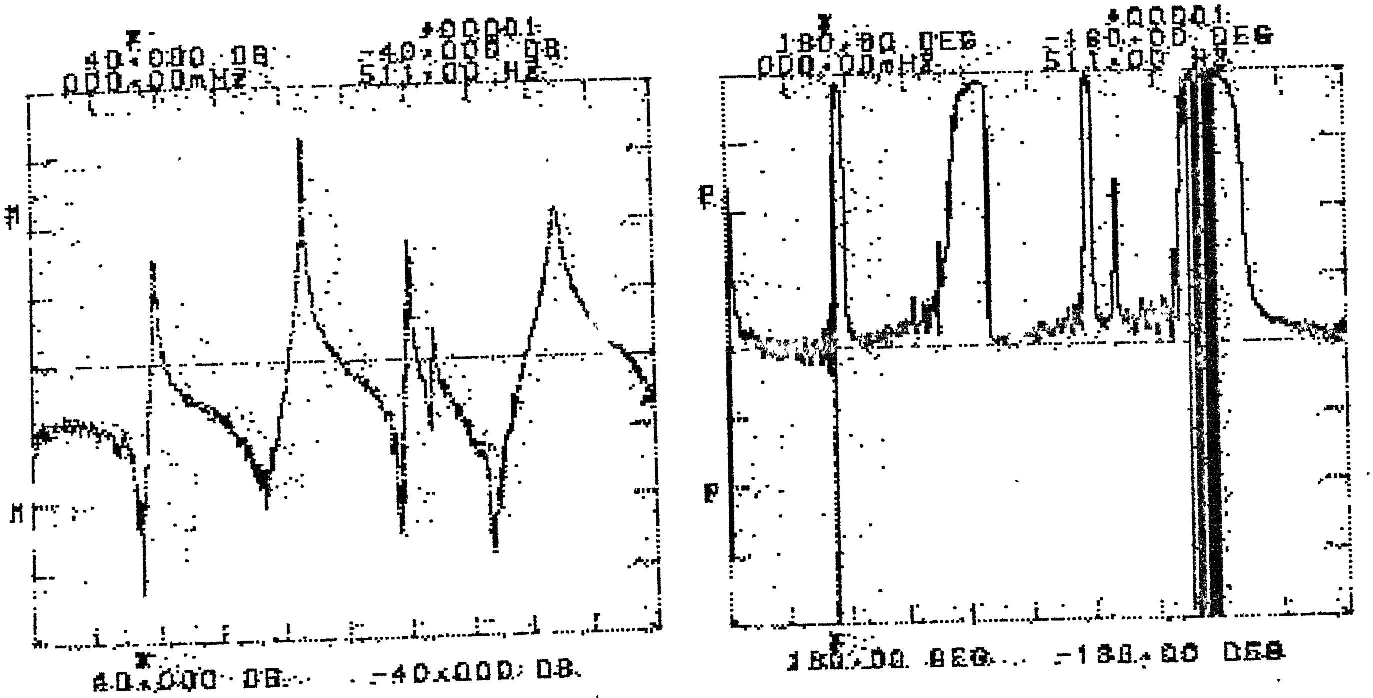

Fig. 6.4 : FRF a_{11}^{*} of Rhombus shaped Jointed Structure

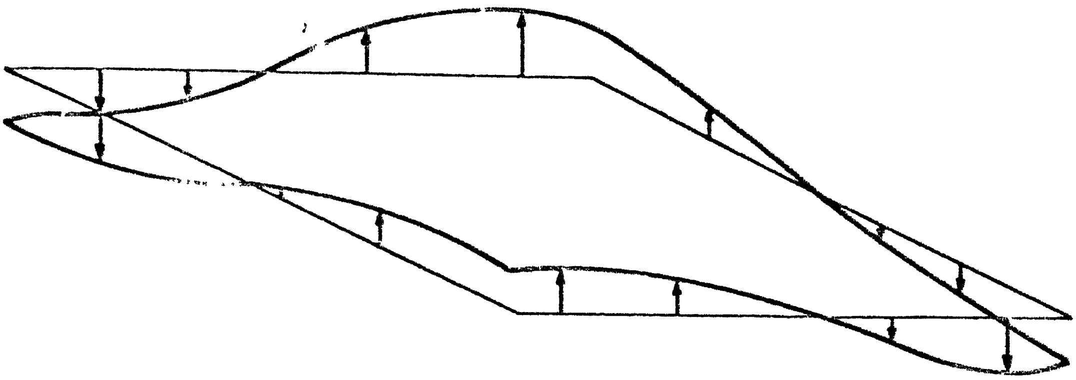

Mode 1

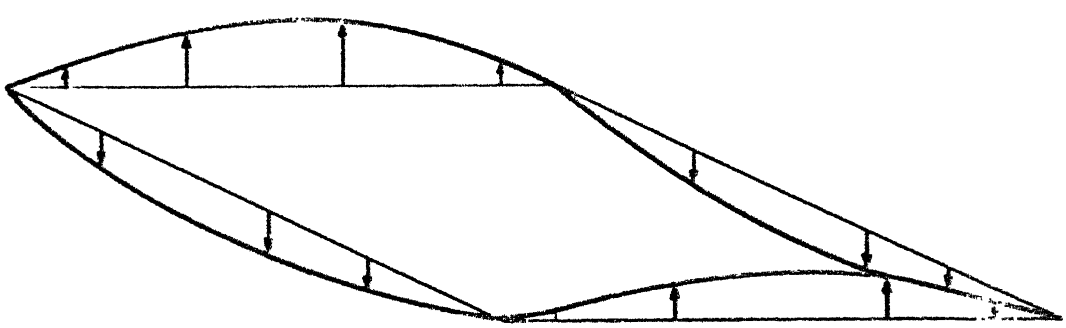

Mode 2

Fig. 6·5 (a)

MODE SHAPES OF RHOMBUS SHAPED STRUCTURE

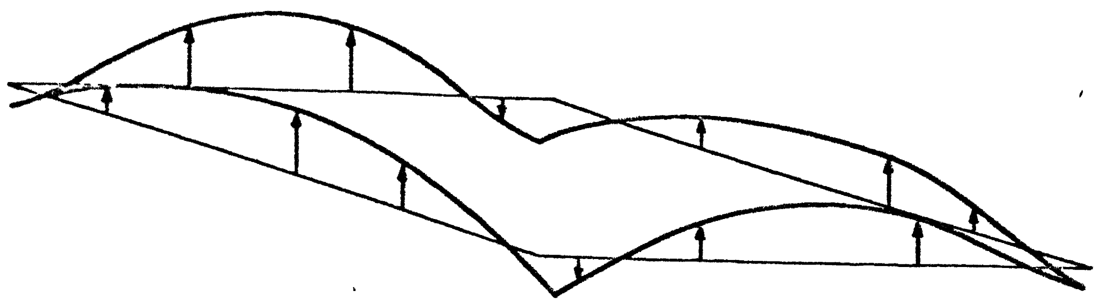

Mode 3

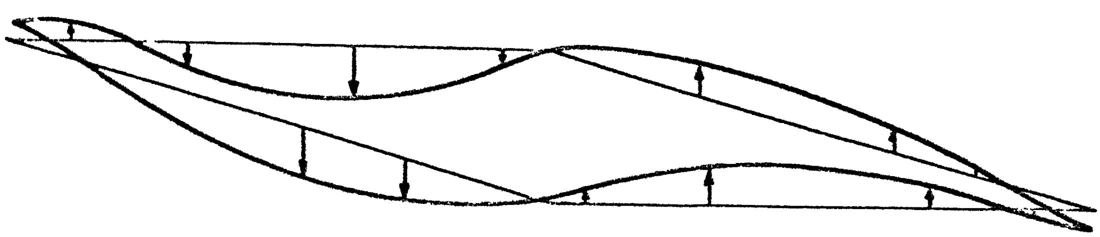

Mode 4

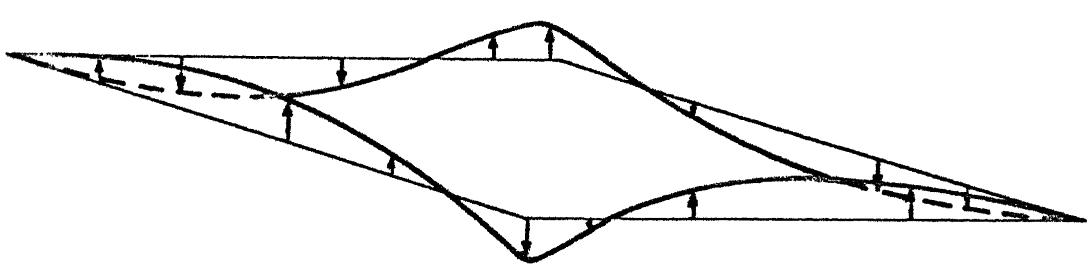

Mode 5

Fig. 6·5 (b)

MODE SHAPES OF RHOMBUS SHAPED STRUCTURE

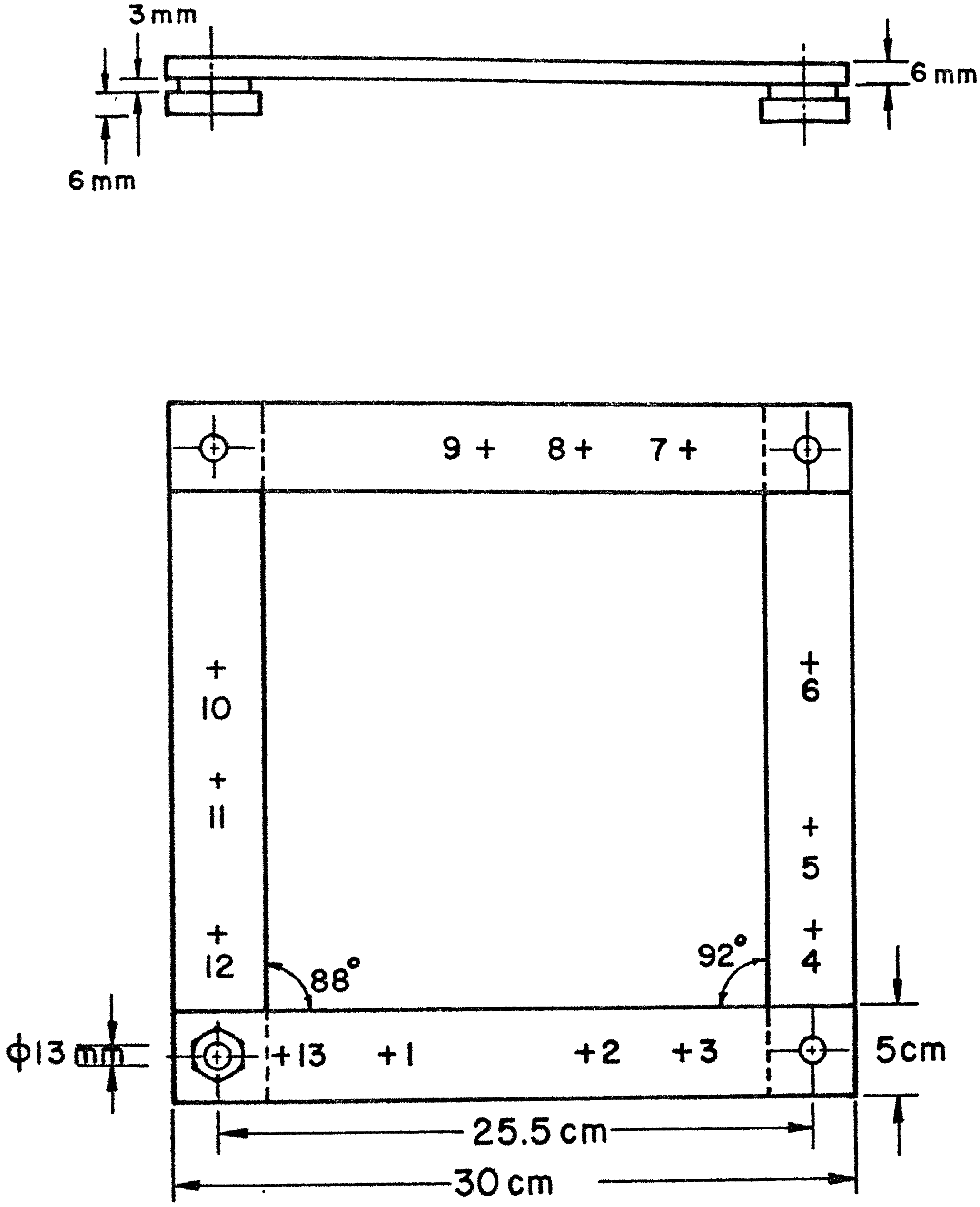

Fig. 6.6 Jointed structure

Fig. 6.7. The fourth and fifth modes are now seen to be quite close to each other. The frequency resolution is 1 Hz and even with this resolution it is difficult to take a sizeable number of data for SDF circle fit method, without zooming facility in the signal analyzer. The modal parameters were calculated using SDF circle fit method and were used to regenerate the FRF. This regenerated FRF, superimposed on the experimentally obtained FRF is shown in Fig. 6.8. It is clear from this figure that the SDF circle fit method does not result in a good regeneration in the region surrounding the fourth and fifth modes, whereas upto the third mode the regeneration is acceptable. The single mode assumption at these last two modes is not really good since each of these two modes will have a significant effect on each other. Moreover, the number of points required for a circle fit, available in this case is very small, which leads to an erroneous circle fit. This is turn leads to erroneous estimation of modal parameters. This configuration indeed gives us a good case for testing the MDF curve fit method.

6.3.2 Improvement of Modal Parameters by MDF Curve Fit Method

The MDF curve fit method, described in Chapter 3, was applied to the jointed structure with configuration described in 6.3.1, the structure having exhibited closely placed fourth and fifth modes.

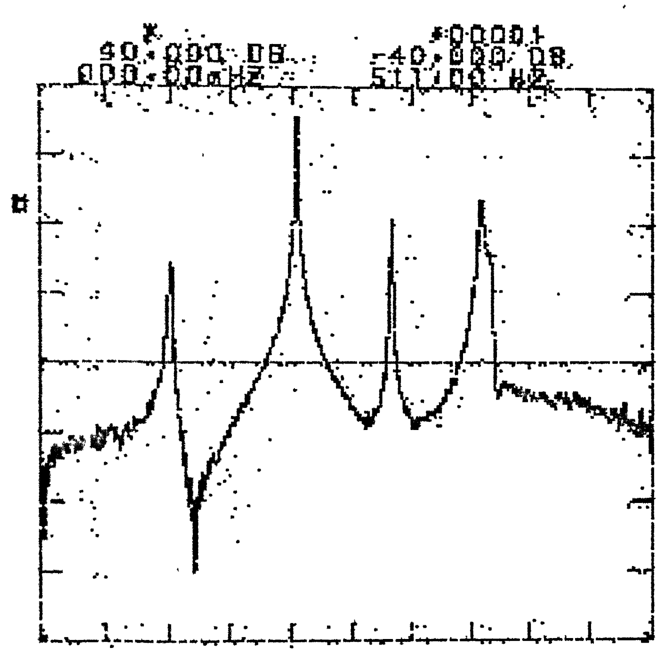

Fig. 6.7 : Measured FRF a^*_{14} of Jointed Structure

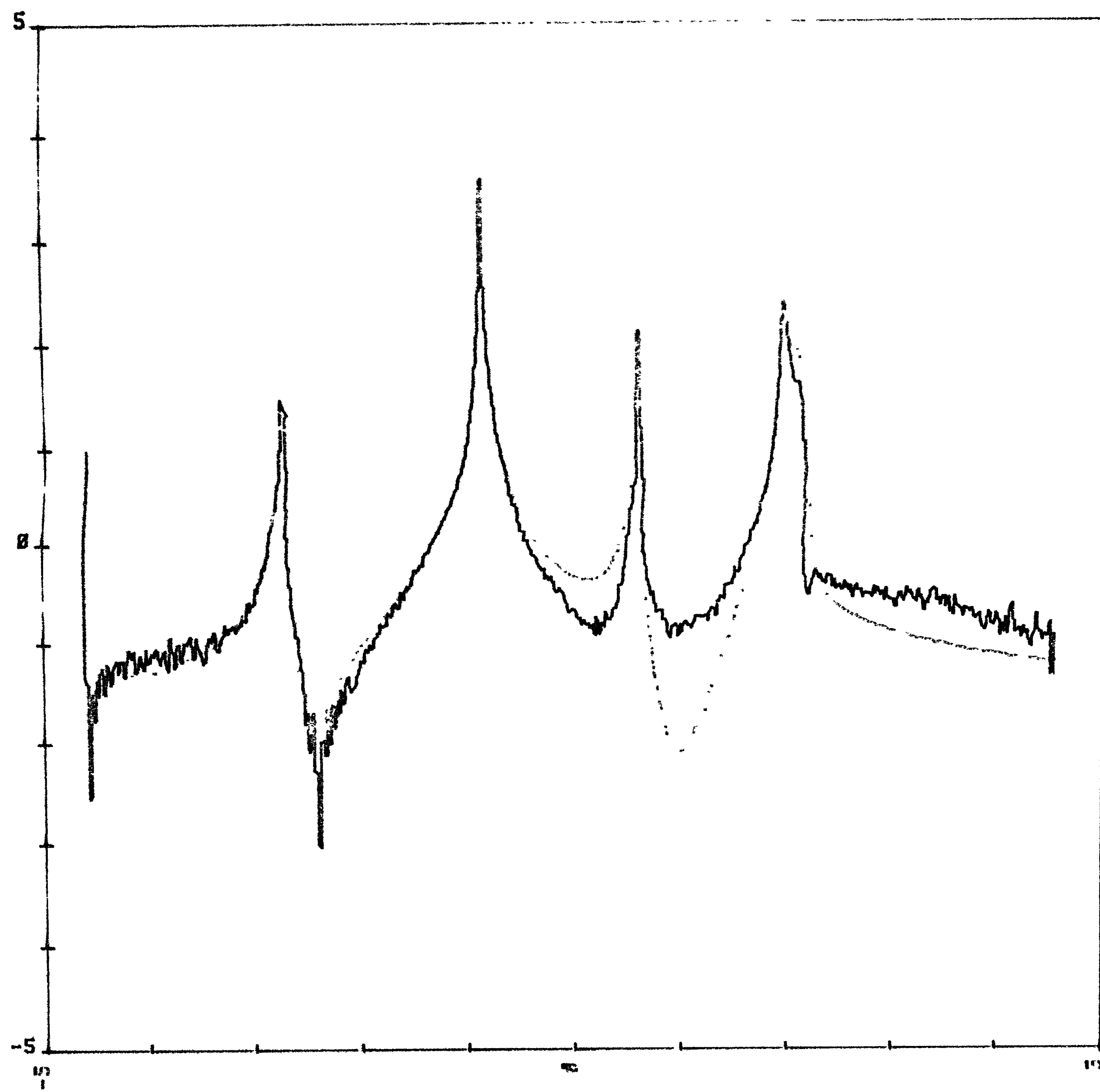

TITLE	SDF 14	
DATE TIME	88/10/06 14:43	
SAMPLE RATE	20mS	
MANUAL TRIG.	NORMAL	
CH	1	2
RANGE	10V	10V
OFFSET	50 %	50 %
COUPLE	DC	DC
ZOOM	* 1	* 1
CALC.		
CH 1	MAX. MIN.	4.55V -4.62V
CH 2	MAX. MIN.	3.47V -2.12V
COMMENT		

Fig.6.8 Measured and regenerated (SDF method) FRF a^*_{14} of Jointed structure

Equation (3.11) is reproduced here as

$$[P]\ \{\delta k\} = \{R\} \qquad (6.1)$$

where the individual elements of $[P]$ matrix, P_{ij} and vector $\{R\}$, R_i are given by (3.6) and (3.7) respectively. These values are calculated over the frequency range using the previous estimates of the modal parameters. From (6.1), $\{\delta k\}$ is then obtained, which represents the incremental change in the modal parameter value vector $\{k\}$. These increments $\{\delta k\}$, are added to the previous estimates to obtain the new estimates, i.e.

$$\left\{\begin{array}{c}\text{Previous}\\ \text{estimate of}\\ \text{parameters}\end{array}\right\} + \{\delta k\} = \left\{\begin{array}{c}\text{New estimate}\\ \text{of}\\ \text{parameters}\end{array}\right\} \qquad (6.2)$$

It was observed that on regeneration of FRF using these new estimates, the error given by (3.4), increased with each iteration drastically indicating the divergence of the solution.

It was also observed that on scaling these increments $\{\delta k\}$ by a factor ε, where $\varepsilon < 1$, the solutions converged monotonically. Therefore the new vector $\{k\}$ is obtained by

$$\left\{\begin{array}{c}\text{Previous}\\ \text{estimate of}\\ \text{parameters}\end{array}\right\} + \varepsilon\ \{\delta k\} = \left\{\begin{array}{c}\text{New estimate}\\ \text{of parameters}\end{array}\right\} \qquad (6.3)$$

The value of ε may not be the same for each iteration. It is chosen by trial and error, keeping in view that the error obtained by using the new parameters is lesser than the error obtained by using the previous estimates.

The explanation for the divergence for $\varepsilon = 1$ and convergence for $\varepsilon < 1$ is due to the following reason. The solution for these FRF's with closely placed modes has a very small stable solution region around the actual solution. If the solution crosses this stable region and reaches the unstable region, the method diverges.

6.3.2.1 MDF Curve Fit Method Applied for Full Frequency Range and all the Parameters

The MDF curve fit method with scaling factor ε was used to obtain the modal parameters for the FRF (a^*_{14}) shown in Fig. 6.7. The initial estimate vector $\{k\}$ was taken as the parameter values obtained from SDF circle fit method. Table 6.3 lists the scaling factor ε and the error e after each iteration. Table 6.4 compares the modal parameters as obtained from SDF circle fit method and as obtained from the MDF curve fit method after 17 iterations. It is evident that the parameters associated with only the fourth and fifth modes get refined. The regenerated FRF using the MDF curve fit results is shown in Fig. 6.9. On comparing this with the regenerated FRF of Fig. 6.8, the improvement near the last two modes is evident. This is better illustrated if the nyquist plots obtained from SDF and MDF results are compared in Fig. 6.10. These nyquist plots are drawn only

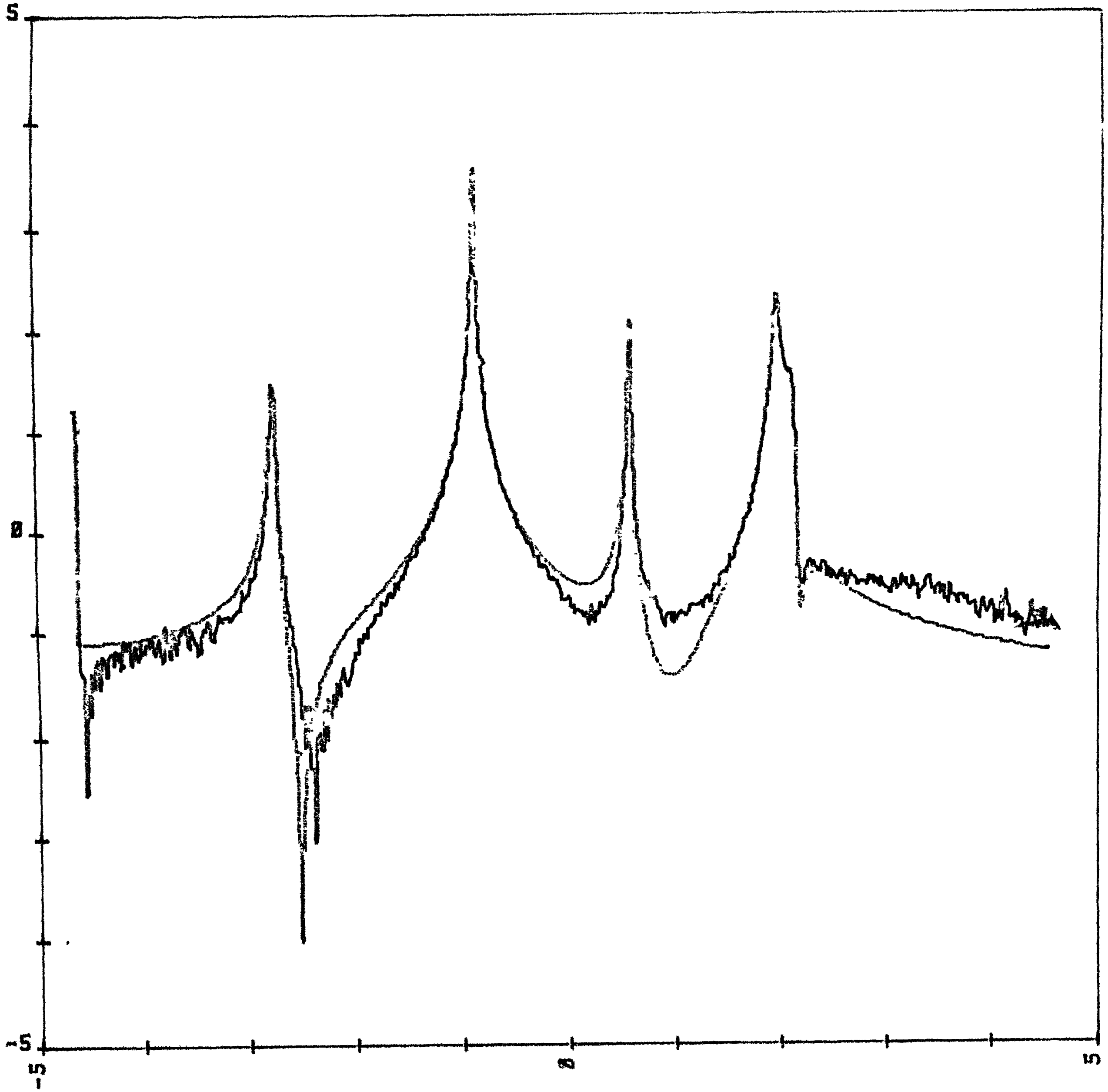

TITLE	MDF 14	
DATE TIME	88/10/06 15:37	
SAMPLE RATE	20mS	
MANUAL TRIG.	NORMAL	
CH	1	2
RANGE	10V	10V
OFFSET	50 %	50 %
COUPLE	DC	DC
ZOOM	* 1	* 1
CALC.		
CH 1	MAX. 4.54V MIN. -4.62V	
CH 2	MAX. 3.57V MIN. -4.03V	

COMMENT

Fig.6.9: Measured and regenerated (MDF method - full frequency range and all parameters) of FRF a^*_{14} of Jointed structure

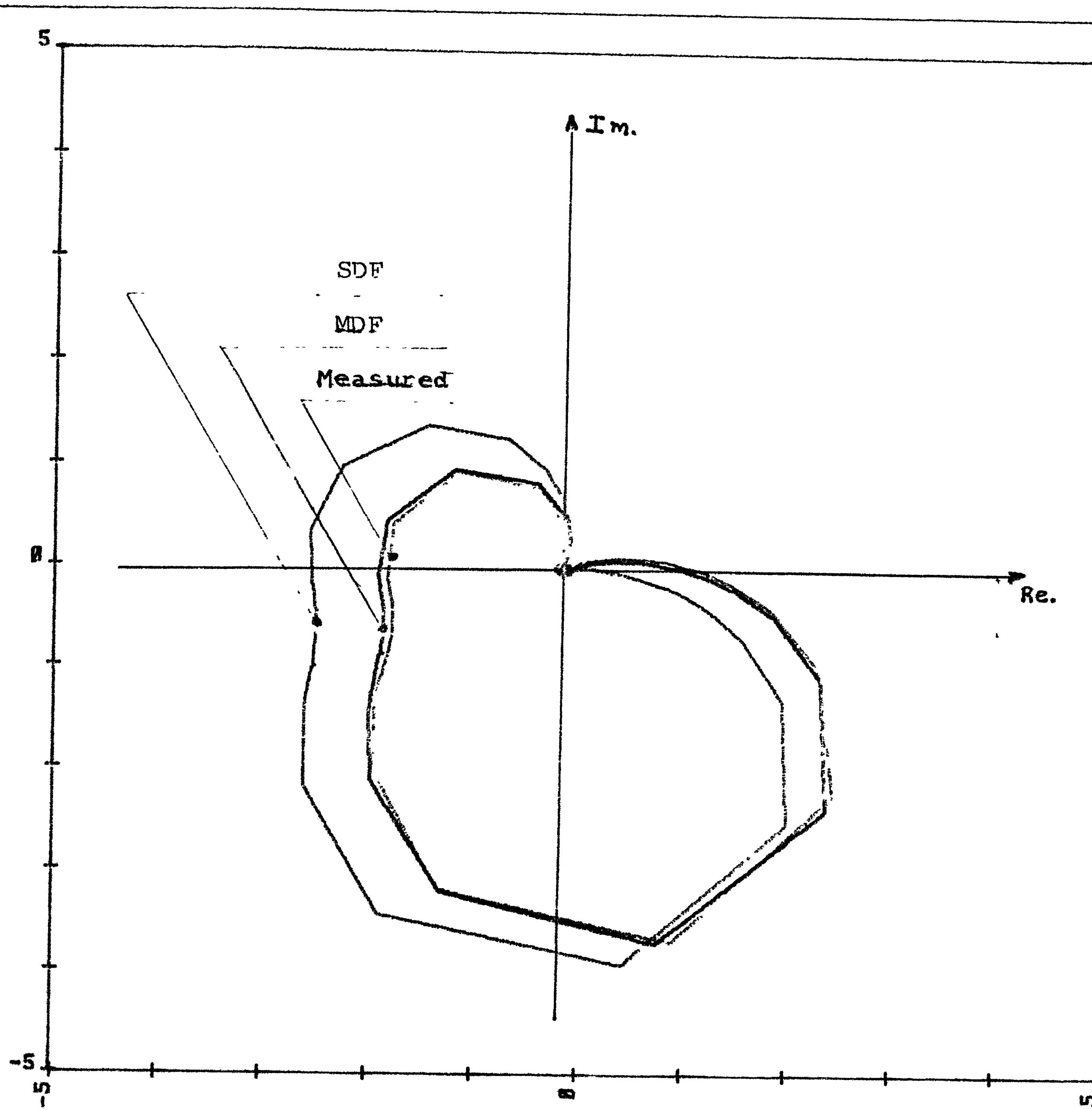

TITLE	COUPLE 11		
DATE TIME	88/10/14 00:46		
SAMPLE RATE	20mS		
MANUAL TRIG.	NORMAL		
CH	1	2	
RANGE	10V	10V	
OFFSET	50 %	50 %	
COUPLE	DC	DC	
ZOOM	* 1	* 1	
CALC.			
CH 1	MAX. 2.30V MIN. -1.99V		
CH 2	MAX. .93V MIN. -3.72V		
COMMENT			

Fig.6.10: Nyquist plots a^*_{14} of measured regenerated. (SDF and MDF methods) FRF, around fourth and fifth modes of Jointed structure

Table 6.3 : Error and scaling factor for each iteration of MDF curve fit method for jointed structure FRF a^{*}_{14}

Error after SDF circle fit method : 323.495

Iteration number	Scaling factor ε	Error after the iteration
1	0.01	307.933
2	0.02	282.319
3	0.03	253.858
4	0.04	226.611
5	0.05	201.634
6	0.06	178.612
7	0.07	156.992
8	0.08	136.523
9	0.10	115.327
10	0.10	98.139
11	0.10	84.139
12	0.20	62.581
13	0.30	42.618
14	0.30	32.299
15	0.30	26.922
16	0.30	24.088
17	0.30	22.782

Time taken for each iteration ≈ 20 minutes.

Table 6.4 : SDF versus MDF for Jointed Structure FRF a^*_{14}

Parameters	From SDF circle fit method	From MDF curve fit method after 17 iteration
Mass term	0.26173388	0.28799294
η_1	0.01412377	0.01474284
ω_1	103.4	103.374934
$({}_1A^*_{14})_{real}$	-0.08636302	-0.09076631
$({}_1A^*_{14})_{imag}$	0.02284896	-0.00158237
η_2	0.00067156	0.00067967
ω_2	207.5	207.55378
$({}_2A^*_{14})_{real}$	-0.2558857	-0.255804
$({}_2A^*_{14})_{imag}$	-0.050539	-0.050442
η_3	0.00163598	0.00231796
ω_3	288.7	288.7808
$({}_3A^*_{24})_{real}$	0.03305854	0.03002156
$({}_3A^*_{14})_{imag}$	0.01132084	0.01052005
η_4	0.00906141	0.00956932
ω_4	365.8	365.93098
$({}_4A^*_{14})_{real}$	-0.143115	-0.1383204
$({}_4A^*_{14})_{imag}$	-0.024972	-0.043329
η_5	0.0087456	0.0095888
ω_5	374.7	374.96568
$({}_5A^*_{14})_{reak}$	0.071151	0.0500657
$({}_5A^*_{14})_{imag}$	0.045904	0.0137109

from 300 Hz to 450 Hz so as to signify the results around fourth and fifth modes.

The time taken for each iteration was about 20 minutes on the PC/AT machine with 8087 chip. This is an enormous computation time considering the fact that MDF method may need many iterations to converge. The next subsections discuss two alternatives to cut down this computation time.

6.3.2.2 Reducing the Number of Parameters to be Improved

As mentioned earlier in 6.3.2.1 and illustrated in Fig. 6.8, the SDF circle fit method gives a satisfactory estimates for the first three modes. The major error is indeed from the estimation of modal parameters of the fourth and fifth modes. So the MDF curve fit method has now been applied for the same FRF a^*_{14}, to improve only the parameters ω_r, η_r, real part of ${}_rA^*_{jk}$ and imaginary parts of ${}_rA^*_{jk}$, where $r = 4$ and 5. The frequency range covered is the full range i.e. upto 500 Hz.Since the number of parameters to be improved are now only 8, the time required is brought down to only about 3½ minutes per iteration. The scaling factor ε and the error after each iteration is given in Table 6.5. The regenerated FRF superimposed on the measured FRF is given in Fig. 6.11 and the regeneration is observed to be quite faithful. The nyquist plots also were seem to match. Table 6.6 compares the parameters obtained by MDF curve fit method with the parameters of SDF circle fit method.

Table 6.5 : Error and scaling factor ε for each iteration of MDF curve fit method of section 6.3.2.2 for Jointed structure FRF a^*_{14}

Iteration No.	Scaling factor ε	Error after each iteration
1	0.01	310.189
2	0.03	279.37
3	0.04	254.304
4	0.08	224.952
5	0.08	207.889
6	0.12	188.944
7	0.08	179.203
8	0.08	170.921
9	0.08	163.863
10	0.1	156.425
11	0.1	150.326
12	0.1	145.316
13	0.1	141.195
14	0.12	137.167
15	0.12	133.976
16	0.12	131.44
17	0.20	128.23
18	0.30	125.147
19	0.3	123.464
20	0.1	123.122

Time taken for each iteration $\approx 3\frac{1}{2}$ minutes.

Table 6.6 : SDF versus MDF of section 6.3.2.2 for FRF a^*_{14} of the Jointed structure

Parameters	SDF circle fit method	MDF curve fit method
η_4	0.00906141	0.0094403
ω_4	365.8	365.942627
$({}_4A^*_{14})_{real}$	-0.143115	-0.13690983
$({}_rA^*_{14})_{imag}$	-0.024972	-0.04398023
η_5	0.0087456	0.00946401
ω_5	374.7	374.99396136
$({}_5A^*_{14})_{real}$	0.071151	0.04734567
$({}_5A^*_{14})_{imag}$	0.045904	0.01151493

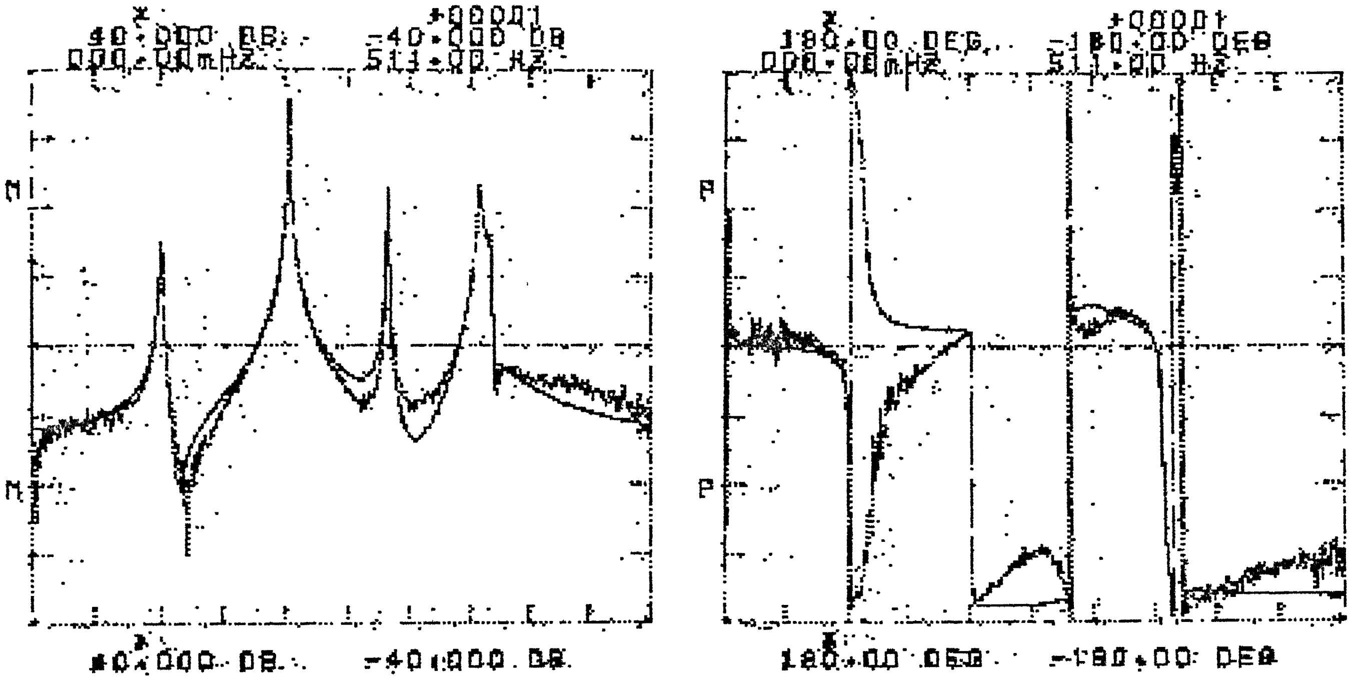

Fig. 6.11 : Measured and regenerated (MDF method - restricting number of parameters) of FRF a^*_{14} of Jointed structure

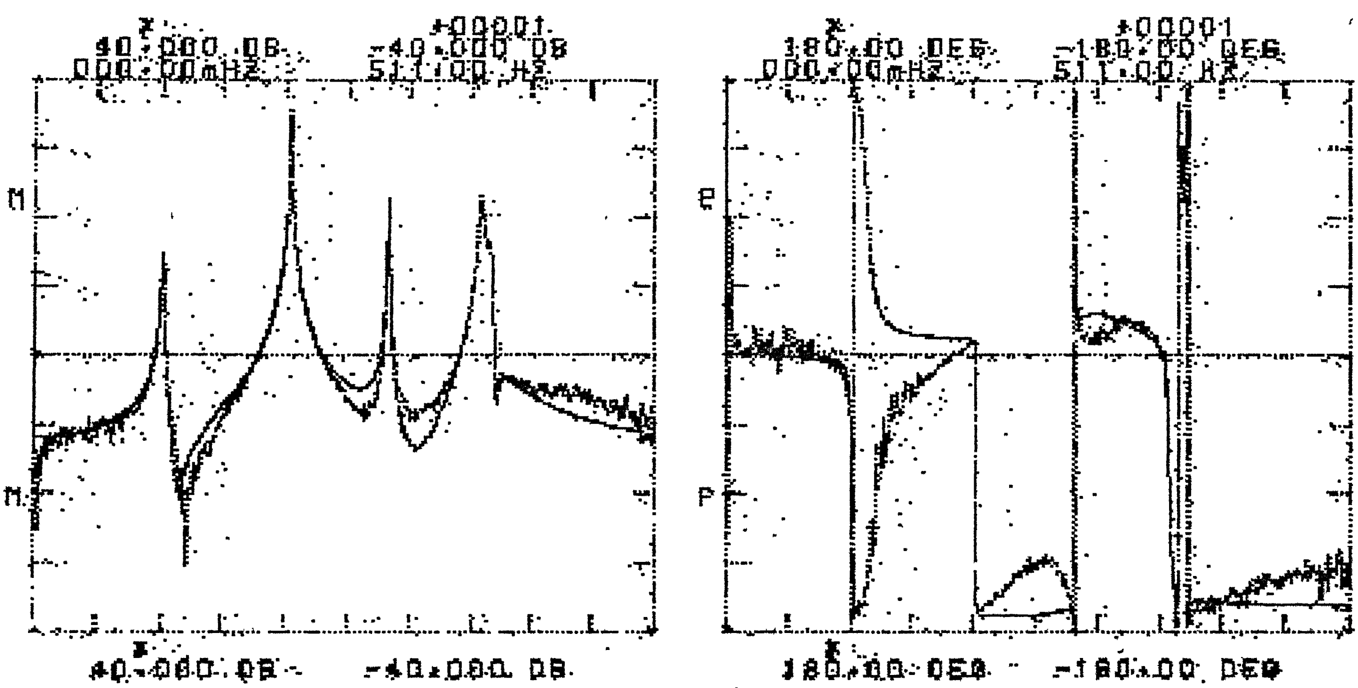

Fig. 6.12 : Measured and regenerated (MDF method - restricting both frequency range and the number of parameters) of FRF a^*_{14} of Jointed structure

6.3.2.3 Restricting the Frequency Range and the Number of Parameters to be Improved

The contribution from the parameters of the fourth and the fifth modes to the frequencies away from these modes are found to be extremely small. Hence the frequency range covered has been restricted to that around the fourth and fifth modes, i.e. from 325 Hz to 410 Hz.

The results for the same FRF a^*_{14}, are shown in Fig. 6.12 and Tables 6.7 and 6.8. As can be seen from Table 6.7, the error has been reduced to almost the same level as in the Table 6.5, though the frequency range now has been reduced.

The advantage of this restriction of frequency range is evident from the fact that the time taken for each vibration is now only 40 seconds compared to the iteration time of about 3½ minutes for the results of Table 6.5.

6.3.3 Mode Shapes for the Jointed Structure

For obtaining the mode shapes for the jointed structure, with included angles very close to 90^o, a total of 13 FRF were measured, one point FRF and 12 transfer FRF's. Out of the 13 FRFs, four FRF's a^*_{11}, a^*_{17}, a^*_{18} and a^*_{19} responded well for SDF circle fit method which is evident from the Fig. 6.13. The fourth and fifth modes appear to contribute

Table 6.7 : Error and scaling ε for each iteration of MDF curve fit method of section 6.3.2.3 for FRF a^*_{14} of the Jointed structure

Error after SDF circle fit method: 323.495

Iteration number	Scaling factor ε	Error after the iteration
1	0.01	310.186
2	0.03	279,368
3	0.04	254.302
4	0.08	224.951
5	0.08	207.888
6	0.12	188.943
7	0.08	179.202
8	0.08	170.92
9	0.08	163.863
10	0.10	156.425
11	0.10	150.326
12	0.12	144.384
13	0.12	139.691
14	0.12	135.977
15	0.08	133.969
16	0.08	132.245
17	0.06	131.121
18	0.06	130.116
19	0.06	129.216
20	0.12	127.656
21	0.20	125.669
22	0.3	123.746
23	0.4	122.406
24	0.5	121.695
25	0.6	121.389

Time taken for each iteration 40 seconds.

Table 6.8 : SDF versus MDF of section 6.3.2.3 for FRF a^*_{14} of the Jointed structure

Parameters	After SDF circle fit method	After MDF curve fit method
η_4	0.00906141	0.00943072
ω_4	365.8	365.93578896
$({}_4A^*_{14})_{real}$	-0.143115	-0.13652802
$({}_4A^*_{14})_{imag}$	-0.024972	-0.04460380
η_5	0.0087456	0.00936464
ω_5	374.7	374.97755729
$({}_5A^*_{14})_{real}$	0.071151	0.04671169
$({}_5A^*_{14})_{imag}$	0.045904	0.01176846

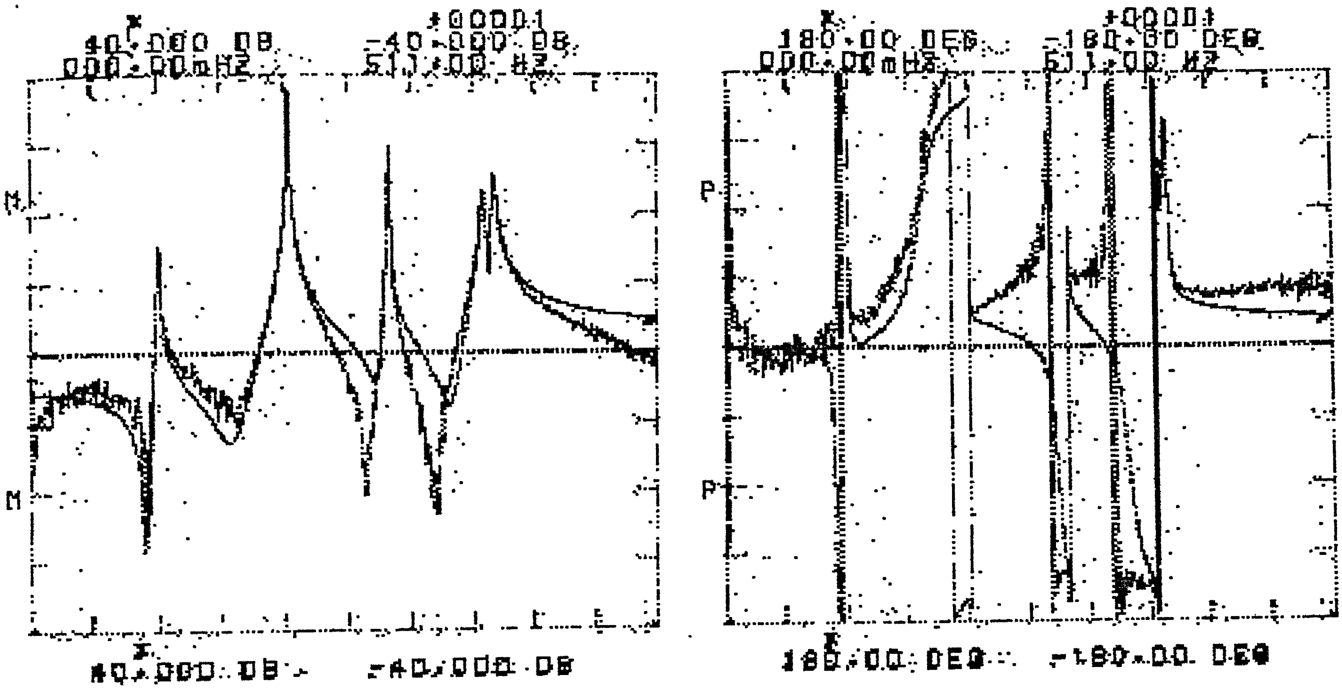

(a) FRF a_{11}^{*}

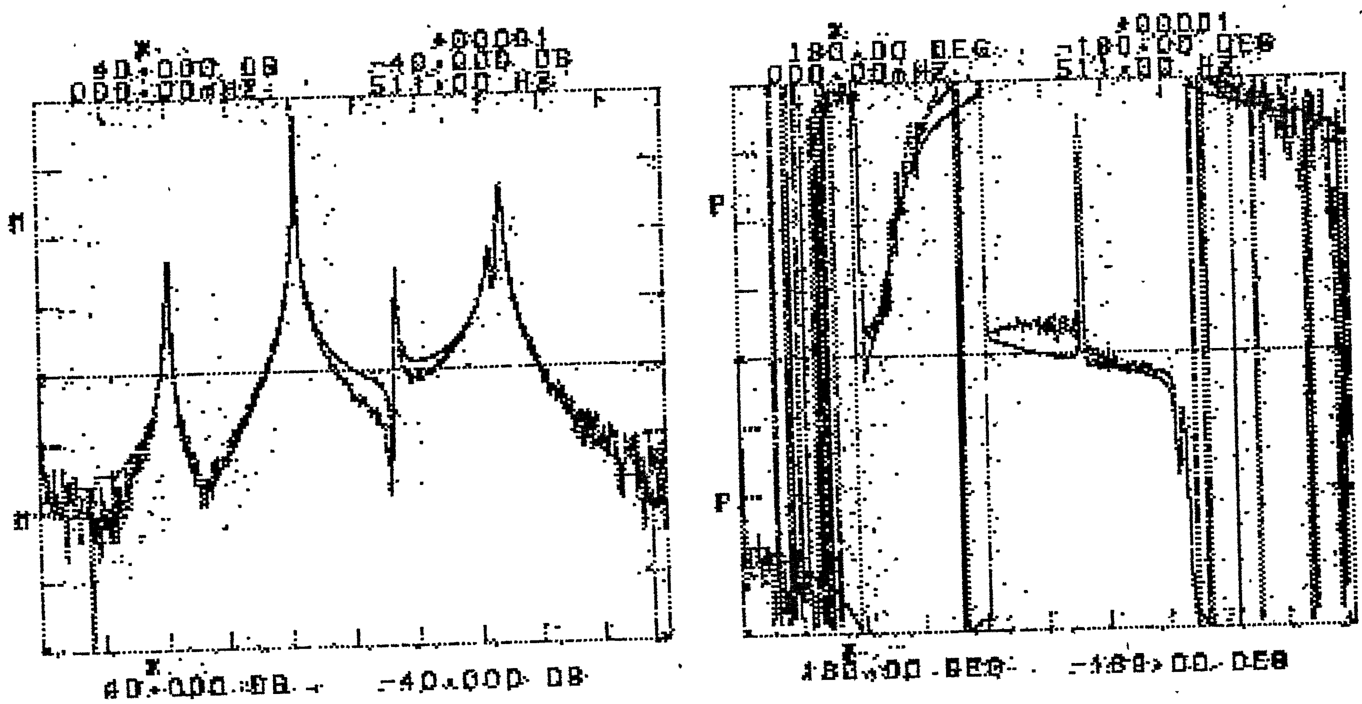

(b) FRF a_{17}^{*}

Fig. 6.13 : Measured and regenerated (SDF method) FRFs of Jointed Structure

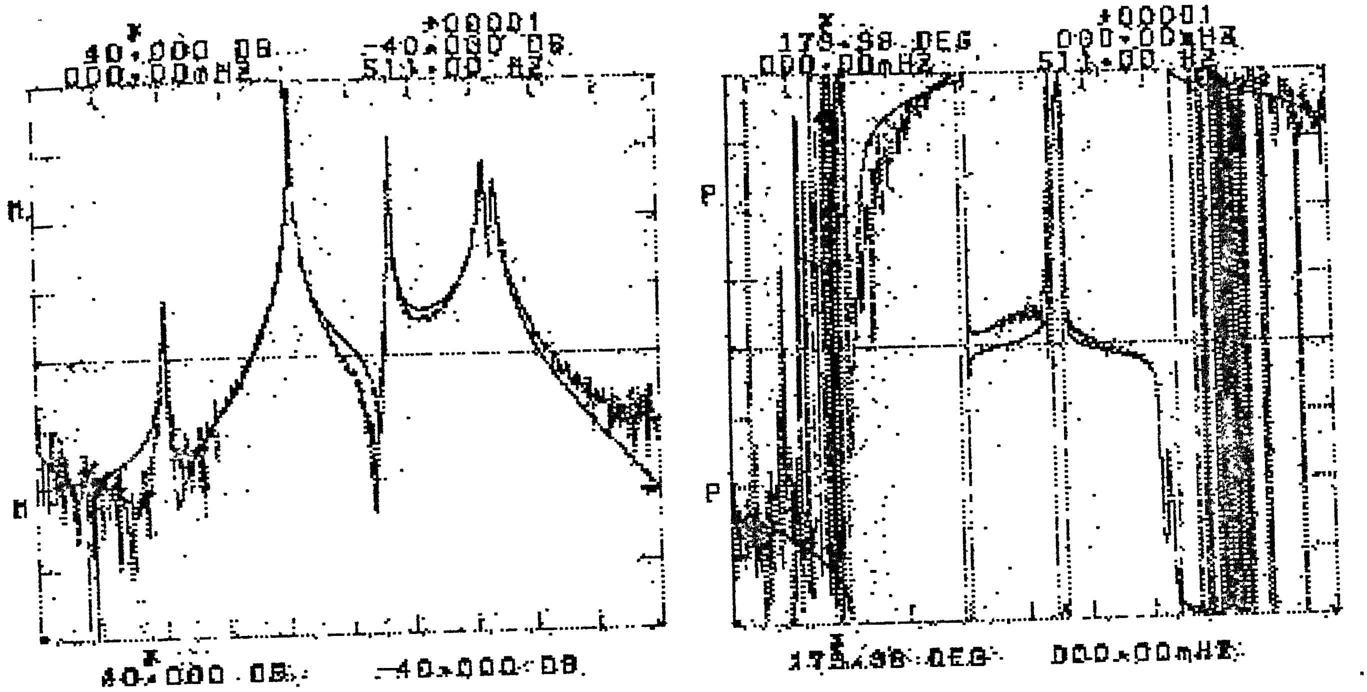

(c) FRF a^{*}_{18}

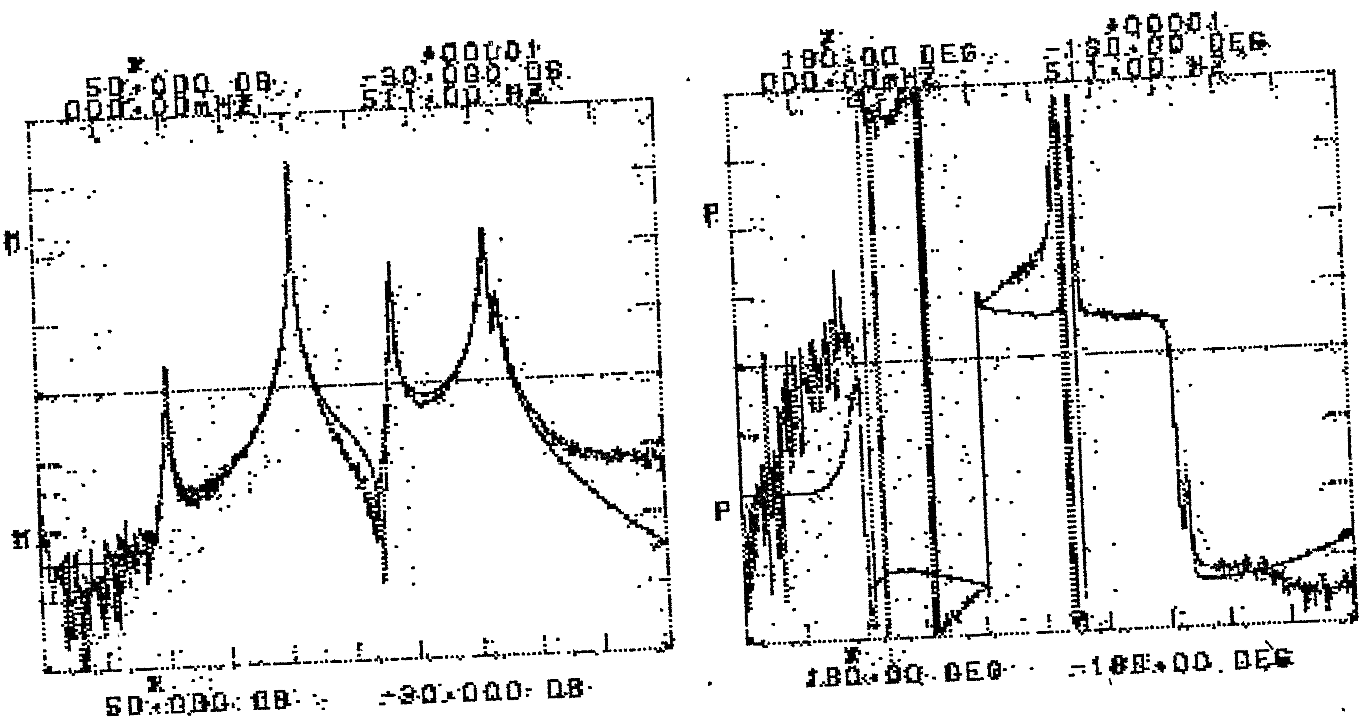

(d) FRF a^{*}_{19}

Figure 6.13

equally for these FRFs, thus providing sufficient number of points to do the circle fit. The other FRFs were all improved over the region covering the fourth and fifth modes by the MDF curve fit method described earlier in section 6.2.2.3. The SDF circle fit method did not yield good estimates for the modal parameters of fourth and fifth modes. Thus the modal parameters corresponding to only the fourth and fifth modes were refined using the MDF curve fit method and the resulting regenerated FRF's are shown in Fig. 6.14.

The modal constants ${}_rA^*_{jk}$ do not explicitly yield the elements of the normalised eigen matrix $[\phi^*]$. In order to extract the individual elements of this matrix $[\phi^*]$, one needs at least one point FRF and other transfer FRFs. These transfer FRF's should have a common excitation point or response point as that for the point FRF. The modal constant ${}_rA^*_{jk}$ is given by

$$ {}_rA^*_{jk} = {}_r\phi^*_j \cdot {}_r\phi^*_k \tag{6.4} $$

For point FRF,

$$ {}_rA^*_{kk} = {}_r\phi^*_k \; {}_r\phi^*_k \tag{6.5} $$

From (6.5) above, the element ${}_r\phi_k$ can be calculated. This corresponds to the k^{th} row of $[\phi^*]$ matrix. For other transfer FRF, say a^*_{jk}, with same excitation (or response) point, the j^{th} row of the $[\phi^*]$ matrix can be evaluated by

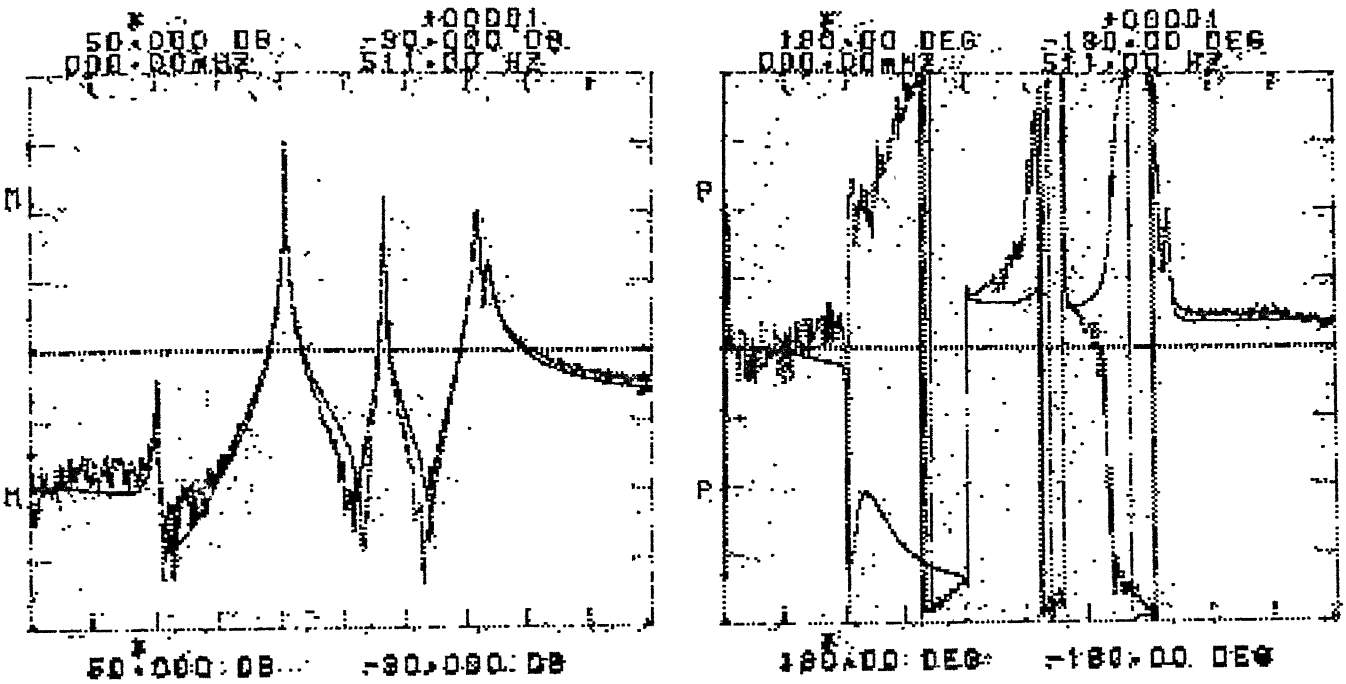

(a) FRF a_{12}^{*}

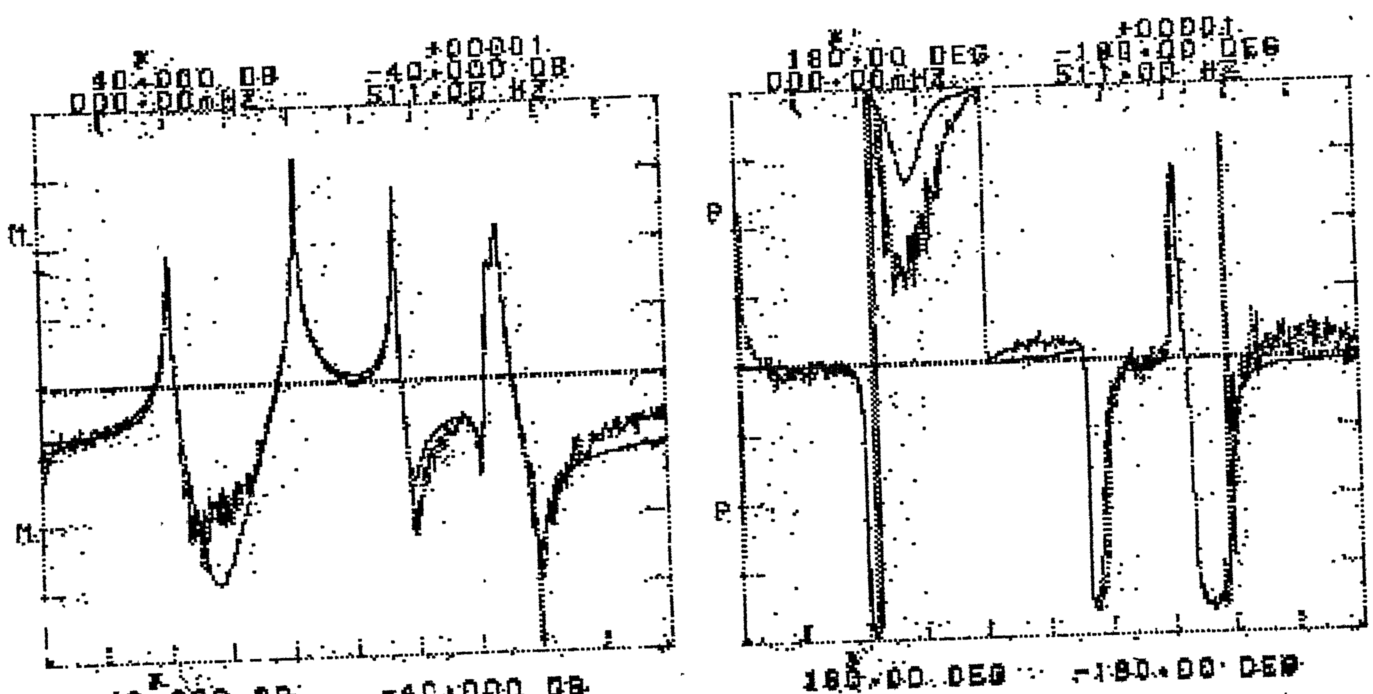

(b) FRF a_{13}^{*}

Figure 6.14 : Measured and regenerated (MDF method) FRF's of Jointed structure

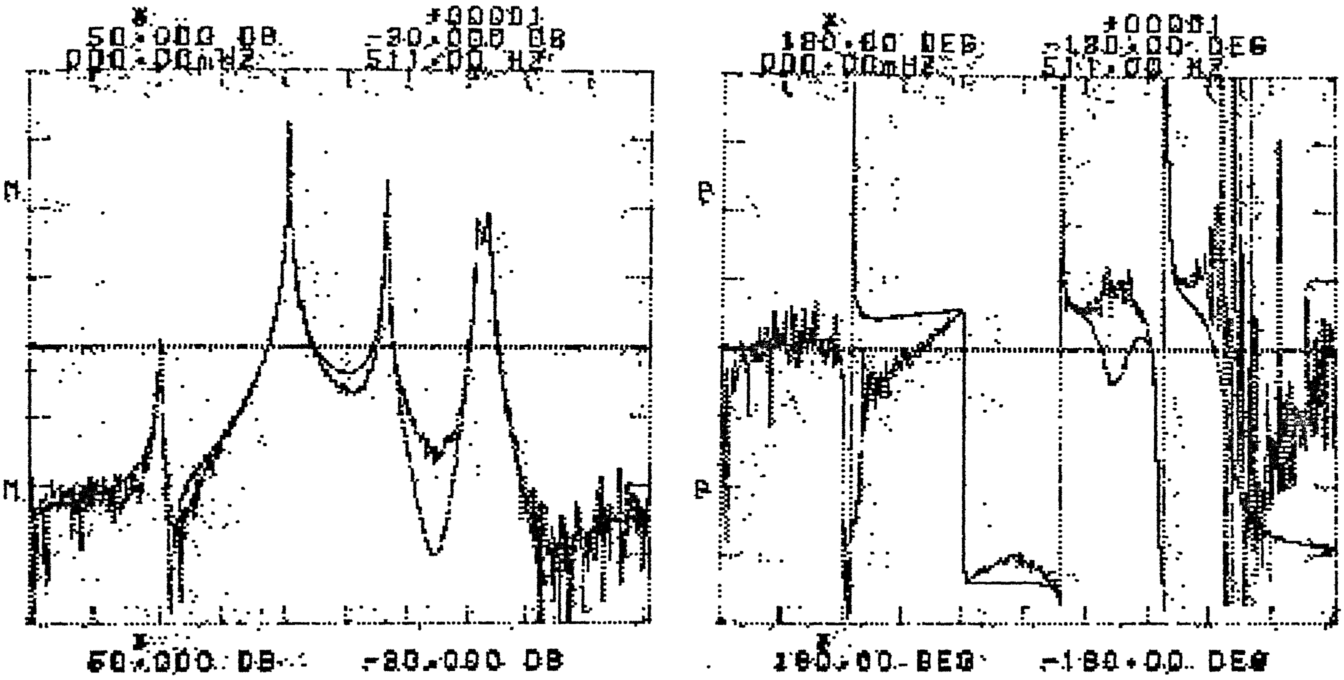

FRF a^*_{15}

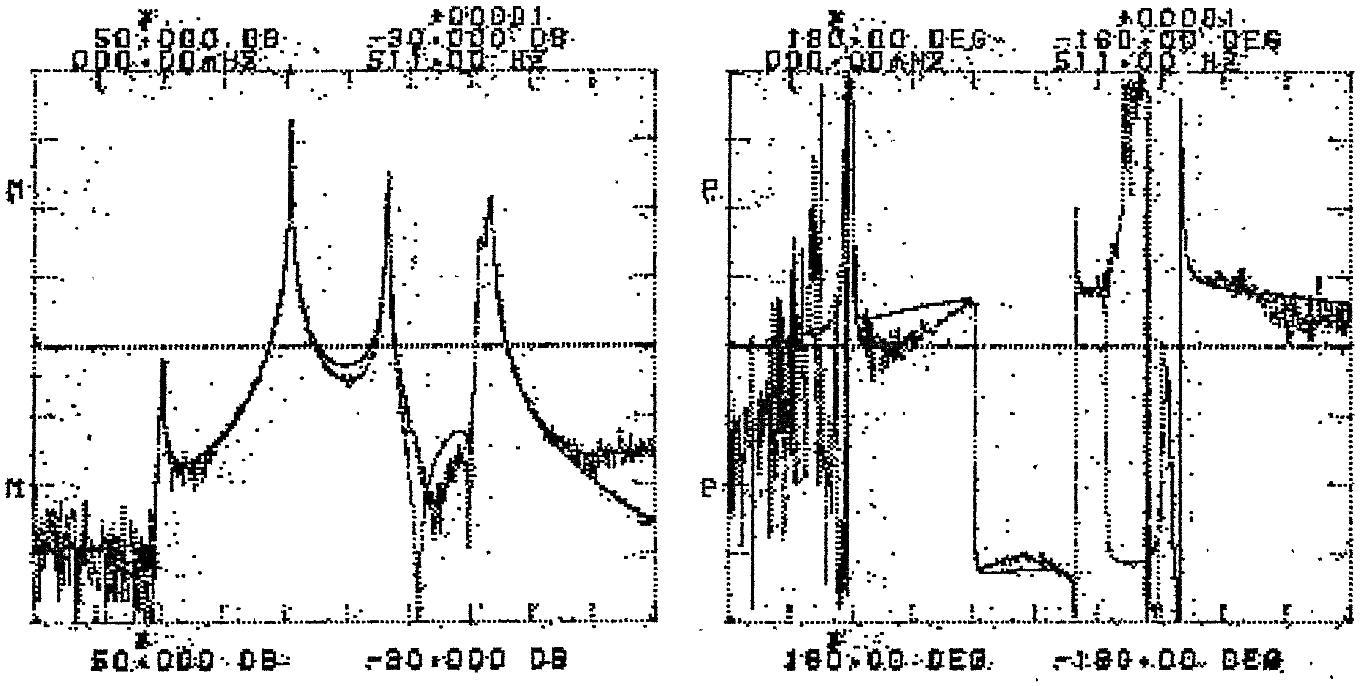

FRF a^*_{16}

Figure 6.14

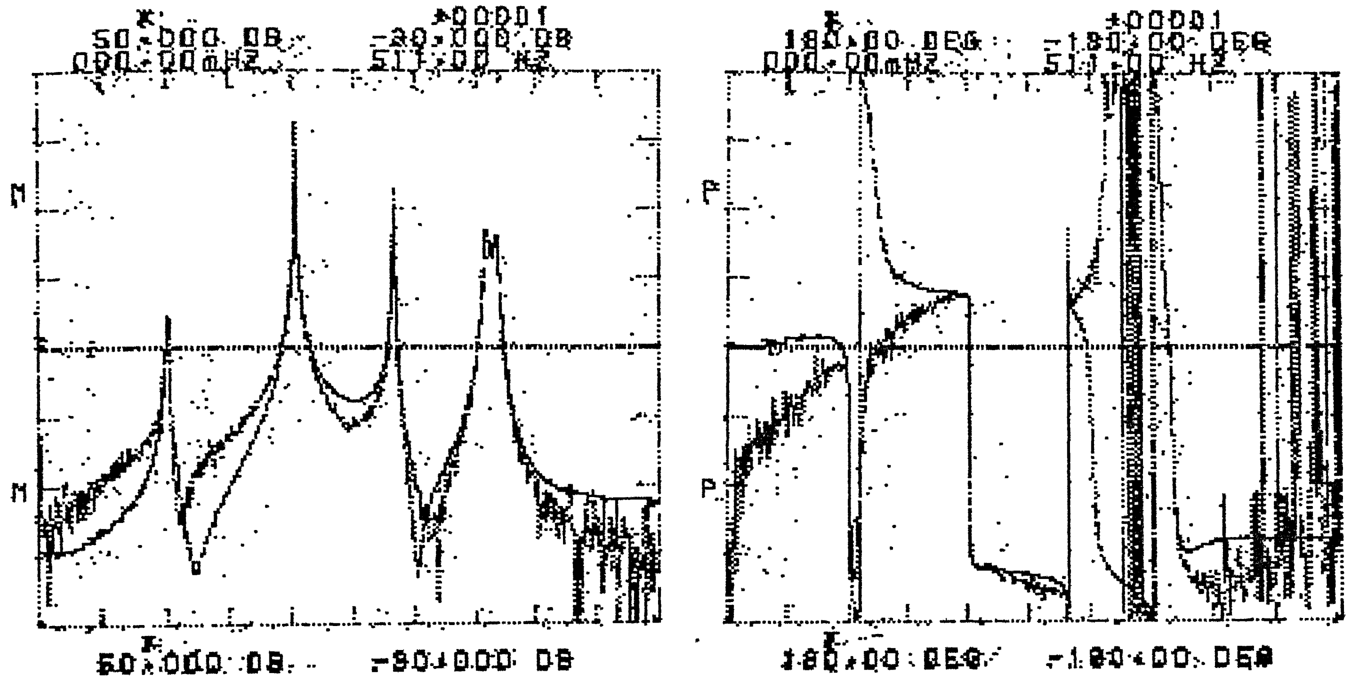

FRF a^*_{1-10}

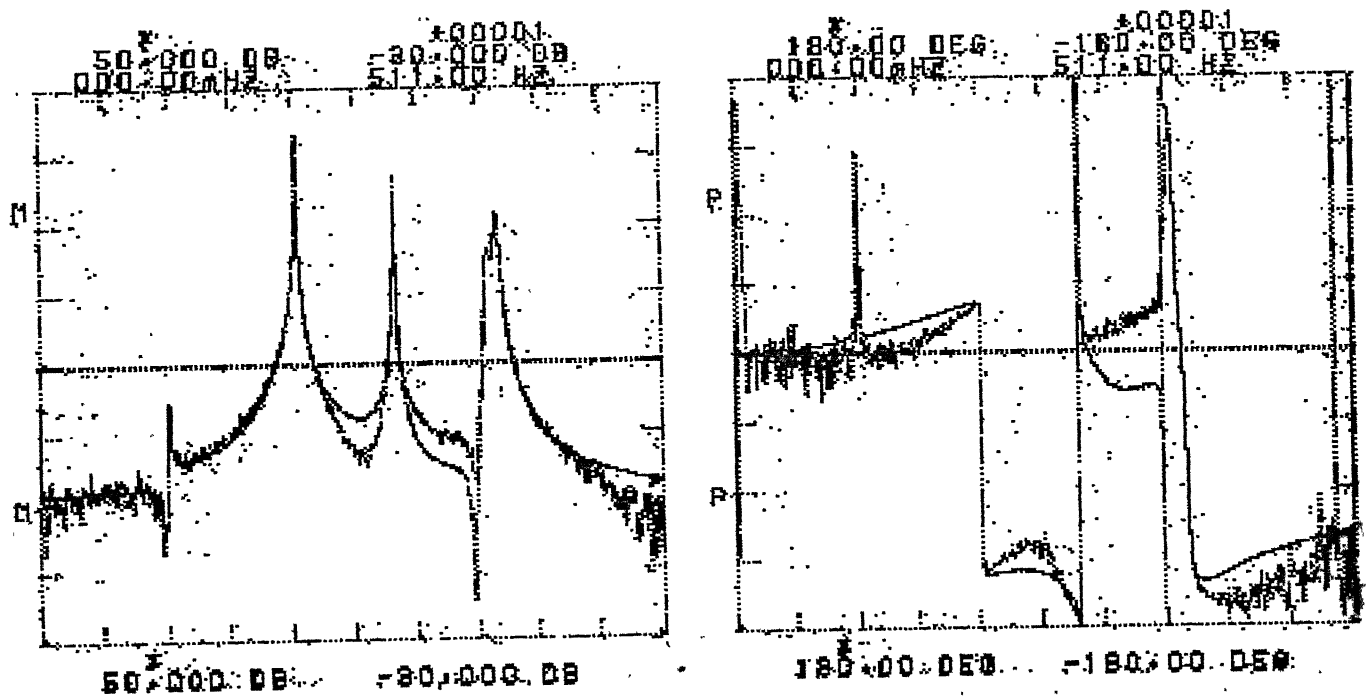

FRF a^*_{1-11}

Figure 6.14

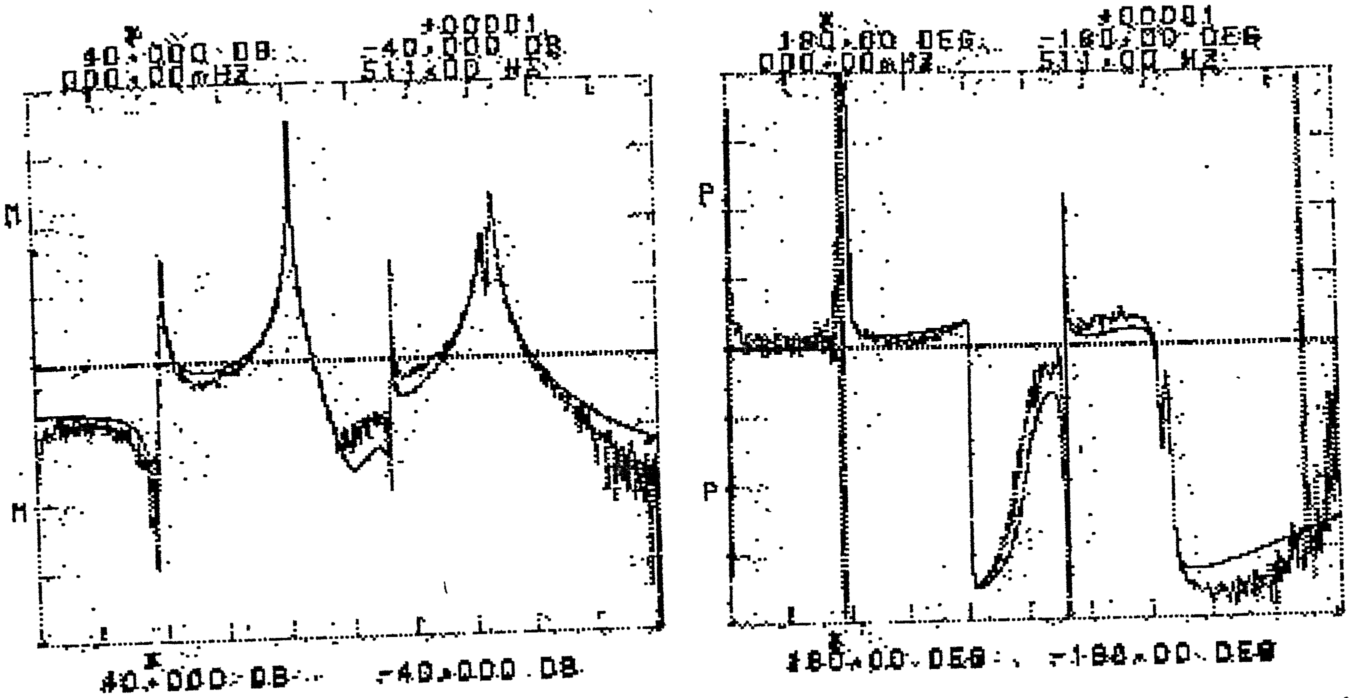

FRF a^*_{1-12}

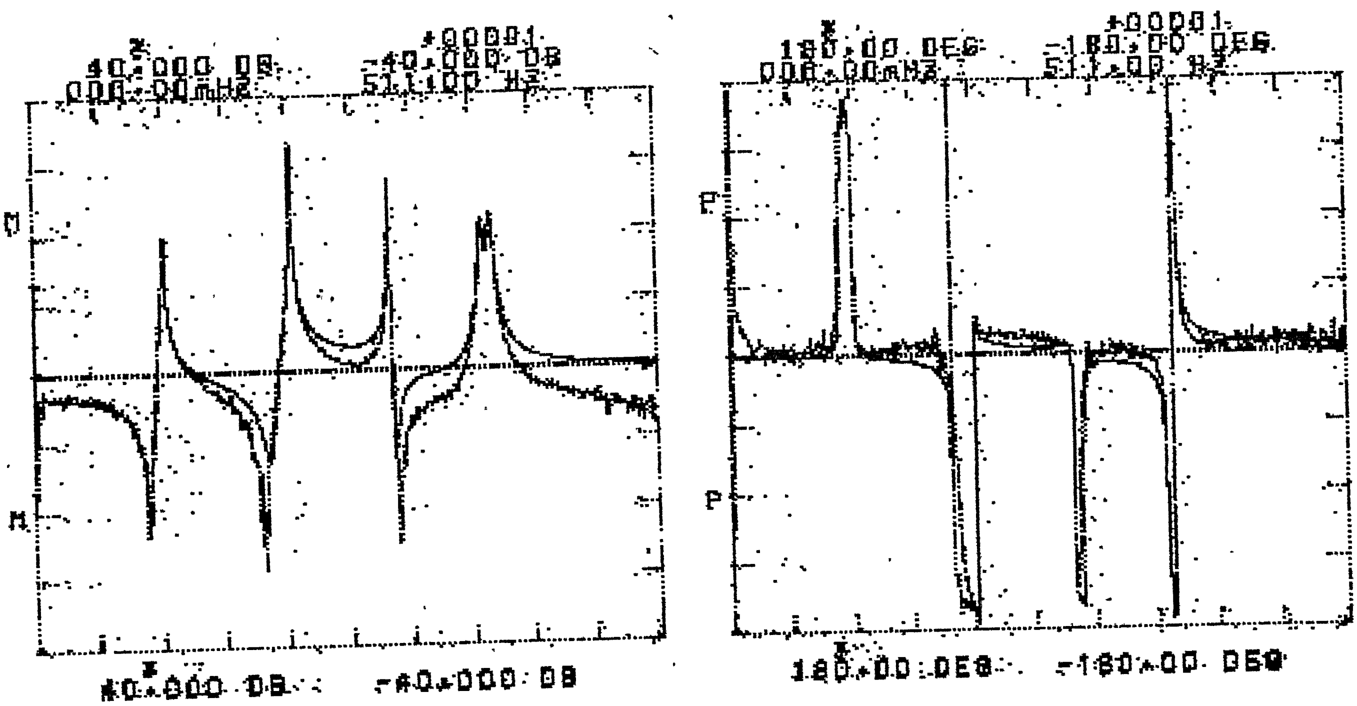

FRF a^*_{1-13}

Figure 6.14

using the relation

$$ {}_r\phi_j^* = {}_rA_{jk}^* \,/\, {}_r\phi_k^* \qquad (6.6) $$

using (6.6) above, all the elements of $[\phi^*]$ can be calculated.

These elements of the eigen matrix are calculated from the previously obtained modal parameters using SDF circle fit method combined with MDF curve fit method. This eigen matrix is given in Table 6.9. The average of natural frequencies and damping obtained for the thirteen FRFs for the five modes are given in Table 6.10.

The eigen matrix $[\phi^*]$ is complex indicating that the motion is not 'Synchronous' in a damped system. Since the imaginary parts are relatively small compared to the real part, the mode shapes are drawn using only the real parts of $[\phi^*]$ considering a synchronous motion. These mode shapes are shown in Fig. 6.15.

On comparing these mode shapes with that of the mode shapes obtained when the included angles are 68° and 112° (Fig. 6.5), one finds that all the five mode shapes are similar for both cases.

6.4 Coupling of Structures by Impedance Coupling Method

The method outlined in Chapter 4 has been applied to the coupling of two substructures - a beam and a 'U' shaped structure. These two substructures and the resulting coupled structure are shown in Fig. 6.16. The coupling of the two

Table 6.9 : Mode Shape Vectors for Jointed Structure

Mode 1

Real Part	Imaginary Part
0.3135	0.00
-0.0979	-0.0082
-0.4364	0.0421
-0.2758	0.0728
-0.1816	-0.0066
0.1193	0.0257
0.3502	0.0053
0.1240	0.0231
-0.0233	-0.0613
-0.2767	-0.013
0.0616	0.0079
0.2714	0.0458
0.5161	-0.0304

Mode 2

0.6115	0.00
0.5684	0.3365
0.3317	-0.00796
-0.4184	-0.0826
-0.8017	-0.3957
-0.7577	-0.4656
0.4677	0.08875
0.6717	0.0606
0.7332	0.4822
-0.4384	-0.3121
-0.6328	-0.4186
-0.3598	-0.1236
0.2647	0.060

Mode 3

0.2787	0.00
0.3431	0.1377
-0.2222	-0.4765
0.1183	0.0408
0.5357	0.2585
0.5587	0.3894
0.0583	-0.1268
0.3181	0.0480
0.3752	0.1875
0.2932	0.1285
0.4122	-0.0482
0.0155	0.0035
-0.1589	-0.0313

Mode 4

0.3360	0.00
0.7448	0.271
0.1792	0.0045
-0.4063	-0.1327
-0.6329	-0.3172
-0.1548	-0.2363
-0.6002	0.5742
-0.8456	0.2825
0.5874	-0.5277
0.5435	0.2121
-0.1980	0.0903
0.2843	-0.0136

Continued....

Mode 5

0.3815	0.00
0.2587	-0.0224
-0.2996	-0.0185
0.1225	0.0308
0.6219	0.3059
0.7381	0.4981
-0.4521	0.1031
-0.3452	0.1162
-0.1957	-0.1541
-0.4472	-0.1989
-0.8431	-0.2131
-0.3033	-0.1358
0.2891	0.0367

Table 6.10 : Natural frequencies and damping loss factors of Jointed structure

Mode	Natural frequency (Hz)	Damping loss factor
1	103.51	0.013878
2	207.50	0.000773
3	288.67	0.002160
4	366.16	0.009186
5	375.11	0.009007

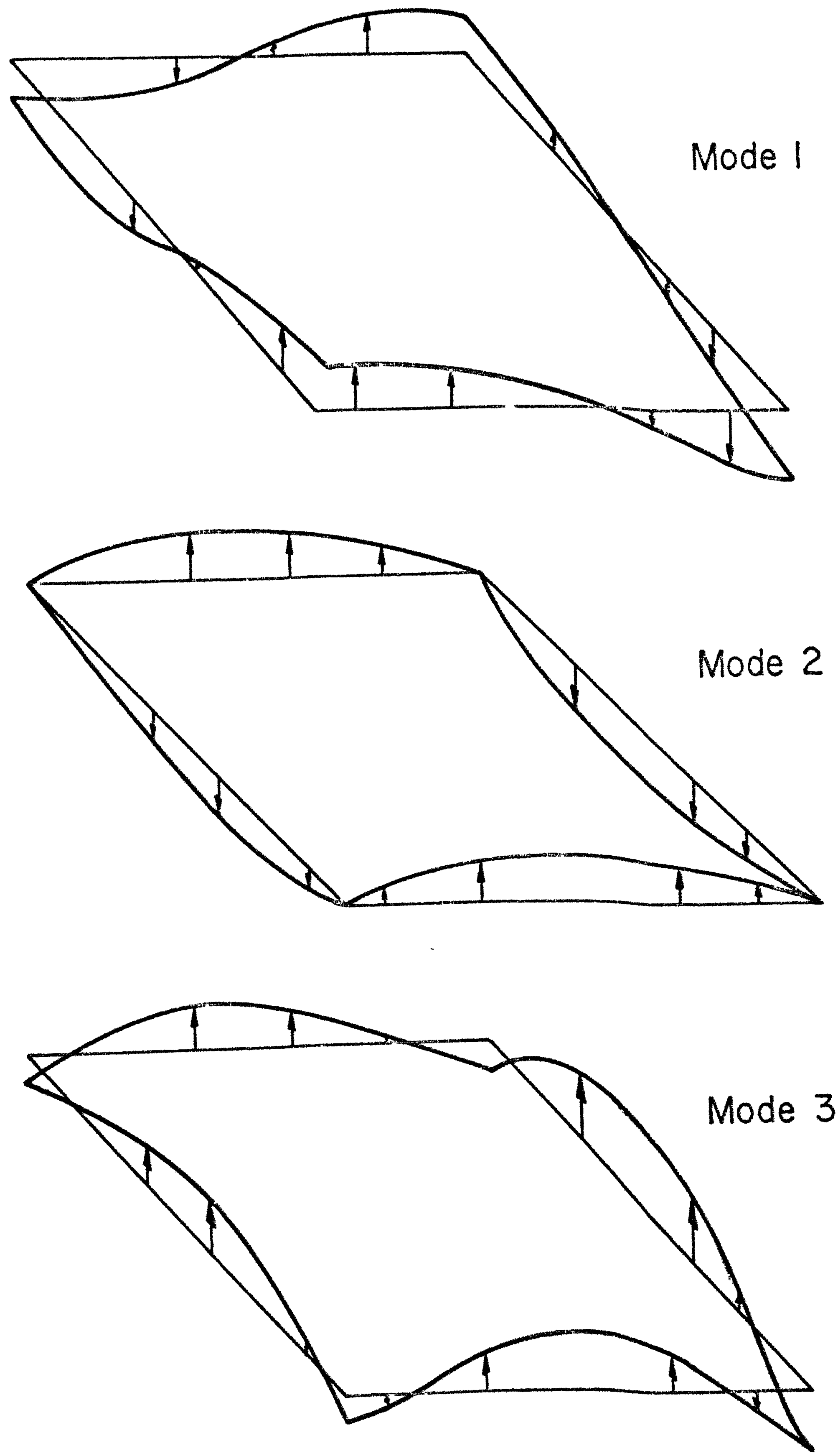

Fig.6.15(a) Mode shapes of jointed structure

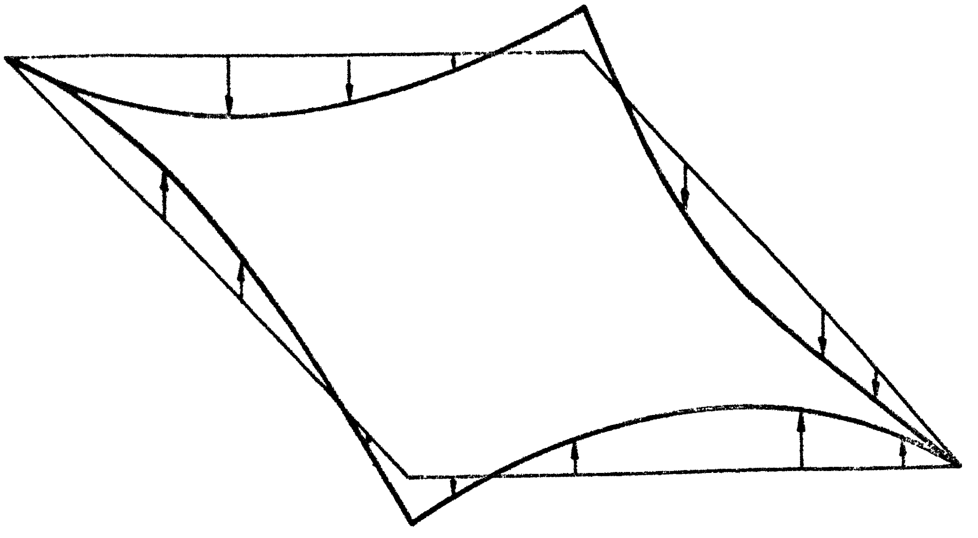

Mode 4

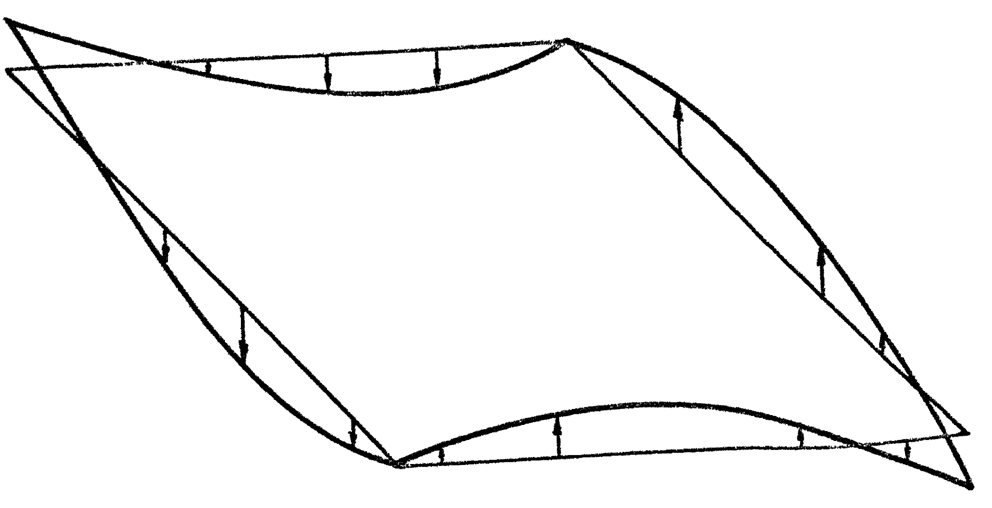

Mode 5

Fig.6.15(b) Mode shape of jointed structre

substructures was done using bolts. A nut was introduced between the two substructures to simulate the point contact within the experimental limits. Upto a frequency range of 2KHz, the beam exhibited four modes and the U-shaped structure two modes. The FRFs taken for analysing the beam were for the points ^{1}b, ^{2}b and ^{3}b shown in Fig. 6.16(a) and for the U-shaped structure the FRFs considered were for the points ^{1}U and ^{2}U shown in Fig. 6.16(b).

As a first step in the coupling procedure for these two substructures to be coupled at points 1 and 2, the FRFs were taken for each substructure separately. The beam thus requires six FRFs and the U-shaped structure requires three FRFs. The modal parameters for these two substructures were calculated using SDF circle fit method. Table 6.11 shows the parameters values for the beam and table 6.12 shows the same for the U-shaped substructure. Figure 6.17 and Figure 6.18 show the regenerated FRFs for the beam and U-shaped structure, respectively. The measured FRFs are also shown in these figures. It is clear from Figs. 6.17 and 6.18, that the regeneration is satisfactory and the modal parameters estimated are acceptable.

The next step requires calculation of impedance as a function of frequency for each substructure by using (4.9). The receptance values for this step are taken from the regenerated FRF rather than the experimentally measured FRF. This is to avoid the noise present in the experimental FRF.

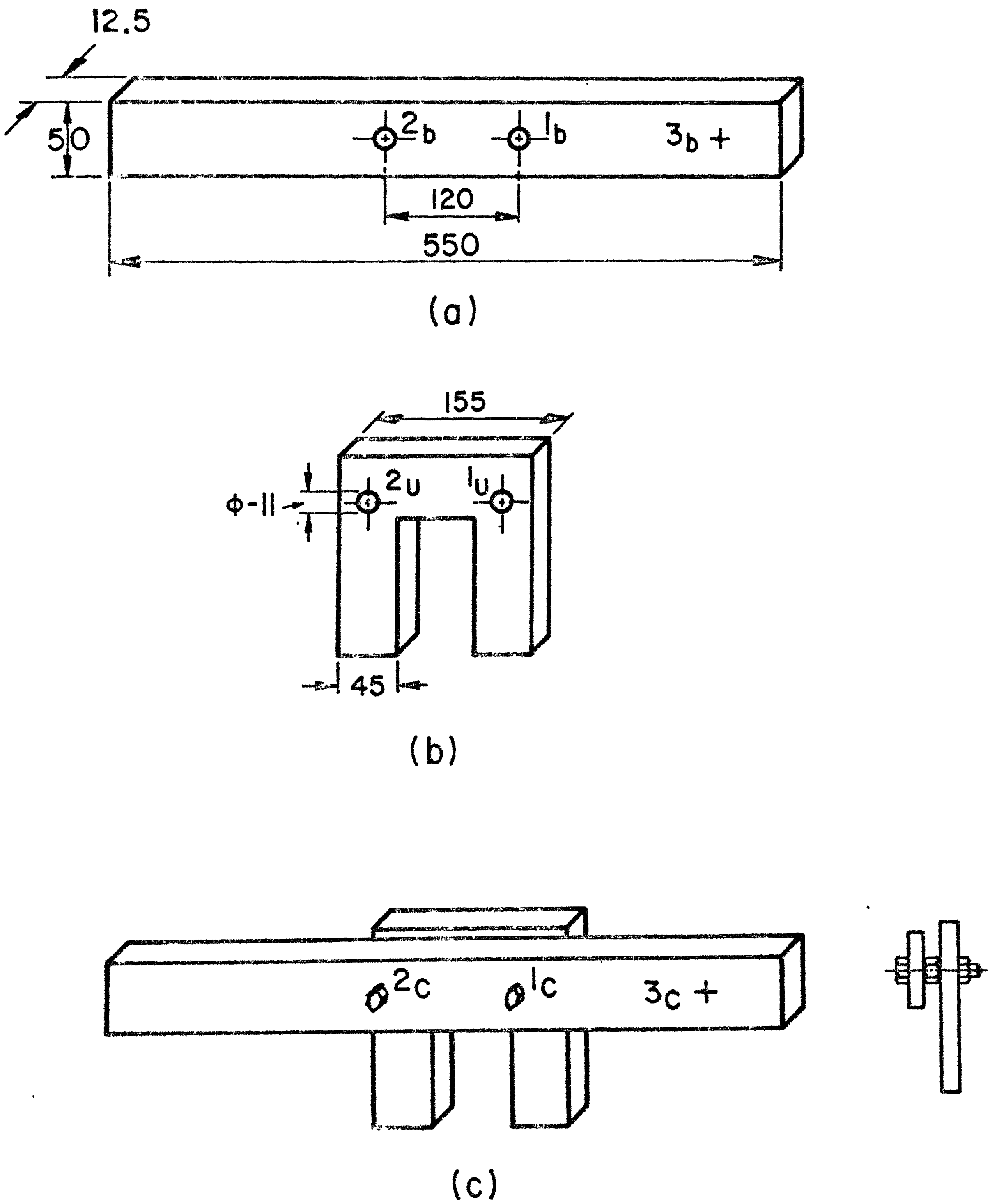

Fig.6.16 Coupling of two substructures

Table 6.11 : Parameters for sub-structure-beam

FRF	Mode	Natural frequency	Damping loss factor	Real part of modal constant	Imaginary part of modal constant
a^*_{11}	1	201.383	0.000946	0.2466	-0.1013
	2	558.469	0.000611	0.1717	0.0689
	3	1098.083	0.00105	0.09941	0.0195
	4	1778.787	0.01024	0.3385	0.00995
a^*_{12}	1	201.361	0.001235	0.31314	-0.1643
	2	558.451	0.00066	-0.2153	-0.0577
	3	1098.204	0.00080	0.0924	0.03315
	4	1774.282	0.00729	-0.3018	-0.1031
a^*_{13}	1	201.406	0.000599	-0.4255	0.188
	2	558.49	0.000680	-0.2839	-0.1045
	3	1098.52	0.00035	0.1240	0.0783
	4	1776.931	0.00283	0.1504	0.0728
a^*_{22}	1	201.458	0.000958	0.2327	-0.0606
	2	558.675	0.000389	0.11986	0.100
	3	1098.682	0.000169	0.07046	0.08312
	4	1781.887	0.001156	0.273	0.104
a^*_{23}	1	201.408	0.001297	-0.3825	0.1247
	2	558.71	0.000514	0.22574	0.1203
	3	1098.686	0.000162	0.1263	0.1203
	4	1781.800	0.00117	-0.2153	-0.1012
a^*_{33}	1	201.421	0.000659	0.1442	0.223
	2	558.63	0.000607	0.1262	0.153
	3	1098.542	0.00025476	0.089	-0.102
	4	1781.867	0.000953	0.132	-0.0137

Table 6.12 : Modal Parameters for the Substructure - U-shaped Structure

FRF	Mode	Damping	Natural frequency	Real part of ${}_{r}A_{jk}$	Imaginary part of ${}_{r}A_{jk}$
a^*_{11}	1	0.004024	661.6602	0.21719	-0.01314
	2	0.003569	1787.5457	0.05566	-0.01672
a^*_{12}	1	0.002613	661.2817	-0.26682	0.03679
	2	0.004865	1782.9799	0.10886	0.02460
a^*_{22}	1	0.002085	661.5231	0.19963	-0.01726
	2	0.006096	1782.6751	0.06809	0.02758

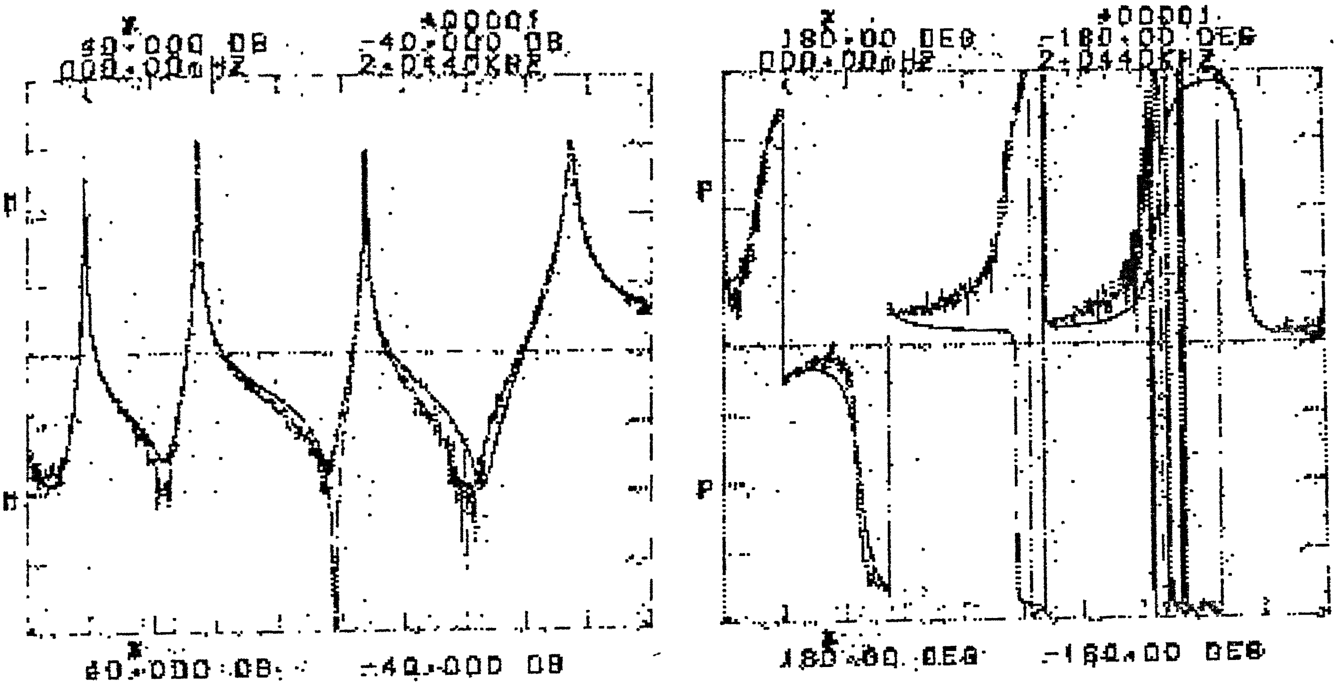

(a) FRF $a^*_{1_b 1_b}$

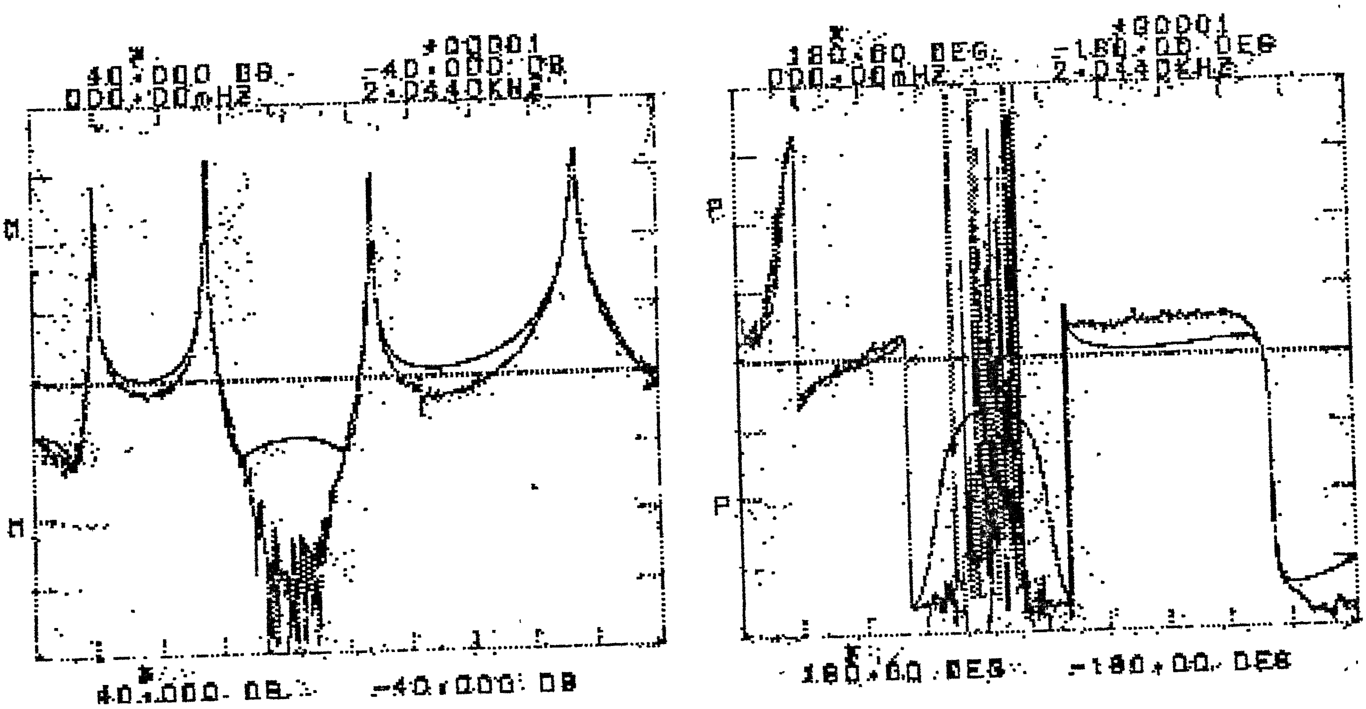

(b) FRF $a^*_{1_b 2_b}$

Figure 6.17: Measured and regenerated FRFs for substructure beam

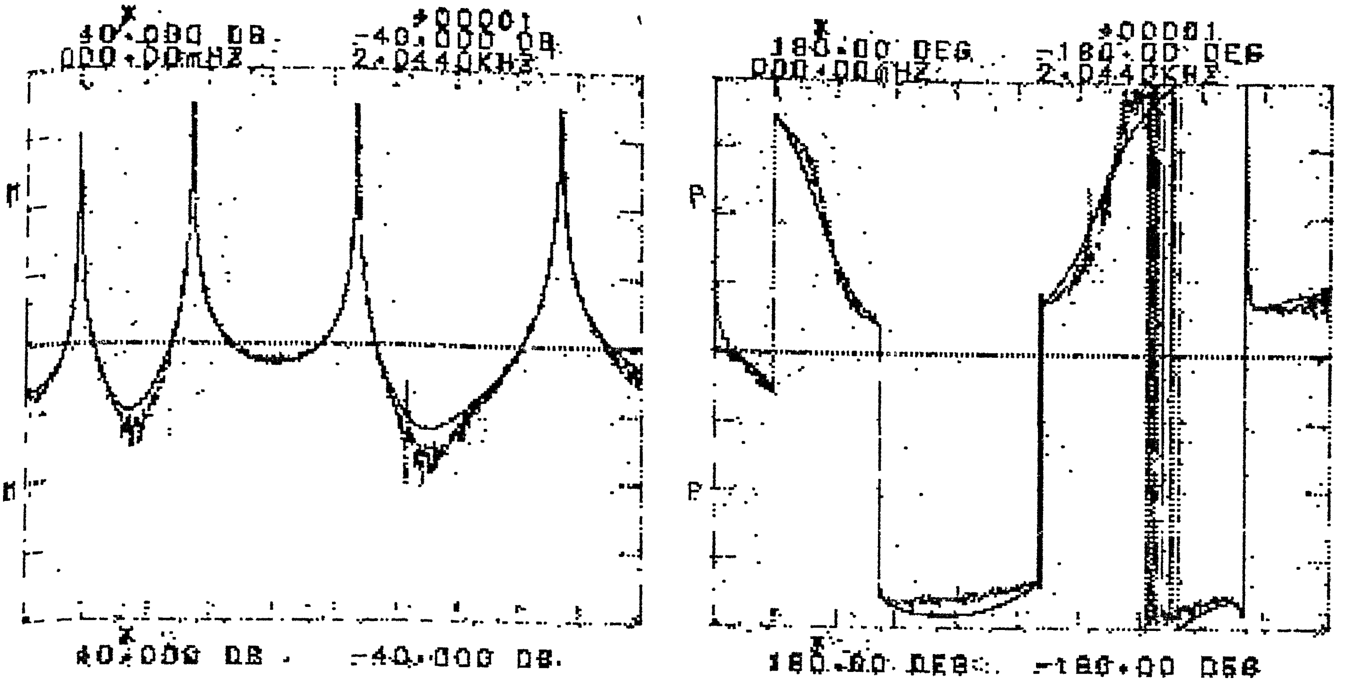

(c) FRF $a^*_{1_b 3_b}$

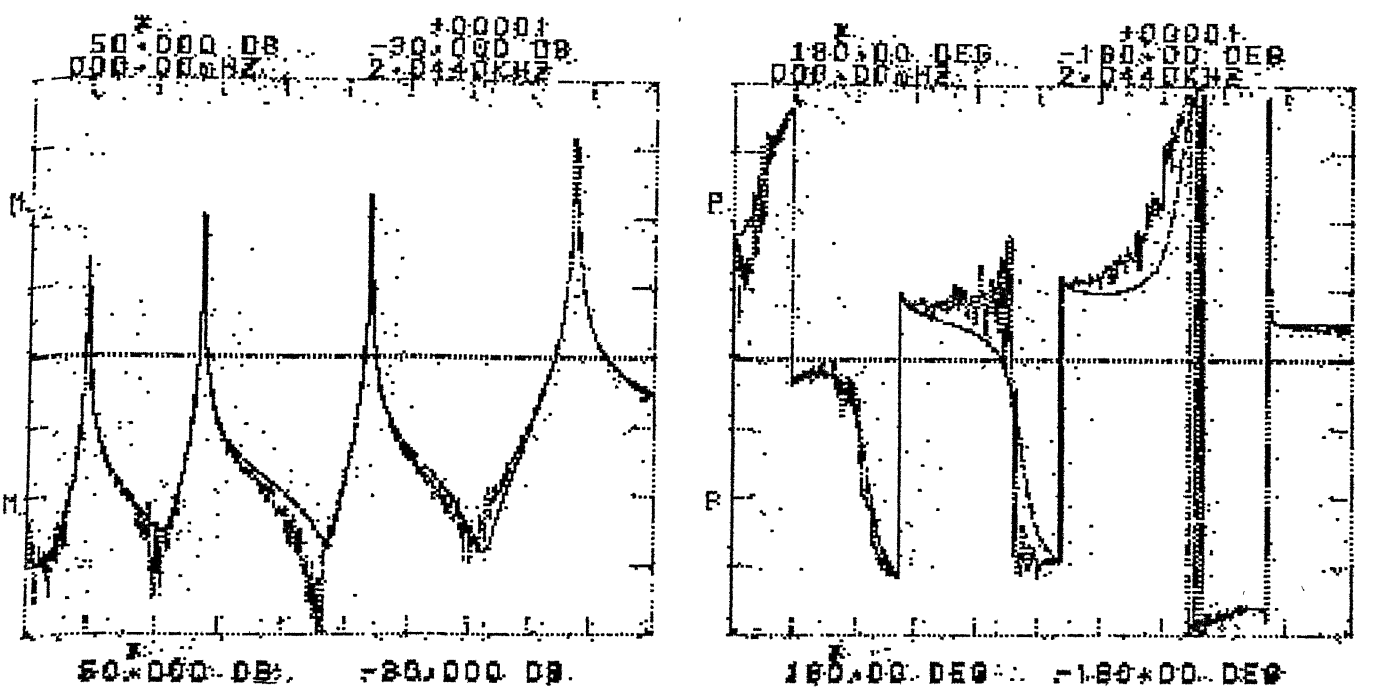

(d) FRF $a^*_{2_b 2_b}$

Figure 6.17

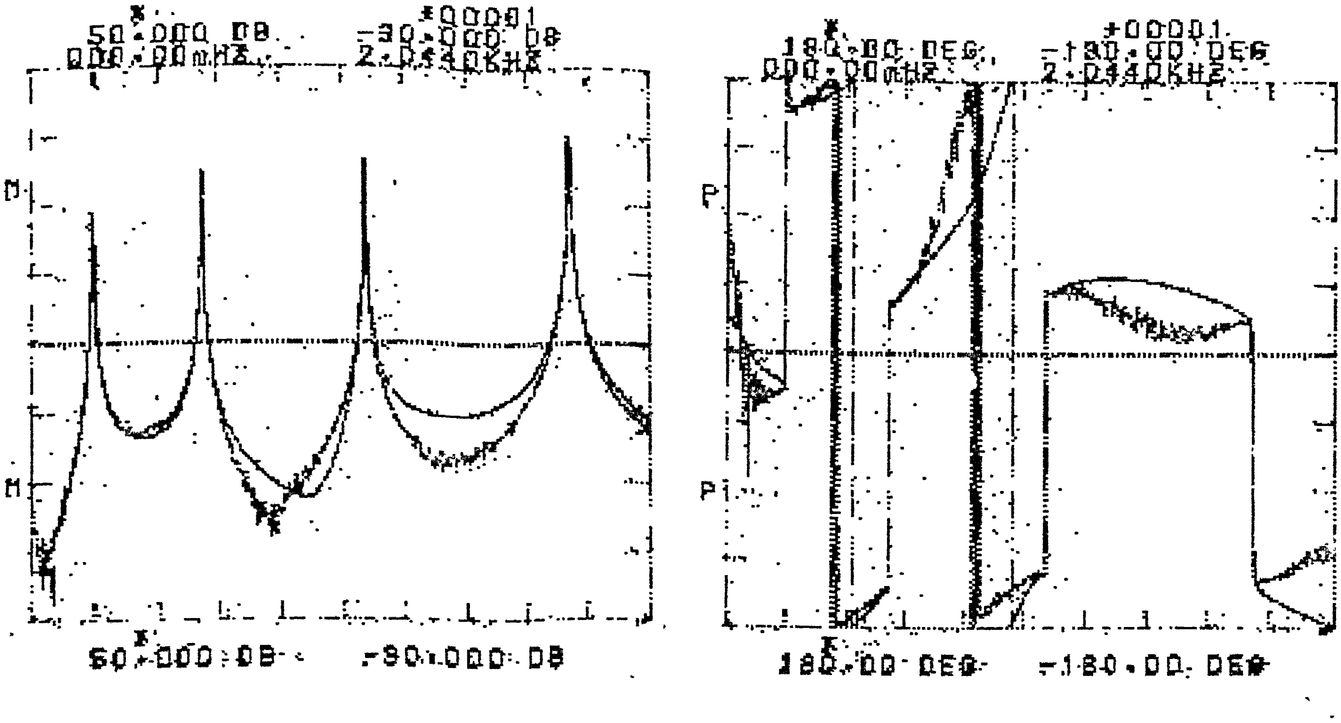

(a) FRF $a^*_{2_b 3_b}$

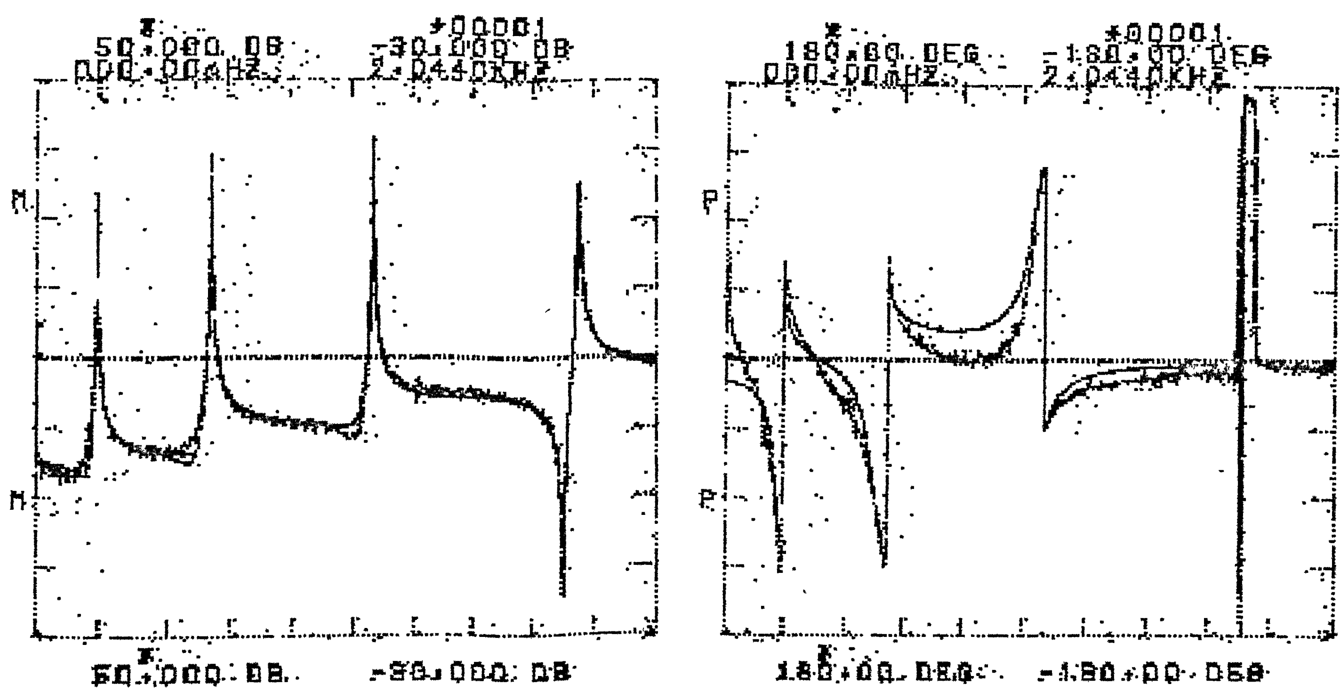

(b) FRF $a^*_{3_b 3_b}$

Figure 6.17

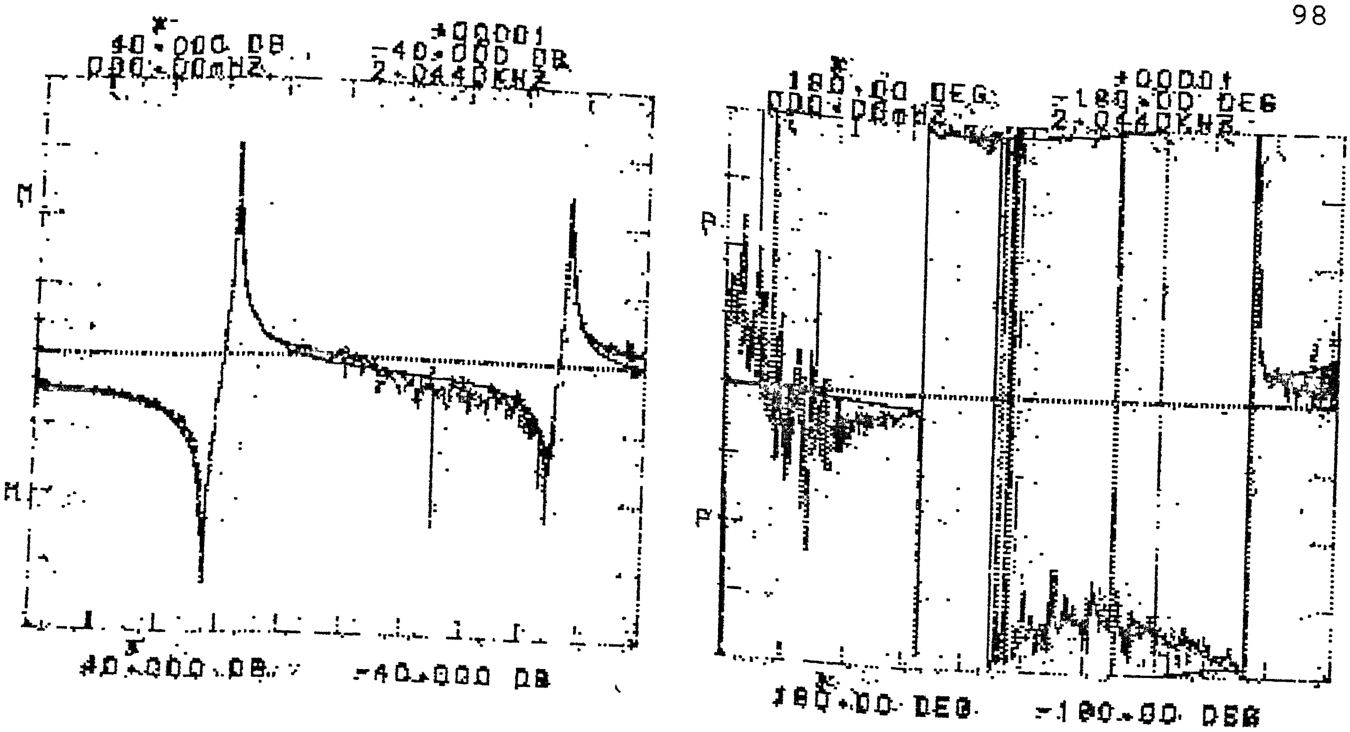

(a) FRF $a^*_{1_u 1_u}$

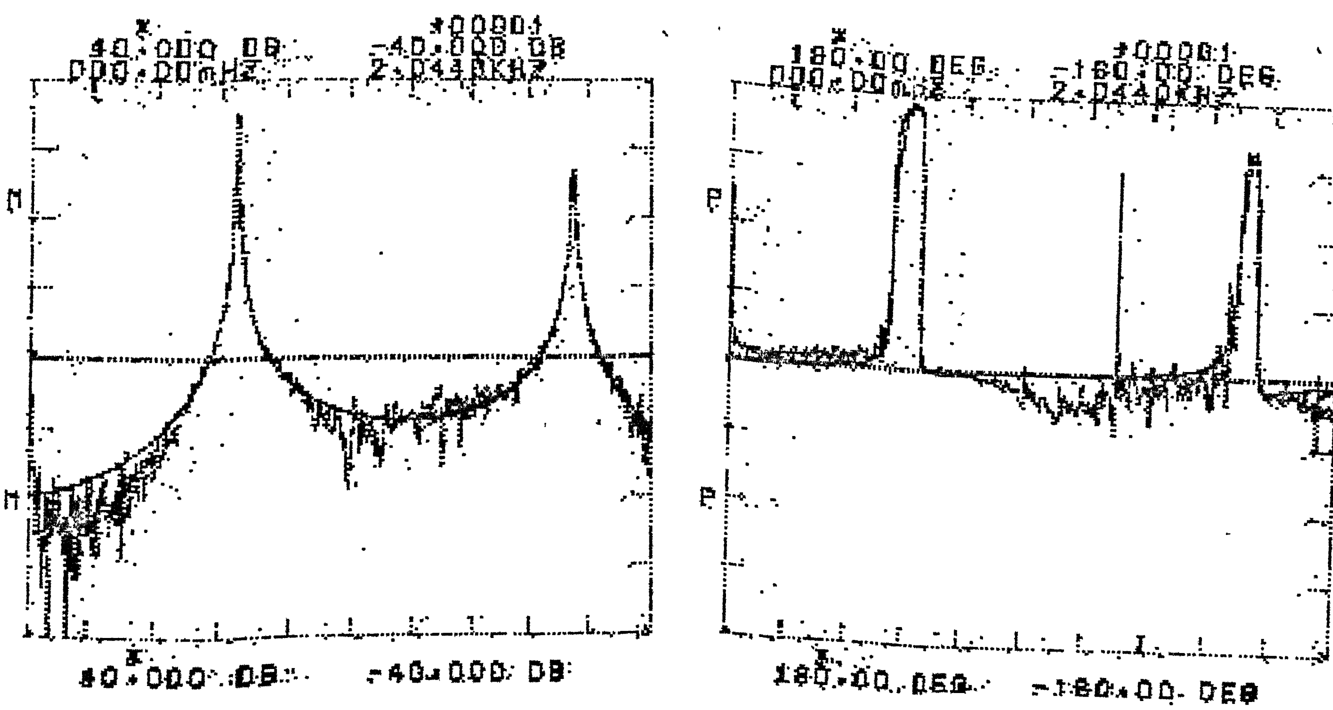

(b) FRF $a^*_{1_u 2_u}$

Figure 6.18 : Measured and regenerated FRFs of U-shaped substructure

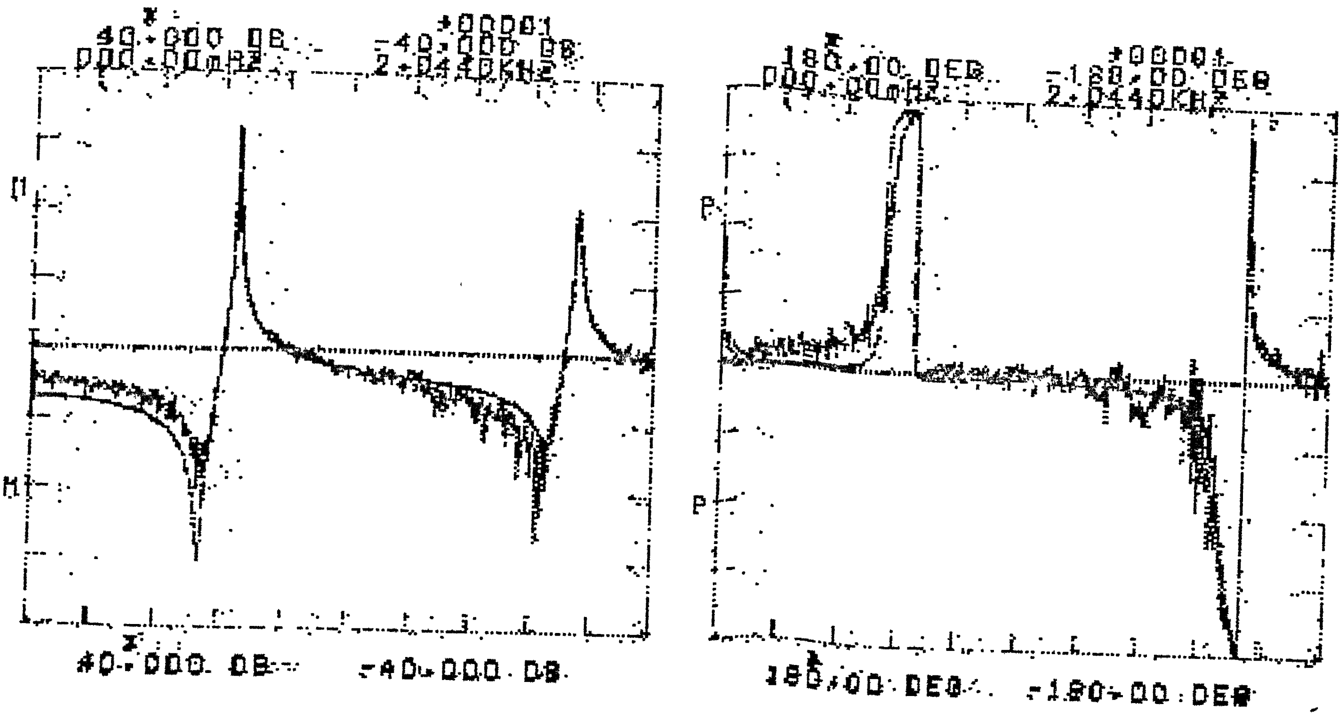

(c) FRF $a^*_{2_u 2_u}$

Figure 6.18

The impedance matrix of each substructure at a particular frequency is obtained by inverting numerically the receptance matrix of each substructure. The method adopted for obtaining this inversion of a complex matrix is given in Appendix D.

The impedance matrix for the beam is obtained by the expression given below:

$$[Z^*_B(\omega)] = [\alpha^*_B(\omega)]^{-1} = \begin{bmatrix} \alpha^*_{1_b1_b} & \alpha^*_{1_b2_b} & \alpha^*_{1_b3_b} \\ \alpha^*_{2_b1_b} & \alpha^*_{2_b2_b} & \alpha^*_{2_b3_b} \\ \alpha^*_{3_b1_b} & \alpha^*_{3_b2_b} & \alpha^*_{3_b3_b} \end{bmatrix}^{-1}_{\text{at frequency } \omega} \tag{6.7}$$

and the impedance matrix for the U-shaped structure, $[Z^*_u(\omega)]$ is given by

$$[Z^*_u(\omega)] = [\alpha^*_u(\omega)]^{-1} = \begin{bmatrix} \alpha^*_{1_u1_u} & \alpha^*_{1_u2_u} \\ \alpha^*_{2_u1_u} & \alpha^*_{2_u2_u} \end{bmatrix}^{-1}_{\text{at frequency } \omega} \tag{6.8}$$

The impedance coupling is done by using (4.11) and is

$$[\, Z_C^*(\omega) \,] = [\, Z_B^*(\omega) \,] + [\, Z_U^*(\omega) \,]$$

$$= \begin{bmatrix} Z^*_{1_b1_b} + Z^*_{1_u1_u} & Z^*_{1_b2_b} + Z^*_{1_u2_u} & Z^*_{1_b3_b} \\ Z^*_{2_b1_b} + Z^*_{2_u1_u} & Z^*_{2_b2_b} + Z^*_{2_u2_u} & Z^*_{2_b3_b} \\ Z^*_{3_b1_b} & Z^*_{3_b2_b} & Z^*_{3_b3_b} \end{bmatrix} \tag{6.9}$$

The receptance matrix for the combined structure is obtained by the inversion of the impedance matrix of (6.9).

$$[\, \alpha_C^*(\omega) \,] = [\, Z_C^*(\omega) \,]^{-1} \tag{6.10}$$

As an example, the values of receptances for the two substructures and the coupled structure at a frequency of 100 Hz is listed in Table 6.13. The receptances for the coupled structure are obtained as point and transfer receptances for the location points 1, 2 and 3. Thus six FRFs of the coupled structure obtained using (6.10) are the plotted in Fig. 6.19, along with the measured FRFs obtained experimentally.

Table 6.13 : Values of Receptances and Impedances of Substructures and Coupled Structure at a Frequency of 100 Hz

(i) Substructure Beam

Receptance:

FRF	Real part	Imaginary part
11	-1.134E-05	3.081E-06
12	-2.188E-06	5.599E-06
13	6.066E-05	-1.559E-06
22	-1.559E-05	1.592E-06
23	8.137E-06	-4.549E-06
33	-1.021E-04	-4.761E-06

Impedance:

FRF	Real part	Imaginary part
11	-2.09E-04	-4.393E-06
12	1.055E-04	-9.429E-05
13	1.198E-04	8.321E-06
22	-6.185E-04	8.295E-06
23	-9.855E-06	3.343E-05
33	2.556E-05	7.572E-08

Continued......

Table 6.13 (Continued):

(ii) Substructure - U-shaped structure

Receptance:

FRF	Real part	Imaginary part
11	5.322E-05	3.812E-08
12	1.165E-05	-9.542E-08
22	4.357E-05	3.280E-08

Impedance:

FRF	Real part	Imaginary part
11	1.996E-04	-3.64E-07
12	-5.335E-05	5.747E-07
22	2.438E-04	-4.541E-07

(iii) Coupled Structure

Impedance:

FRF	Real part	Imaginary part
11	-9.434E-06	-4.757E-06
12	5.214E-05	-9.371E-05
13	1.198E-04	8.321E-06
22	-3.747E-04	7.841E-06
23	-9.855E-06	3.343E-05
33	2.556E-05	7.572E-08

Continued.....-

Table 6.13 (Continued):

Receptance:

FRF	Real part	Imaginary part
11	-1.263E-05	4.607E-06
12	-1.765E-06	1.065E-05
13	7.393E-05	-1.129E-05
22	-2.282E-05	2.483E-06
23	6.136E-06	-1.859E-05
33	1.908E-05	1.361E-05

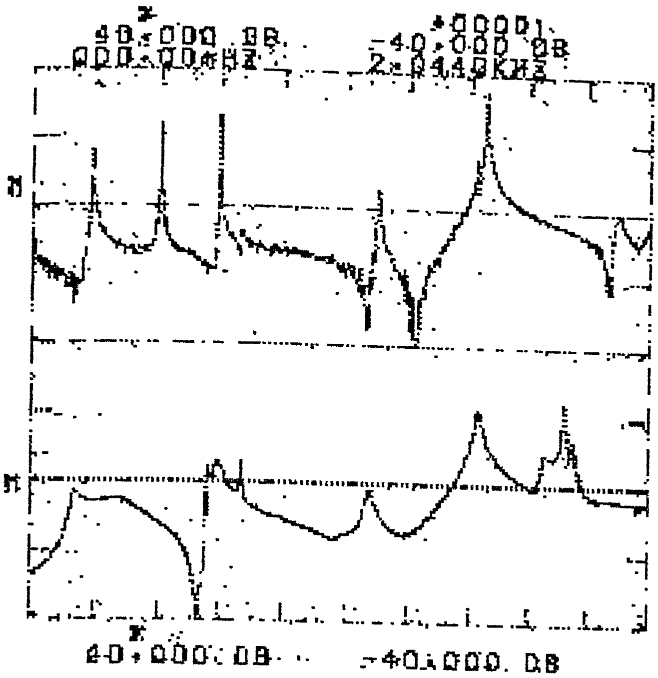

(a) FRF $|a^*_{1_c 1_c}|$

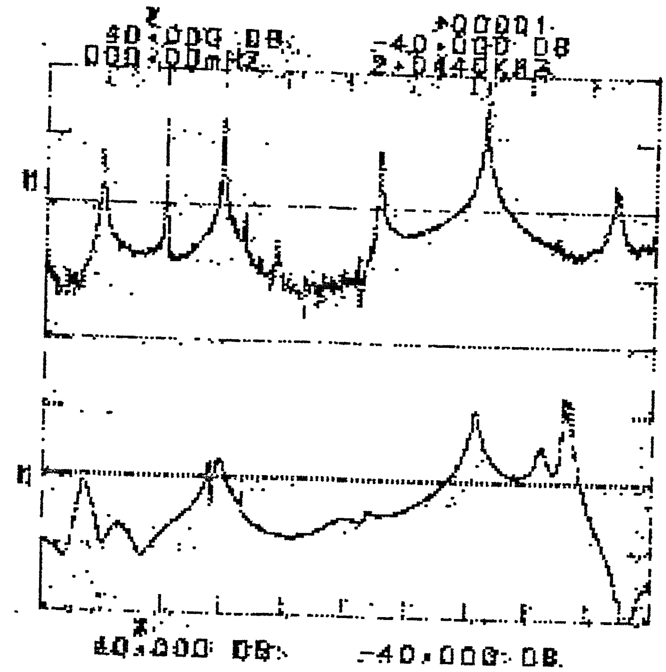

(b) $|a^*_{1_c 2_c}|$

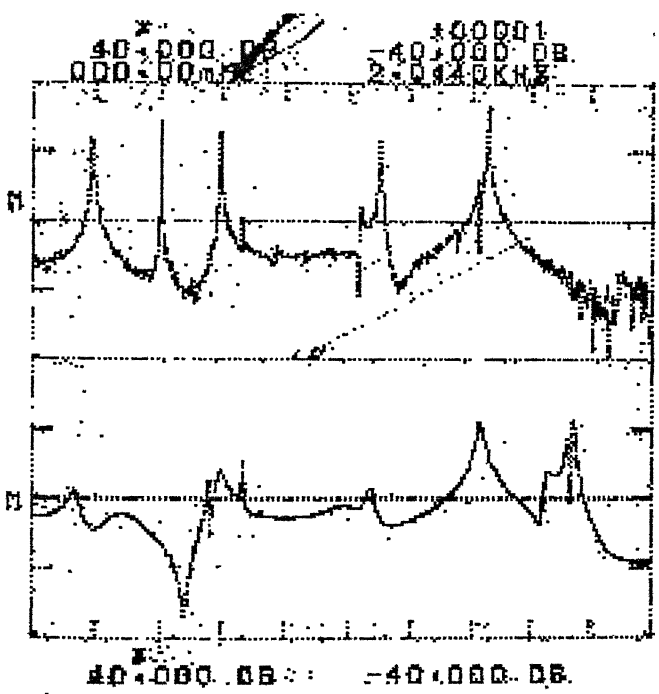

(c) $|a^*_{1_c 3_c}|$

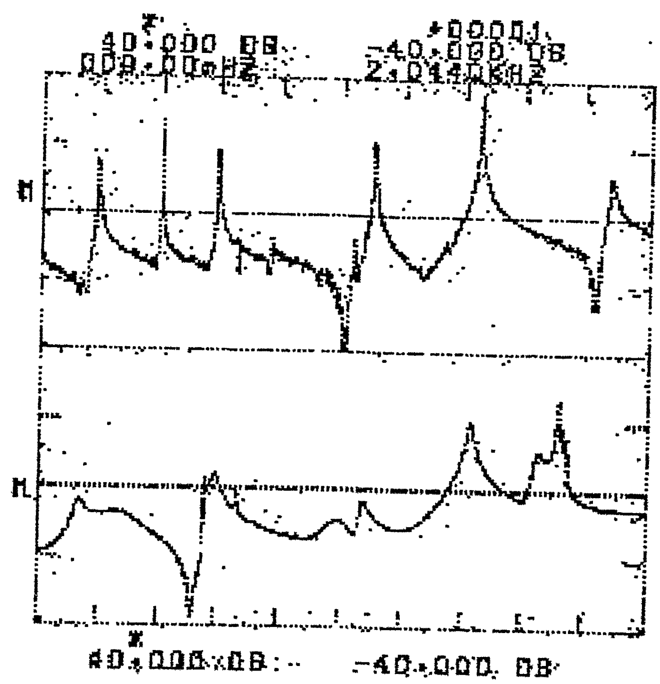

(d) $|a^*_{2_c 2_c}|$

Fig.6.19 : Measured and predicted FRF's of coupled structure

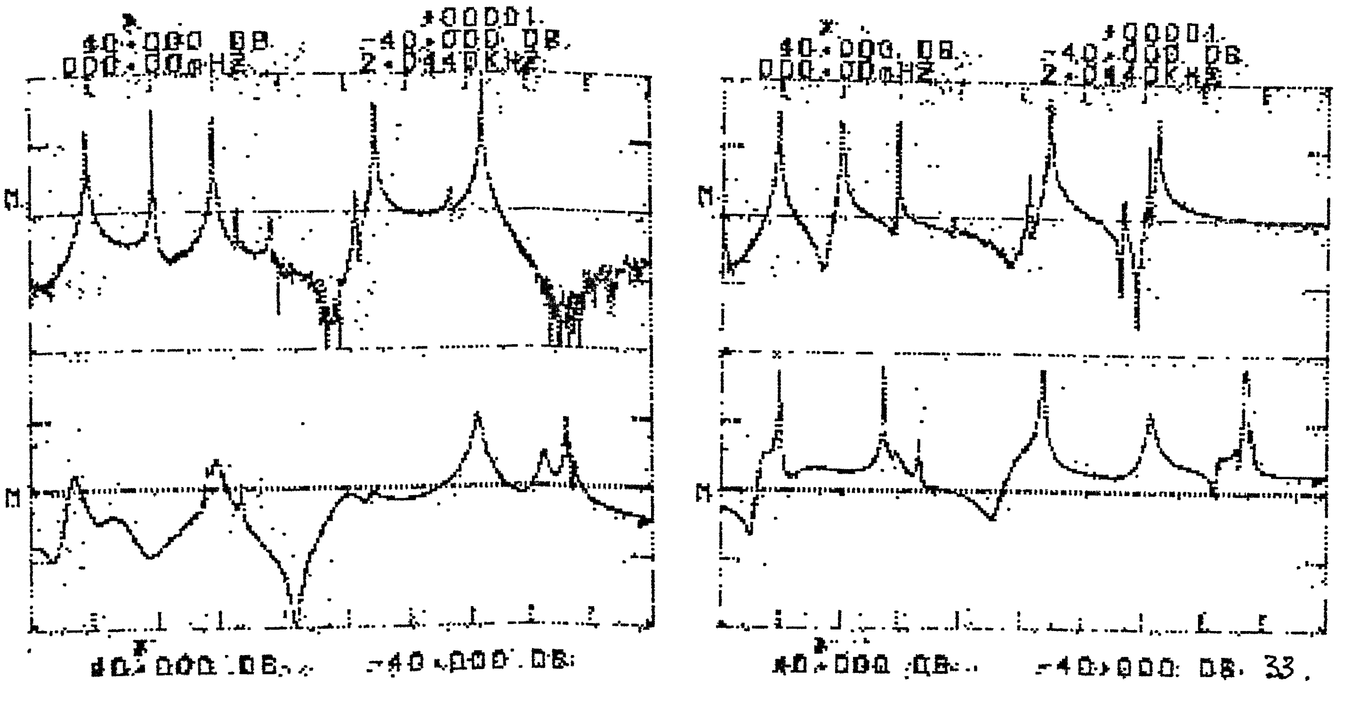

(e) $a^*_{2_c 3_c}$ (f) $a^*_{3_c 3_c}$

Figure 6.19.

Figure 6.20 shows the theoretical FRF, $|a_{11}^{*}|$, superimposed on the experimental FRF. The theoretical results do not exactly coincide with the experimental results for the coupled structure, but the overall nature of theoretical FRF is acceptable. As a comparison, the theoretical and experimental results obtained in [8] are reproduced in Fig. 6.21.

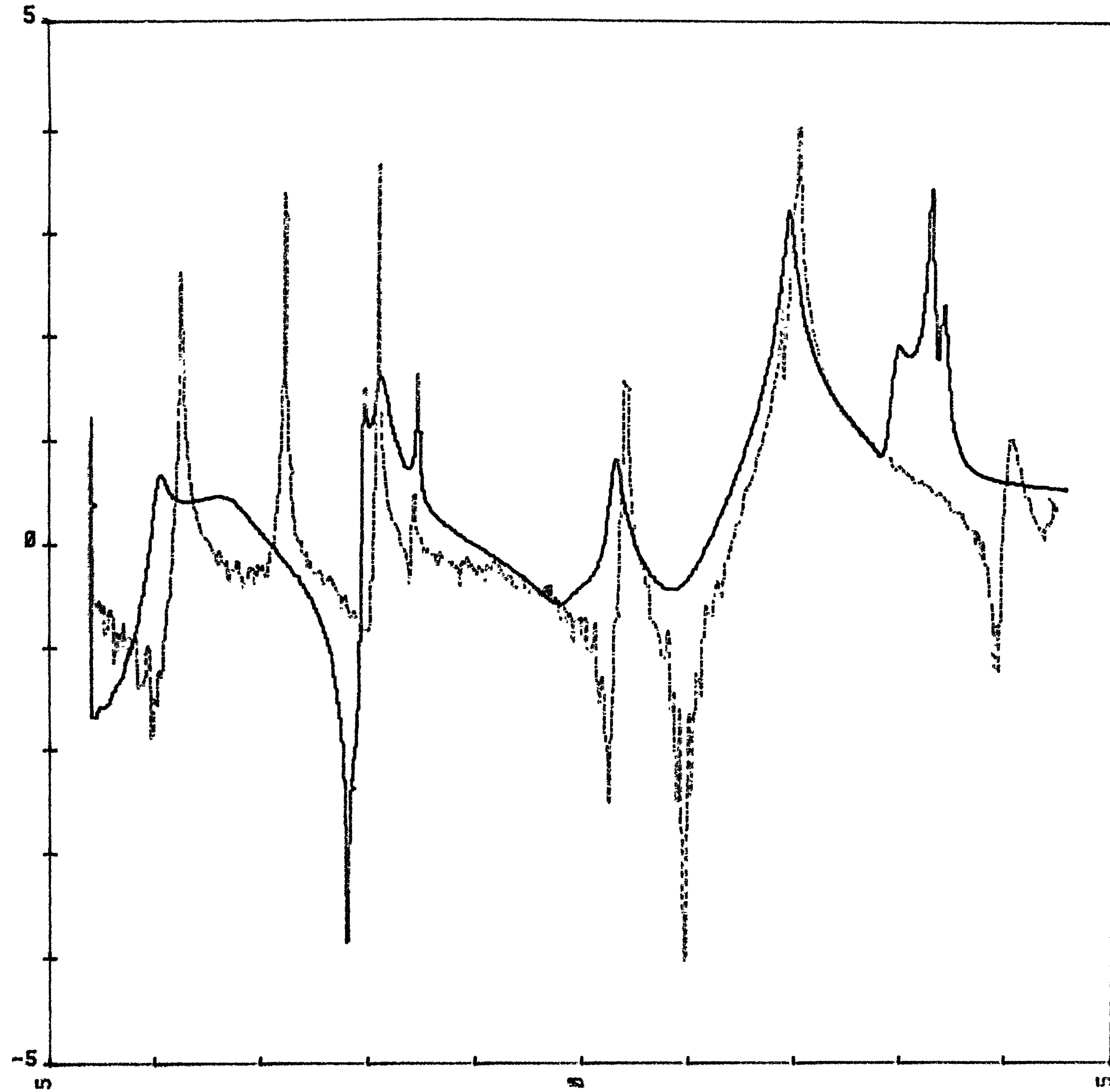

TITLE	COUPLE 11	
DATE TIME	88/10/14 00:01	
SAMPLE RATE	20m?	
MANUAL TRIG.	NORMAL	
CH	1	2
RANGE	10V	10V
OFFSET	50 %	50 %
COUPLE	DC	DC
ZOOM	* 1	* 1
CALC.		
CH 1	MAX. 4.55V MIN. -4.62V	
CH 2	MAX. 3.44V MIN. -3.86V	

COMMENT

Fig.6.20: Measured and predicted FRF, $|a^{*}_{1_c 1_c}|$ of coupled structure

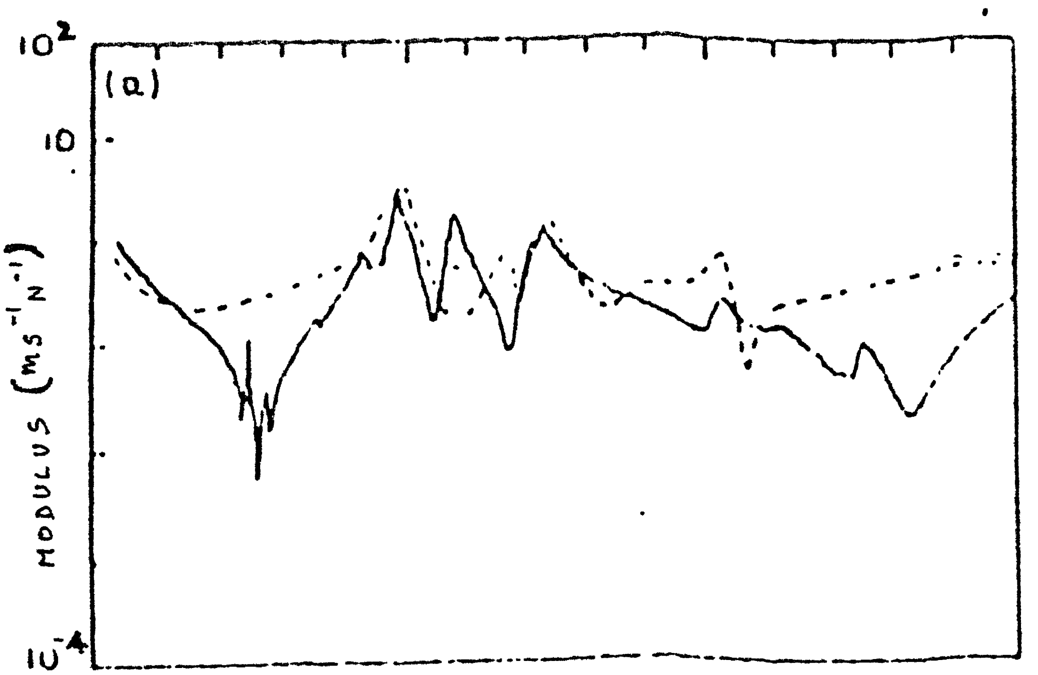

Fig. 6.21 : Measured and Predicted FRF (Reproduced from [8]).

CHAPTER - 7

CONCLUSIONS

The SDF circle fit method for modal parameter extraction is simple and requires little computation time. The present work has tried to identify the cases, where this SDF method does not yield acceptable results. These cases corresponded to system with high damping and system with closely placed natural frequencies. If the two closely placed modes are of equal strength and are highly damped then the circle fit method is still capable of generating good estimates of modal parameters. Otherwise, MDF curve fit method was found to be necessary to obtain the acceptable estimates of the modal parameters.

For the heavily damped system, the MDF method, which is iterative in nature, was observed to converge monotonically to the correct solution. For the other case of a lightly damped structure with two closely placed modes with one mode being predominant over the other, the MDF method was found to be stable in only a narrow zone around the actual solution. This prompted the idea of reducing the incremental change vector ($\{\delta k\}$ of (6.1)) by a factor ε so that the new estimates also lie in the stable zone.

If all the modal parameters are attempted to be modified by the MDF curve fit, the curve fit being done over the entire frequency range is very time consuming. Instead, it is suggested that the MDF curve fit may be used only for the modal parameters corresponding to closely placed modes and the curve fit should be done only over the frequency range encompassing the two modes. For all other modes, the circle fit method is acceptable.

This work also attempted to verify the theory of impedance coupling to predict the response of a coupled structure, when the responses of the individual substructures are known. The predicted responses, though observed to be similar in nature with the experimental responses, were not exhibiting complete informations about the modal parameters corresponding to some of the modes observed in experimental response. This may be attributed to the fact that i) the rotational coordinates at the coupling points were not included, and ii) the coupling was idealized to be a perfectly rigid one. With a proper model of coupling, the predicted responses are expected to be closer to the theoretical ones.

REFERENCES

1. EWINS D.J.
"Modal Testing : Theory and Practice"
Research Studies Press Ltd., 1986.

2. KENNEDY C.C. AND PANCU C.D.P.
"Use of Vectors in Vibration Measurement and Analysis"
Journal Aero. Sciences 14(11), 1947.

3. JASPAL SINGH
"Some Investigations of Modal Analysis Technique"
M.Tech. Thesis, IIT Kanpur, July 1988.

4. HALVORSEN W.G. AND BROWN D.L.
"Impulse Technique for Structural Frequency Response Testing".

5, ZAVERI K.
"Modal Analysis of Large Structures - Multiple Exciter Systems", Bruel and Kjaer Publication.

6. BRANDON J.A. AND COWLEY A.
"A Weighted Least Squares Method for Circle Fitting to Frequency Response Data".

7. GAUKROGER D.R., SKINGLE C.W. AND HERON K.H.
"Numerical Analysis of Vector Response Loci".
J. of Sound and Vibration, 29(3), 341-353, 1973.

8. GOYDER H.G.D.
"Methods and Application of Structural Modelling from Measured Structural Frequency Response Data"
J. of Sound and Vibration, 68(2), 209-230, 1980.

9. EWINS D.J. AND GLEESON P.T.
"A Method of Modal Identification of Lightly Damped Structures", J. of Sound and Vibration, 84(1), 57-79, 1982.

10. EWINS D.J., SILVA J.M.M., MALECI G.
"Vibration Analysis of a Helicopter Plus an Externally Attached Structure".
Shock and Vibration Bulletin 50, Part 2, 155-171, Sept. 1980.

11. FRITZEN P.T.
"Identification of Mass, Damping and Stiffness Matrices of Mechanical Systems"
J. of Vib. Acoustics, Stress and Reliability in Design, 108, 9-16, Jan. 1986.

12. G.T.S. DONE , A.D. HUGHES,
"The Response of a Vibrating Structure as a Function of Structural Parameters".
J. of Sound and Vibration, 38, 255-266, 1975.

13. G.T.S. DONE, A.D. HUGHES AND J. WEBBY
"The Response of a Vibrating Structure as a Function of Structural Parameters -- Application and Experiment".
J. of Sound and Vibration, 49, 149-159, 1976.

14. RANDALL R.B.
"Frequency Analysis"
Bruel and Kjaer Publication, Sept. 1977.

15. SVEND GADE AND HENRIK HERLUFSEN
"Use of Weighting Functions in DFT/FFT Analysis
(Part I and II).
Bruel and Kjaer Publication, No. 3, 1987.

APPENDIX A

LEAST SQUARES CIRCLE FITTING

Let real and imaginary parts of a point on the frequency response function is denoted x_k and y_k respectively. A number of points (say n) around a resonance is taken to fit a circle, using the equation given below:

$$\begin{bmatrix} \Sigma x_k^2 & \Sigma x_k y_k & \Sigma x_k \\ \Sigma x_k y_k & \Sigma y_k^2 & \Sigma y_k \\ \Sigma x_k & \Sigma y_k & n \end{bmatrix} \begin{Bmatrix} a \\ b \\ c \end{Bmatrix} = \begin{Bmatrix} -\Sigma(x_k^2 + y_k^2)\, x_k \\ -\Sigma(x_k^2 + y_k^2)\, y_k \\ -\Sigma(x_k^2 + y_k^2) \end{Bmatrix} \tag{A.1}$$

The summation in the above equation is for k = 1...n. Equation (A.1) is solved to obtain a, b and c . The radius (r) and the centre (x_c, y_c) of the fitted circle is given by

$$r = \sqrt{(a^2/4) + (b^2/4) - c} \tag{A.2}$$

$$x_c = -a/2$$

$$y_c = -b/2$$

Appendix - B

LEAST SQUARE ERROR MINIMISATION

The Least square error e is given by

$$e = \sum_{\substack{\text{over each}\\ \text{frequency}\\ \text{of interest}}} (\alpha_e^* - \alpha_m^*)\,(\bar{\alpha}_e^* - \bar{\alpha}_m^*) \tag{B.1}$$

where $\bar{\alpha}_e^*$ and $\bar{\alpha}_m^*$ are the conjugates of α_e^* (measured receptance) and α_m^* (mathematical receptance) respectively.

This error has to be minimised w.r.t. each of the parameters to be improved, k_i, $i = 1.....(4N+2)$.

$$\frac{\partial e}{\partial k_i} = -\sum (\alpha_e^* - \alpha_m^*)\frac{\partial \bar{\alpha}_m^*}{\partial k_i} + (\bar{\alpha}_e^* - \bar{\alpha}_m^*)\frac{\partial \alpha_m}{\partial k_i} = 0 \tag{B.2}$$

$$i = 1....(4N+2)$$

If ${}_rA_{jk}^* = F_r + iG_r$, then

$k_1 = 1/{}_RM_{jk}$

$k_2 = F_1$, $k_3 = G_1$, $k_4 = \eta_1$, $k_5 = \omega_1$

.

.

.

$k_{4N+2} = 1/{}_RK_{jk}$.

$$\text{If } F_i\,(k_1,\ k_2 \ldots\ldots k_{(4N+2)}) \quad = \quad \frac{\partial e}{\partial k_i} \tag{B.3}$$

then let

$$F_i\ (k_1' + \delta k_1,\ \ k_2' + \delta\ k_2, \ldots\ldots k'_{(4N+2)} + \ \delta k_{(4N+2)}) = 0 \tag{B.4}$$

k_j' $(j = 1 \ldots (4N+2))$ are the initial estimates of k_j and may be obtained by SDF methods. δk_j is small compared to k_j's for all j and is the value which are to be found henceforth.

By Taylor's theorem,

$$\begin{aligned} F_i(k_1' + \ \delta k_1,\ \delta k_2' + \ k_2, \ldots\ldots) &= F_i(k_1', k_2' \ldots\ldots) \\ &+ \sum_{j=1}^{4N+2} \frac{\partial F_i}{\partial k_j}\ (k_1', k_2' \ldots) \\ &+ \text{higher order terms} \end{aligned} \tag{B.5}$$

By ignoring the higher order terms and using Eq. (B.4) the above equation becomes,

$$F_i(k_1',\ k_2', \ldots) + \ \sum_{j=1}^{4N+2} \ \delta k_j \ \frac{\partial F_i}{\partial k_j}\ (k_1',\ k_2' \ldots) = 0 \tag{B.6}$$

Using eq. (B.3), the above equation may be expressed as follows

$$\frac{\partial e}{\partial k_i} + \sum_{j=1}^{4N+2} \delta k_j \frac{\partial^2 e}{\partial k_i \, \partial k_j} \tag{B.7}$$

or expressed conveniently in the matrix form,

$$\lfloor P \rfloor \{ \delta k \} + \{R\} = \{0\} \tag{B.8}$$

where any element of $[P]$ matrix P_{ij} is given by

$$P_{ij} = \frac{\partial^2 e}{\partial k_i \partial k_j} = - \sum_{\substack{\text{over each} \\ \text{frequency} \\ \text{of interest}}} (\alpha_e^* - \alpha_m^*) \frac{\partial^2 \bar{\alpha}_m^*}{\partial k_i \partial k_j}$$

$$- \frac{\partial \alpha_m^*}{\partial k_j} \cdot \frac{\partial \bar{\alpha}_m^*}{\partial k_i} + (\bar{\alpha}_e^* - \bar{\alpha}_m^*)$$

$$\frac{\partial^2 \alpha_m^*}{\partial k_i \partial k_j} - \frac{\partial \bar{\alpha}_m^*}{\partial k_j} \cdot \frac{\partial \alpha_m^*}{\partial k_i} \tag{B.9}$$

In P_{ij} above, the second differentials are difficult to obtain. Also being very small, can be neglected

$$P_{ij} = \sum_{\substack{\text{over each} \\ \text{frequency} \\ \text{of interest}}} \left(\frac{\partial \alpha_m^*}{\partial k_j} \cdot \frac{\partial \bar{\alpha}_m^*}{\partial k_i} + \frac{\partial \bar{\alpha}_m^*}{\partial k_j} \frac{\partial \alpha_m^*}{\partial k_i} \right) \tag{B.10}$$

Each element of vector $\{R\}$, R_i is given by

$$R_i = \frac{\partial e}{\partial k_i} = - \sum_{\substack{\text{over each}\\ \text{frequency}\\ \text{of inter-}\\ \text{est}}} (\alpha_e^* - \alpha_m^*) \frac{\partial \bar{\alpha}_m^*}{\partial k_i}$$

$$+ (\bar{\alpha}_e^* - \bar{\alpha}_m^*) \frac{\partial \alpha_m^*}{\partial k_i} \qquad \text{(B.11)}$$

APPENDIX C

FOURIER TRANSFORMATION FROM TIME DOMAIN

Equation (5.1) is

$$x(t) = \int_{-\infty}^{\infty} h(\tau) \; f(t-\tau) \, d\tau \tag{C.1}$$

Fourier transform $X^*(\omega)$ of $x(t)$ is defined as

$$X^*(\omega) = \int_{-\infty}^{\infty} x(t) \, e^{-2\pi\omega t i} \, dt \tag{C.2}$$

Substituting (C.1) in (C.2),

$$X^*(\omega) = \int_{-\infty}^{\infty} e^{-2\pi\omega t i} \, dt \int_{-\infty}^{\infty} h(\tau) \, f(t-\tau) \, d\tau$$

$$= \int_{-\infty}^{\infty} dt \int_{-\infty}^{\infty} e^{-2i\pi\omega(t-\tau)} \, f(t-\tau) \, e^{-2\pi\omega\tau i} h(\tau) d\tau \tag{C.3}$$

By setting $(t-\tau)$ as ξ in (C.3)

$$X^*(\omega) = \int_{-\infty}^{\infty} h(\tau) \, e^{-i2\pi\omega\tau} \, d\tau \int_{-\infty}^{\infty} f(\xi) e^{-i2\pi\omega\xi} \, d\xi$$

or

$$X^*(\omega) = H^*(\omega) \cdot F^*(\omega) \tag{C.4}$$

APPENDIX D

INVERSION OF A COMPLEX MATRIX

If the inverse of a complex matrix $[[A] + i[B]]$ is given by $[[C] + i[D]]$, then

$$([A] + i[B]) + ([C] + i[D]) = [1] + i[0]$$

$$([A][C] - [B][D]) + i([B][C] + [A][D]) = [1] + i[0] \tag{D.1}$$

From (D.1),

$$([A][C] - [B][D] = [1] \tag{D.2}$$

$$([B][C] + [A][D]) = [0] \tag{D.3}$$

Solving (D.2) and (D.3) for C and D we get

$$[C] = ([A] + [B][A]^{-1}[B])^{-1} \tag{D.4}$$

$$[D] = -[A]^{-1}[B]([A] + [B][A]^{-1}[B])^{-1}$$

The real matrix inversion required above, was done using usual inversion process by Gauss-Jordan's method.

104235

Date Slip

This book is to be returned on the date last stamped.